INFORMATION TO USERS

This manuscript has been reproduced from the microfilm master. UMI films the text directly from the original or copy submitted. Thus, some thesis and dissertation copies are in typewriter face, while others may be from any type of computer printer.

The quality of this reproduction is dependent upon the quality of the copy submitted. Broken or indistinct print, colored or poor quality illustrations and photographs, print bleedthrough, substandard margins, and improper alignment can adversely affect reproduction.

In the unlikely event that the author did not send UMI a complete manuscript and there are missing pages, these will be noted. Also, if unauthorized copyright material had to be removed, a note will indicate the deletion.

Oversize materials (e.g., maps, drawings, charts) are reproduced by sectioning the original, beginning at the upper left-hand corner and continuing from left to right in equal sections with small overlaps. Each original is also photographed in one exposure and is included in reduced form at the back of the book.

Photographs included in the original manuscript have been reproduced xerographically in this copy. Higher quality 6" x 9" black and white photographic prints are available for any photographs or illustrations appearing in this copy for an additional charge. Contact UMI directly to order.

U·M·I

University Microfilms International
A Bell & Howell Information Company
300 North Zeeb Road, Ann Arbor, MI 48106-1346 USA
313/761-4700 800/521-0600

Order Number 9325122

Ballistic and diffuse ultrafast laser pulses propagation in model random media and biological tissues

Liu, Feng, Ph.D.

City University of New York, 1993

U·M·I

300 N. Zeeb Rd.
Ann Arbor, MI 48106

Ballistic and Diffuse Ultrafast Laser Pulses Propagation in Model Random Media and Biological Tissues

by

Feng Liu

A dissertation submitted to the Graduate faculty in Physics in partial fulfillment of the requirements for the degree of Doctor of Philosophy, the City University of New York

---1993---

This manuscript has been read and accepted for the Graduate Faculty in Physics in satisfaction of the dissertation requirement for the degree of Doctor of Philosophy.

2/26/93
Date

Robert R Alfano
Chair of the Examining Committee

Professor R. R. Alfano

2/26/93
Date

Joseph B. Krieger
Executive Officer

Professor J. B. Krieger

Supervisory Committee

Professor K. M. Yoo (co-chair)

Professor J. L. Birman

Professor M. Tomkiewicz

Professor P. P. Ho

The City University of New York

Abstract

Ballistic and Diffuse Ultrafast Laser Pulses Propagation in Model Random Media and Biological Tissues

by

Feng Liu

Advisors: R. R. Alfano and K. M. Yoo

The goal of this thesis is to study light scattering and ultrashort laser pulse propagation in the model discrete random media and biological tissues. The temporal profiles of the scattered ultrashort laser pulses were measured by using ultrashort laser pulses, streak camera with 10 ps time response and the femtosecond cross correlation technique.

The intensity of the diffuse pulse is found to be preferentially reduced by the absorption with respect to the intensity of the ballistic light because the diffuse light on the average travel through a longer path than the ballistic light. A simple experiment was performed to demonstrate that one can image through a highly scattering medium by increasing the absorption in the medium. The speed of the ballistic pulse was measured by the femtosecond second harmonic cross correlation method and was found to be reduced by the scattering. This speed reduction can be accounted for by by the volume fraction combination of the indices of refraction of the scatterers and the water or by the coherent interference between the scattered waves and the primary wave.

No distinct ballistic pulse was observed when the laser pulse transmitted through a thin tissue. The continuous random variation of the dielectric constant in tissue may account for the lack of a distinct ballistic pulse. Nevertheless, the early arriving portion of the transmitted pulse was shown to carry image information. The earlier arriving photons were found to produce image of the hidden object with better quality. The intensity of the early arriving transmitted photons was found to decay exponentially with increasing tissue thickness. The earlier the photons arrive, the quicker their intensity decay. Diffusion theory was found to describe the overall transmitted pulse profiles well, but it underestimates the intensity of the early arriving photons. Compressing tissue was found not to change the key optical parameters of the tissue.

The scattered laser pulse profile in an infinite and semi-infinite random medium were measured and analyzed with the photon density and the photon flux of the diffusion theory. The photon density are found to describe the scattered pulse profile measured inside the scattering medium. Both photon density and the photon flux can be used to describe the scattered pulse profile from the surface of the medium.

Acknowledgement

I greatly appreciate the patient guidance, the encouragement, and the help of Professor R. R. Alfano and Professor K. M. Yoo during the course of this thesis work. I would like to especially thank Professor Alfano for giving me an opportunity to study with him during a critical period in my career. I also thank the members of the Institute of Ultrafast Spectroscopy and Lasers for their help during the course of this thesis work. Special thanks to Dr. W. Cai and Dr. P. Hu for their help with the computation work of this thesis. I thank S. H. Zheng and his wife for their encouragement and friendship.

This thesis study was made possible from the educational and financial support provided in part by the Department of Physics of the City College of the City University of New York, Mediscience Technology Corporation, Hamamatsu Photonics K. K., and National Institutes of Health.

TABLE OF CONTENTS

List of Figures

Chapter 1

Introduction

1.1 Background

Over the past twenty years, ultrafast laser and spectroscopy technologies have been developed and are now widely available[1-4] for research and development works. The state-of-the-art ultrafast laser technology can produce high power, ultrashort duration, femtosecond (10^{-15} second) and picosecond (10^{-12} second), laser pulses, at different wavelength covering from ultraviolet (UV) to infrared (IR). These ultrashort laser pulses have been widely used to solve problems in physics, chemistry, biology, and medicine. This thesis presents experimental studies of ultrashort laser pulse propagation and light scattering in random scattering media.

Light scattering in random medium is common in nature, such as sun light being scattered in the cloud, and room light being scattered in the wall paint. Transport theory, multiple scattering theory, and the diffusion approximation are used to describe the light scattering in random medium.[5] When light enters a disordered scattering medium, it is inevitably scattered randomly in all directions. The degree of light scattering depends on the spatial distribution and time variation of the dielectric constant (index of refraction) of the medium. The gross properties of light scattering by a random medium are characterized by three key parameters: the scattering mean free path l_s, the transport mean free path l_t, and the absorption length l_a.

The scattering mean free path l_s is the mean distance between scatterings. $l_s = 1/(n\sigma_s)$, where n is the number density of the scatterer in the medium, and σ_s is the scattering cross-section of a single scatterer. The scattering cross-section depends

on the shape of the particle, the size of the particle with respect to the wavelength of the light, and the refractive index of the particle with respect to the background. The total scattering cross section σ_s is related to the differential scattering cross section $\sigma(\theta, \phi)$ by:

$$\sigma_s = \int \sigma(\theta, \phi)\sin\theta d\theta d\phi \quad . \tag{1.1}$$

The differential scattering cross section $\sigma(\theta, \phi)$ is quantitative measurement of probability of light being scattered in the direction (θ, ϕ) by a scatterer. For a particle of size much smaller than the wavelength of the light the light is scattered almost uniformly (isotropic scattering) in all directions (Rayleigh scattering). For a large particle the light is scattered mostly in the forward direction (anisotropic scattering) within an angle of $1.2\lambda/d$, where λ is the wavelength of the light and d is the diameter of the particle. For particles of intermediate size, $\sigma(\theta,\phi)$ is rapidly changed with scattering angle θ.

The momentum transferred scattering cross-section σ_m is quantitative measurement of the light scattered away from the forward direction and is given by:

$$\sigma_m = \int \sigma(\theta, \phi)(1 - \cos\theta)\sin\theta d\theta d\phi \quad . \tag{1.2}$$

The momentum transferred scattering cross-section is often written as: $\sigma_m = (1-g)\sigma_s$, where g is the anisotropic scattering parameter or mean cosine average of the scattering. In the case of isotropic scattering, $g = 0$. The larger value of g, the light are scattered more anisotropicly.

The transport mean free path is defined as $l_t = 1/n\sigma_m$. Thus, l_t is the mean distance between off angle scattering events, or the mean length of the random walk step of the multiple scattered photons. The transport mean free path is related to the

scattering mean free path by:

$$l_t = l_s/(1 - g). \tag{1.3}$$

$l_t = l_s$ in the case of the isotropic scattering. When light are scattered anisotropicly, $l_t > l_s$, and the transport mean free path can be many times of the mean scattering path. For example, in the case of 625 nm wavelength light scattered by the latex beads sphere (index 1.59) solution in water (index 1.33), $g = 0.06$ and $l_t = 1.07 l_s$ for beads diameter of 0.09 μm (small particle). For large size particle of diameter 11.9 μm, $g = 0.91$ and $l_t = 11 l_s$. The absorption length is the mean distance of the light travels before it is being absorbed due to inelastic scattering in the medium.

In general, $\sigma(\theta, \phi)$ for particle of arbitrary shape can not be computed. Only for a few kind of particles such as spherical, cylindrical particles $\sigma(\theta, \phi)$ can be obtained theoretically. The formal solution of the problem of light scattering by a homogeneous sphere was worked out by Mie[6] and Debye[7], and it is called Mie theory. The details of Mie theory can be found in many standard electrodynamics and light scattering books[8-10] and will not be repeated in this thesis.

When an ultrashort laser pulse is incident on a slab of random medium, photons are scattered randomly. The transmitted laser pulse is split into a ballistic (coherent) and a diffuse (incoherent) component. The ballistic component traverses through the medium in a straight line path and arrives first. Its intensity is attenuated by a factor of $e^{-(w/l_a + w/l_s)}$, where w is the thickness of the slab. The diffuse component consists of multiple scattered photons which undergo random walks inside the medium. Thus the diffuse component is temporally broadened. The gross properties of the diffuse component can be described by parameters l_t and l_a using the diffusion theory when the medium is sufficiently strong in scattering.

Imaging through a thick random scattering medium has many potential practical applications such as seeing an airplane through a cloud and detecting a tumor hidden in human breast. The ballistic photons which traverse through the medium in a straight line path and the early arriving diffuse photons which traverse through the medium almost in the same direction as the ballistic light carry the image information, while the diffuse photons contribute the background noise. The image will be lost if the medium is sufficiently strong in scattering by using the steady state transillumination imaging technique. Recently, time resolved detection techniques have been used to improve the image quality of the hidden object by detecting only the early arriving photons of the transmitted pulse.

1.2 Thesis Statement and Organization

In this thesis, the light scattering, ultrashort laser pulse propagation and imaging through model scattering medium and biological tissues are experimentally studied using ultrashort laser pulses and various ultrafast time resolved detection techniques. The thesis is organized as follows.

In Chapter 2, the effect of the absorption in the random medium on the intensity of the ballistic and diffuse light is studied. First, the diffusion equation is used to derive the temporal profile and the total intensity of the diffuse component of a ultrashort laser pulse transmitted through a slab of random medium. These solutions will also be used in later Chapters. The experimental results are compared with the theoretical results. The intensity of the diffuse light is found to be preferentially reduced with respect to the intensity of the ballistic light as the absorption of the medium increases. This observation is because the diffuse light on average travel over a longer distance inside the medium than the ballistic light, so these longer

paths diffuse photons will be attenuated more by the absorption. This finding indicates that adding the absorption to the medium can increase the signal (ballistic light) to noise (diffuse light) ratio, thus allowing one to image through an otherwise opaque medium. A simple experiment is performed to illustrate the imaging of an object behind a highly scattering random medium wall by using the absorption.

In Chapter 3, I studied the effect of light scattering on the speed of the ballistic pulse propagation through a discrete random medium. In Chapter 4, I studied the pulse propagation through biological tissues. It is found that the pulse profile of the 100 fs ballistic pulse propagating through discrete medium is not broadened but its speed is reduced by the scattering. On the other hand, no distinct ballistic pulse is observed upon transmitting through the tissue, instead a broadened pulse is observed. We also demonstrate that the early arriving photons through tissue do carry the image information.

In Chapter 5, the temporal profiles of the transmitted pulse through slabs of compressed and uncompressed tissues of different thickness were measured using streak camera and analyzed by using the diffusion theory. The attenuation of the intensity of the photons arriving at various time intervals are computed and analyzed with the diffusion theory. This study yields information about the detectability of the early arring photons which carry the image information.

In Chapter 6, the temporal profiles of the scattered laser pulses in different experimental geometry were measured and analyzed with diffusion theory. The question of whether the measured scattered pulse is better described by the photon density or by the commonly used photon flux is examined.

Finally, in Chapter 7, I summarize the results of this thesis study and in Chapter 8, I point out some future research directions.

References

1 R. L. Fork, B. J. Greene, and C. V. Shank, Appl. Phys. Lett. **38**, 671(1981).

2 H. R. Dorsinville, R. R. Alfano, and N. H. Schiller, "Calibrating a picosecond streak camera", *The photonics design and applications handbook*, H23-25(1986).

3 S. L. Shapiro ed., *Ultrafast Laser Pulses*, (Springer-Verlag, Berlin, 1984).

4 *Ultrafast Phenomena*, Vol. I-VII(Springe-Verlag, Berlin).

5 A. Ishimaru, *Wave propagation and scattering in random media*, Vol. **1 & 2**,(Academic Press, New York, 1978).

6 G. Mie, Ann. Physik. **25**, 377(1908).

7 P. Debye, Ann. Physik. **30**, 59(1909).

8 M. Born and E. Wolf, *Principles of Optics,* 4^{th} Edition, (Pergamon, New York, 1970), Pg. 633-664.

9 H. C. van de Hulst, *Light Scattering by Small Particles,* (Dover, New York, 1981).

10 J. D. Jackson, *Classical Electrodynamics,* 2^{nd} Edition, (Wiley, New York, 1975).

Chapter 2

Imaging through Scattering Wall using Absorption

2.1 Introduction

To see an object hidden in or behind a highly scattering random medium is one of the most challenging physics and engineering problems. Many different techniques have been introduced for this purpose, such as, phase conjugation,[1] stellar interferometry,[2] inverse scattering,[3,4] time of flight,[5] spatial filter, and fluorescence.[6] Recently, two new techniques have been proposed: Freund et al.[7] suggested that the memory effect[7-9] may be used to see through a random medium, while White et al.[10] suggested that the inverse problem of pulse backscattering may be used to probe 1-dimensional random medium. Nevertheless, most of the above methods are difficult to realize which involve sophisticated mathematical problems, long numerical programs, and complex experimental setups. In this Chapter, we introduce an exceedingly simple, yet novel and important technique to improve our ability to see through a highly scattering random wall. This technique simply makes use of the absorption presence in the random medium at propagating light's wavelength. The absorption is shown to reduce the intensity of multiple scattered light (noise) below the ballistic signal intensity (image). This reduction in noise to signal ratio allows us to see through a random scattering wall which would otherwise be opaque in the absence of absorption. An experimental realization of seeing through a random medium with the help of absorption is also presented in this Chapter.

Light propagating through a random medium undergoes multiple scattering. Multiple light scattering in random medium of discrete scatterers splits the incident

light into two components: a coherent and an incoherent components.[11] The coherent component constitutes the ballistic signal; it propagates through the medium undeviated in the forward direction and carries the object information. The incoherent component constitutes the noise because the light had undergone random scattering in all directions in which the signal information is lost. Multiple scattering of light reduces the intensity of the signal and increases the noise. The signal intensity can be reduced by several orders of magnitude below that of multiple scattered noise, which is the primary reason why one cannot see through an optically thick scattering random medium (e.g. a cloud). The noise due to multiple light scattering is commonly reduced by a spatial filter which removes light scattered away from the collinear direction of the signal. However, there is a substantial portion of multiple scattered light traveling in the collinear direction of the ballistic signal in an highly scattering medium.[11] This multiply scattered light collinear to the signal direction cannot be eliminated using a spatial filter, but can be substantiately reduced by absorption because of longer light path travel.

The image of an object hidden in a random medium can be improved by increasing the amount of absorption in the medium. The underlying physical principle is multiple scattered light travels over a longer pathlength than the ballistic signal. The average distance the multiple scattered light travel in the medium is w^2/l_t, which is longer than w, the distance the ballistic light transverses through a slab of thickness w. Light traveling over a longer pathlength has a higher probability of being attenuated. Thus, an introduction of absorbing dye into a random medium will preferentially absorb the multiple scattered light over the ballistic light.

2.2 Theory

The properties of light scattering in random media can be described by the transport theory.[12] In general, transport equation is difficult to solve analytically. Even in most simple cases, the solution of the transport equation are complicate. When the medium is highly scattering, the transport theory can be approximated by the diffusion theory.[12] Diffusion theory has now been widely used to describe the properties of the multiple scattered (diffuse) light. Analytic solutions of the diffusion equation for various experimental geometries are available and are simple to use. The temporal profile of the diffuse component of the scattered ultrashort laser pulse in a random medium depends on the photon transport mean free path l_t and the absorption length l_a of the random medium, the distance between the source and detection sites, and the boundary conditions. The temporal profile of the photon density $n(\vec{r},t)$ at distance $\vec{r}$ from the source can be obtained from the solution of the diffusion equation as follows[12-14]

$$\frac{\partial n(\vec{r},t)}{\partial t} = D\nabla^2 n(\vec{r},t) - \frac{v}{l_a}\cdot n(\vec{r},t) + \delta(\vec{r})\delta(t) \quad , \tag{2.1}$$

where the δ- function term represents the impulse photon source at time $t = 0$ and position $\vec{r} = 0$, $D = \frac{1}{3}vl_t$ is the diffusion constant, and v is the speed of light in the scattering medium. The first term on the right hand side of eq. (2.1) is the diffusion term and the second term is the absorption term. The temporal profiles of the diffuse pulse are commonly described by the photon flux. The photon flux is related to the photon density by: $j(\vec{r},t) = \vec{j}(\vec{r}, t)\cdot\hat{s} = -D\hat{s}\cdot\vec{\nabla}n(\vec{r},t)$, where $\hat{s}$ is the direction of detection. The question about whether the scattered pulse profile under different experimental geometries should be described by the photon density or by the photon flux

will be addressed in Chapter 7. In the case of transmission through a slab of random medium which we considered in this Chapter, both photon density and photon flux can be used to describe the scattered pulse profile.

In the case of diffusion in an infinite slab of random medium of thickness w located between $z = z_0$ (z_0 will be defined later) and $z = w + z_0$, with the boundary condition that photon density n vanishes at $z = 0$ and $z = w + 2z_0$, the temporal profile of the photon density at point (x, y, z) with an impulse source at $(x'=0, y'=0, z')$ can be obtained from the solution of the diffusion equation and is given by:[13, 14]

$$n(\vec{r}, t) = \frac{e^{-R^2/4Dt}}{(4\pi Dt)^{3/2}} \sum_{m=-\infty}^{\infty} \left\{ e^{-(2md + z' - z)^2/4Dt} - e^{-(2md - z' - z)^2/4Dt} \right\} e^{-vt/l_a}, \quad (2.2)$$

where $R^2 = x^2 + y^2$, $z_0 = 0.71 l_t$ is the extrapolation length, and $d = w + 2z_0$. This solution is obtained with the methods of images. In the case of infinite medium, ie. $w \sim \infty$, eq. (2.2) gives the usual solution of the diffusion in an infinite random medium:

$$n(\vec{r}, t) = \frac{1}{(4\pi Dt)^{3/2}} e^{-[R^2 + (z - z')^2]/4Dt} \cdot e^{-vt/l_a} \quad . \quad (2.3)$$

The sum in eq. (2.2) can also be written as a sum over the reciprocal space by using the Poisson sum formula.[15] The result is

$$n(\vec{r}, t) = \frac{e^{-R^2/4Dt}}{(4\pi Dt)d} \sum_{m=-\infty}^{\infty} \left\{ \sin\frac{\pi m z'}{d} \sin\frac{\pi m z}{d} e^{-Dt(m\pi/d)^2} \right\} \cdot e^{-vt/l_a}. \quad (2.4)$$

In the case of transmission through a slab, $z' = z_0$ and $z = w + z_0$. This gives the temporal profile of the photon density and photon flux as

$$n_z(t) = \frac{e^{-R^2/4Dt}}{(4\pi Dt)d} \sum_{m=1}^{\infty} (-1)^m \left(1 - \cos\frac{2\pi m z_0}{d}\right) e^{-Dt(m\pi/d)^2} \cdot e^{-vt/l_a} \quad , \quad (2.5)$$

and

$$j_z(t) = \frac{D \cdot e^{-R^2/4Dt}}{\pi w^2 (4\pi D t)} \sum_{m=1}^{\infty} m \left(\frac{\pi w}{d}\right)^2 \sin\frac{m\pi w}{d} e^{(-Dt(m\pi/d)^2} \cdot e^{-vt/l_a} \quad . \tag{2.6}$$

In our experiment performed in this Chapter, a plane wave ultrashort laser pulse (large beam diameter) was incident normally onto a slab of random medium, the temporal profile of the scattered pulse exiting at a point on the opposite side of the slab is obtained by integrating eq. (2.6) over the whole surface of the slab. The result is

$$I_z(t) = \frac{D}{\pi w^2} \sum_{m=1}^{\infty} m(\pi w/d)^2 \sin(m\pi w/d)\, e^{(-Dt(m\pi/d)^2)} e^{-vt/l_a} \quad . \tag{2.7}$$

This equation has been found to consistently describe the measured scattered pulse profile in the diffusion region.[16]

The total intensity of the diffuse light is obtained by integrating eq. (2.7) with respect to time from 0 to ∞, results in:

$$I_{total} = \int_0^{\infty} I_z(t)\, dt = \frac{\sinh\left[(3/l_t l_a)^{1/2}(d - w)\right]}{2\sinh[(3/l_t l_a)^{1/2} d]} \quad . \tag{2.8}$$

The average arrival time, t_{ave}, of the transmitted photons can also be obtained:

$$t_{ave} = \int_0^{\infty} t \cdot I_z(t)\, dt \,/ \int_0^{\infty} I_z(t)\, dt = \frac{(l_t l_a/3)^{1/2}}{4D} \cdot$$

$$\cdot \frac{w\sinh[(3/l_t l_a)^{1/2}(2d - w)] - (2d - w)\sinh[(3/l_t l_a)^{1/2} w]}{\sinh[(3/l_t l_a)^{1/2}(d - w)] \cdot \sinh[(3/l_t l_a)^{1/2} d]} \quad . \tag{2.9}$$

In the absence of the absorption ($l_a = \infty$), eq. (2.8) is reduced to the simple form

$$I_{total} = (1 - w/d)/2 = z_0/(w + 2z_0) \quad . \tag{2.10}$$

The average time that the transmitted photons take is

$$t_{ave} = w(w + 2z_0)/2vl_t \quad . \tag{2.11a}$$

When the thickness of slab is many transport mean free path thick $w/l_t \gg 1$, i.e. the medium in the diffusion region, the total transmission of light is:

$$T \approx l_t/w, \tag{2.11b}$$

that is the intensity of the total transmission decreases inversely with the increase of the medium thickness.

The average time is:

$$t_{ave} \approx w^2/2vl_t, \tag{2.11c}$$

that is the average time taken by the diffuse photons to traverse through the medium $w/2l_t$ times of the ballistic time w/v.

The average distance the diffuse light travel in the medium is:

$$<L> = vt_{ave} \approx w^2/2l_t, \tag{2.11d}$$

which is many times of slab thickness w in the diffusion region ($w/l_t >> 1$).

The transmitted diffuse light is scattered in all directions. Thus, the measured intensity of the diffuse light scattered within a fraction of solid angle Ω is given by

$$I_{dif} = \Omega\, I_{total} \quad , \tag{2.12}$$

where I_{total} is given by eq. (2.8). On the other hand, the intensity of the ballistic signal transversing a distance z is reduced by

$$I_c = e^{-w(1/l_s+1/l_a)} \quad , \tag{2.13}$$

where l_s is the photon scattering mean free path. Eqs. (2.12) and (2.13) are used to

compute the diffuse and ballistic intensity of the transmitted laser pulse, respectively.

2.3 Experimental Method

In this section, we present the angle- and time-resolved detection technique which has been used through out this thesis work. A schematic diagram of the experimental setup utilizing this technique is shown in Fig. 2.1. A beam of ultrafast laser pulses of 100 fsec pulse duration, repetition rate of 82 MHz, average laser power of 10 mW, laser wavelength centered at 620 nm, and beam diameter of 3 mm were generated from a Argon laser (515 nm) pumped colliding pulse mode-locked (CPM) dye laser system. Part of the laser beam was split to trigger the measurement instruments. The main part of the laser beam was expanded by two lens to a beam diameter of 20 mm, and was incident on a slab of random medium. The random medium consists of 0.3 % of spherical latex beads of diameter 0.296 μm suspended in water in a cylindrical glass cell of 50 mm in diameter and 10 mm thick. A black pinhole of 2 mm diameter was placed at the center on the opposite side of the cell. The temporal distribution of the photons emerging from this pin hole within 4 mrad in the forward direction was angle resolved by a collecting lens (10 cm focal length) and time resolved by by a 3-dimensional (intensity, time, angle) Hamamatsu syn-chroscan streak camera. The horizontal input slit of the streak camera was placed at the focal plane of the collecting lens. Thus the direction along the slit corresponds to the angle the scattered photons travel. The typical time response for this detecting system is about 10 ps. In our experiment, further increase of the incident beam diameter did not change the measured scattered pulse profile. Thus, the measured temporal profile can be approximated by the plane wave incident case and can be described by eq. (2.7). The synchroscan operation of the streak camera greatly

improve the signal to noise ratio. Each temporal profile was acquired by accumulating a total of $1.23 \cdot 10^9$ laser pulses in 15 second integration time. The data were then saved and analyzed by computer. Absorbing dye (malachite green) was added into the random medium to increase the absorption. The absorption length at different wavelength corresponding to certain absorbing dye concentration was determined by measuring the transmission through the dye solution (no scatterer added) using a spectrophotometer.

2.4 Results on the Intensity Attenuation of Ballistic and Diffuse Pulses by Absorption

Absorption in random media can substantiately reduce the noise below the signal intensity. This is an important point which has not been realized before. The reduction of noise over signal using absorption were measured using time- and angle-resolved ultrafast laser pulse measurements. The intensity of the diffuse and ballistic light predicted by the diffusion theory are computed using eq. (2.12) and eq. (2.13), and plotted in Fig. 2.2 by solid and broken lines, respectively. The squares and the triangles are experimental data to be presented later. This figure illustrates a case for scattering medium consisting of 0.3 % volume concentration latex beads of 0.296 μm diameter suspended in water. $l_t = 1\ mm$ is found experimentally, $l_s = 1/n\sigma_s = 0.3\ mm$, where $n = 2.2\times10^{17}\ m^{-3}$ is the scatterer density, $\sigma_s = 1.54\times10^{-14}\ m^2$ is the scattering cross-section computed numerically from the Mie theory. The thickness of the slab of random medium $w = 10\ mm$, and the absorption length is varied from 1000 mm to 0.1 mm. The intensity of diffuse light is much higher than the intensity of ballistic when the medium is less absorbing. e.g. when l_a=1000 mm, the diffuse intensity is 130 times that of the ballistic signal. The

solid angle of collection Ω for the diffuse light is taken to be 7×10^{-12}. As the absorption in the medium is increased (smaller absorption length), the diffuse intensity decreased faster than the ballistic intensity. The diffuse intensity is decreased below the ballistic intensity when l_a is 2 mm. This reduction of diffuse light with respect to ballistic signal will substantially increase the quality of image of an object hidden in a highly scattering random medium.

The temporal profiles of ballistic pulse and diffuse light pulses in the forward direction for different amounts of absorbing dye added into the random medium are displayed in Fig. 2.3. The narrow peak at time 44 psec corresponds to the ballistic signal which travels undeviated in the forward direction. The pulse width is same as the time response time of the streak camera which is about 10 ps. In contrast, the diffuse light pulse component which had undergone multiple scattering in the random medium shows a broad temporal distribution of photons arrival at later times. Fig. 2.3(a) presents the result of a latex beads medium when no dye is added. The intensity of the tiny ballistic peak at 44 ps is much smaller than the large and broad temporal distribution of the diffuse pulse. The total intensity of the diffuse light is found to be 130 times greater than the intensity of the ballistic signal. It is impossible to see through such a cloudy medium. To study how the diffuse intensity may decrease with respect to the ballistic signal, an increasing amounts of absorbing dye (malachite green) is added into the random medium. Both the ballistic and diffuse intensity are found to be decreased, but the intensity of the diffuse light decreased faster than the ballistic light. Fig. 2.3(d) shows the case where the diffuse intensity becomes equal to the ballistic intensity.

The photon transport mean free path l_t and the absorption length of the 0.3% latex beads solution (no dye added) were found to be 1 mm and 550 mm,

respectively, by fitting eq. (2.7) to the experimental result in curve (a) of Fig. 2.3. The theoretical plot of the best fit is showing in Fig. 2.4(a). The fitting was done numerically using a standard least square fitting program.[17] The scattering mean free path is computed to be 0.3 mm. This slab of random medium is (w/l_s=10mm/0.3mm) 33 scattering mean free paths thick, or (w/l_t=10mm/1mm) 10 transport mean free paths thick. The transmitted pulse profiles shown in Figs. 2.3(b), (c) and (d) demonstrate how the diffuse light intensity decrease with respect to ballistic intensity as increasing amount of absorbing dye (malachite green) is presence in the random medium. The diffuse scattered light at later times which travel over a longer distance is attenuated more. The intensity of the diffuse light is shown to decrease faster as compare to ballistic light as more absorbing dye is added. The absorption lengths from these media were measured by a spectrophotometer. Measurements of absorption were performed on dye solutions (no beads in it). The corresponding absorption lengths were measured and computed to be 13.5, 3.4, and 1.8 mm for Fig. 2.3(b), (c), and (d), respectively. The temporal profile in Fig. 2.3(d) shows that the diffuse light intensity is substantially reduced with respect to signal intensity as compared with the profile in Fig. 2.3(a).

The experimentally measured diffuse and ballistic intensity for medium with different amount of absorption are presented in Fig. 2.2 plotted by triangles and squares, respectively. The intensities of the ballistic and the diffuse component are obtained by integrating the corresponding temporal profiles. The intensity of the diffuse light is almost equal to the ballistic signal when the absorption length of the medium is 1.8 mm. If the solid angle of collection is made smaller, then the intensity of the diffuse intensity is below that of the ballistic signal.

The theoretical transmitted pulse profiles of the diffuse component for increasing absorption cases are computed from eq. (2.7) using the transport mean free path $l_t = 1$ mm and the corresponding absorption length l_a. The absorption lengths decrease as more absorbing dye is added to the medium. Fig. 2.4 shows theoretical plots which correspond to the cases shown in Fig. 2.3 where the absorption lengths are 550, 13.5, 3.4, and 1.83 mm, respectively. These curves show quite good fit to the corresponding diffusive pulse profiles shown in Fig. 2.3.

2.5 Imaging Enhancement using Absorption

Using the basic knowledge gain above, we experimentally demonstrated that an hidden object behind a *random scattering wall* can in fact be seen and imaged with the aid of absorption. A CROSS of 3 mm and 2 mm wide bars to be imaged through a highly scattering medium is shown in the Inset of Fig. 2.5. A cylindrical glass cell (5 cm diameter and 1 cm thick) in which the random medium to be created was placed between the object (CROSS) and the video detector (streak camera in focus mode). A laser beam was incident upon the CROSS, and traveled through the medium in the glass cell and transmitted light was detected by the streak camera. Photograph (a) of Fig. 2.5 shows the image of the CROSS including diffraction fringes when there is no scatterer in the cell. When a random medium was introduced in the glass cell, which was 0.23 % concentration of latex beads of 0.296 μm diameter suspended in water, the image of the CROSS was completely lost. Only a cloudy diffuse image was seen as shown in photograph (b) of Fig. 2.5. The scattering mean free path for this medium computed from Mie theory is found to be 0.4 mm. This medium of 10 mm thick corresponds to w/l_s = 10/0.4 = 25 scattering mean free path thick which is definitely in the multiple scattering regime. When an

absorption was introduced into the random medium by the addition of malachite green (the absorption length at 620 nm of the medium is l_a = 4.6 mm), a clear image of the CROSS reappeared including the diffraction fringes as shown in photograph (c) of Fig. 2.5. The reduction of image intensity due to absorption is small, only by a factor of 30%. There is sufficient intensity to be detected for imaging. When the laser wavelength was changed to 515 *nm*, where the malachite green dye becomes less absorbing (l_a = 75 mm), the image disappeared as shown by photograph (d) of Fig. 2.5.

The simplicity as well as the importance of this method on its diverse applications in imaging of objects in highly scattering medium must be stressed. Examples are airplanes hidden in clouds or a tumor in a breast. In each case, the spectral region of light for imaging should be selected for an appropriate amount of absorption such that the noise is reduced below the signal. A low power laser such as HeNe laser normally emits light of 1 mW mm^{-2} power at 633 nm which corresponds to 3.2 x 10^{15} photons s^{-1} mm^{-2}. If this laser passes through a highly scattering wall with $w = 10\ mm$ thick, $l_s = 0.5\ mm$, and $l_t = 1.67\ mm$. Then, (w/l_s = 20), the ballistic intensity will be reduced by a factor of $e^{-20} \approx 2\times10^{-9}$. The number density of the ballistic photon will be equal to 6.6 10^6 photon s^{-1} mm^{-2} after passing through the scattering wall. A good intensifier cooled charge coupled device photon detector (such as Hamamatsu VIM) is able to detect very low light with intensity as low as 1 photon s^{-1} mm^{-2}. Thus, the ballistic photons may be further reduced by absorption to 1 photon s^{-1} mm^{-2} and is still detectable. That is, a reduction factor of 1.5 10^{-7} is available for absorption. This reduction factor corresponds to the absorption length of the medium $l_a = w/15.7$. If the thickness of the scattering wall w=10 *mm*, l_a = 10/15.7 *mm* = 0.64 *mm*. The total intensity for the transmitted multiple

scattered light is obtained from eq. (2.12), and is reduced to be $I_{dif} = 7.\times10^{-3}$ photon s^{-1} mm^{-2} for a solid angle of collection $\Omega = 10^{-5}$. That is the total detected diffuse light is 2 order of magnitude below the ballistic signal. This reduction in noise to signal will substantiately improve the quality of the image.

2.6 Conclusion

We have shown that the diffuse noise can be substantially reduced with respect to ballistic signal by the absorption presence in the random medium. The enhancement of signal to noise ratio with the aid of absorption in the medium is important in remote sensing and many other imaging applications in random medium. To image through a biomedical tissue with optical radiation, one should select a wavelength which is within the absorption region of the media.

References

1 A. Yariv and P. Yeh, *Optical Waves in Crystal: Propagation and Control of Laser Radiation,* (Wiley, New York, 1984), Pg. 549

2 J. C. Dainty, ed., *Laser Speckle and Related Phenomena,* (Springer-Verlag, Berlin, 1975). Pg. 203-278

3 Z. S. Agranovich and V. A. Marchenko, "The Inverse Problem of Scattering Theory," (Gorden and Breach, New York, 1963).

4 H. P. Baltes, editor, *Inverse Source Problems in Optics,* (Springer-Verlag, Berlin, 1978).

5 J. G. Fujimoto, S. De Silversti, E. P. Ippen, R. Margolis, and A. Oseroff, Opt. Lett. **11**, 150 (1986)

6 G. T. Reynolds, Microsc. Acta **83**, 55 (1980)

7 I. Freund, M. Rosenbluh, and S. Feng, Phys. Rev. Lett. **61**, 2328 (1988)

8 S. Feng, C. Kane, P. A. Lee, and A. D. Stone, Phys. Rev. Lett. **61**, 834 (1988).

9 M. J. Stephen and G. Cwilich, Phys. Rev. B **34**, 7564 (1986).

10 B. White, P. Sheng, M. Postel, and G. Papanicolou, Phys. Rev. Lett. **63**, 2228 (1989).

11 K. M. Yoo and R. R. Alfano, Opt. Let. **15**, 320 (1990).

12 A. Ishimaru, *Wave propagation and scattering in random media*, Vol. **1 & 2**, (Academic Press, New York, 1978).

13 M. Lax, V. Nayaramamurti, and R. C. Fulton, " Classical diffusive photon transport in a slab," in *Proceedings of the Symposium on Laser Optics of Condensed Matter, Leningrad, June 1987*, edited by J. L. Birman, H. Z. Cummins

and A. A. Kaplyanskii (Plenum, New York, 1987), Pg. 229-235.

14 G. H. Watson, S. L. McCall, P. A. Fleury, and K. B. Lyons, Phys. Rev. B, **41**, 10947(1990).

15 M. Lax, *Symmetry principles in solid state and molecular physics*, page 198(Wiley, New York, 1974).

16 K. M. Yoo, Feng Liu, and R. R. Alfano, "When does the diffusion approximation fail to describe photon transport in random media?" Phys. Rev. Lett. **64**, 2647-2650(1990); errata, **65**, 2210-2211(1990).

17 W. H. Press, B. P. Flannery, S. A. Teukolsky, and W. T. Vetterling, *Numerical Recipes*, (Cambridge, New York, 1986).

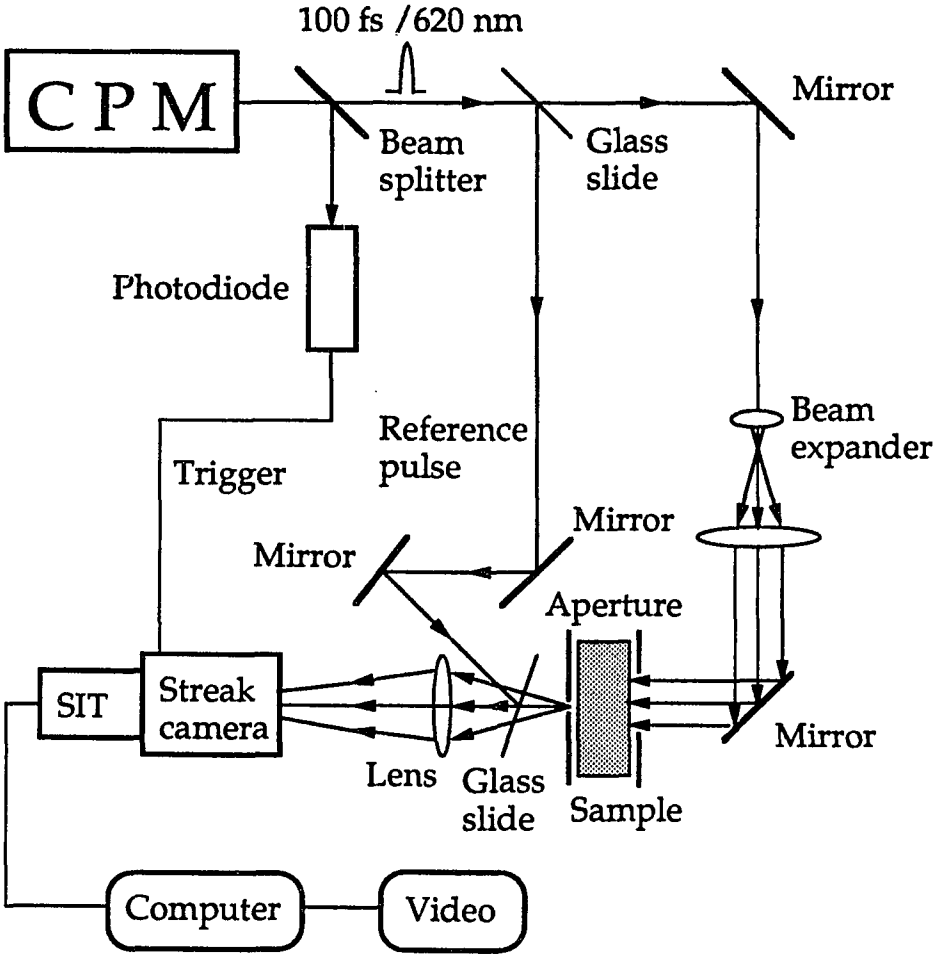

Fig.2.1 Schematic diagram of experimental arrangement.

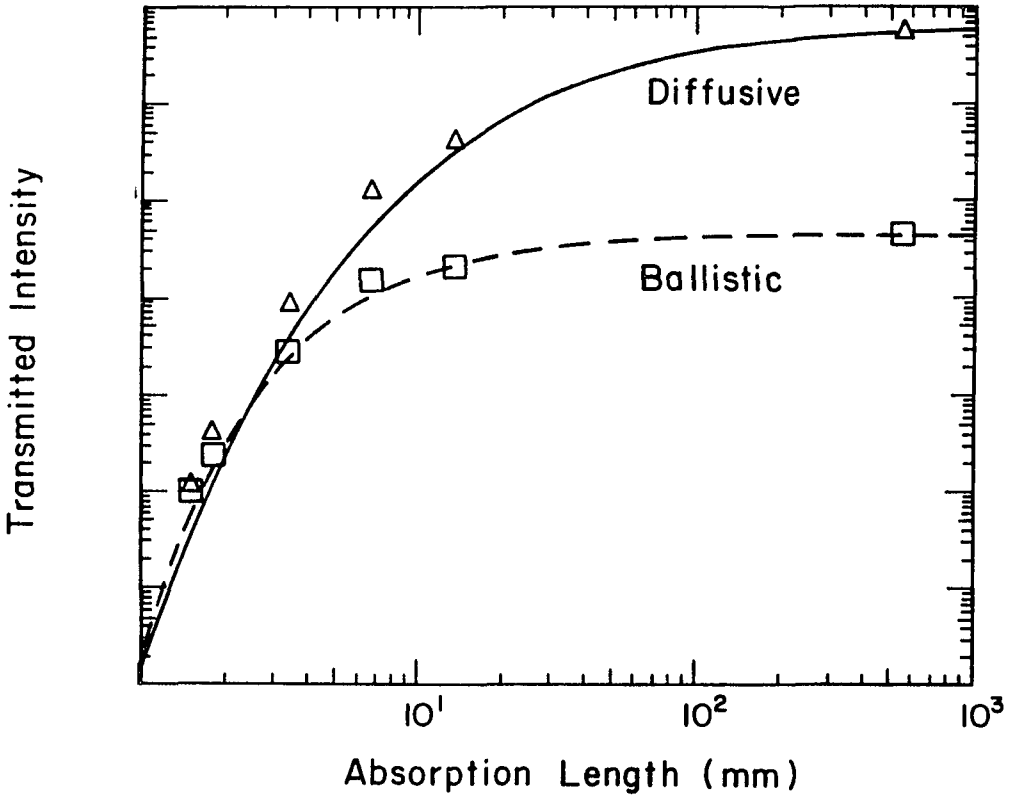

Fig.2.2 Theoretical prediction and experimental results of the total diffuse light and signal intensity for light transmitted through a random medium with different absorption lengths, using $\Omega = 7\times10^{-12}$, w = 10 mm, l_s= 0.3 mm. and l_t=1.0 mm. The solid and dotted curves correspond to the ballistic and diffuse light intensity, respectively, as computed by eq. (2) and (3). The square and triangle correspond to the measured ballistic and diffuse light intensity, respectively.

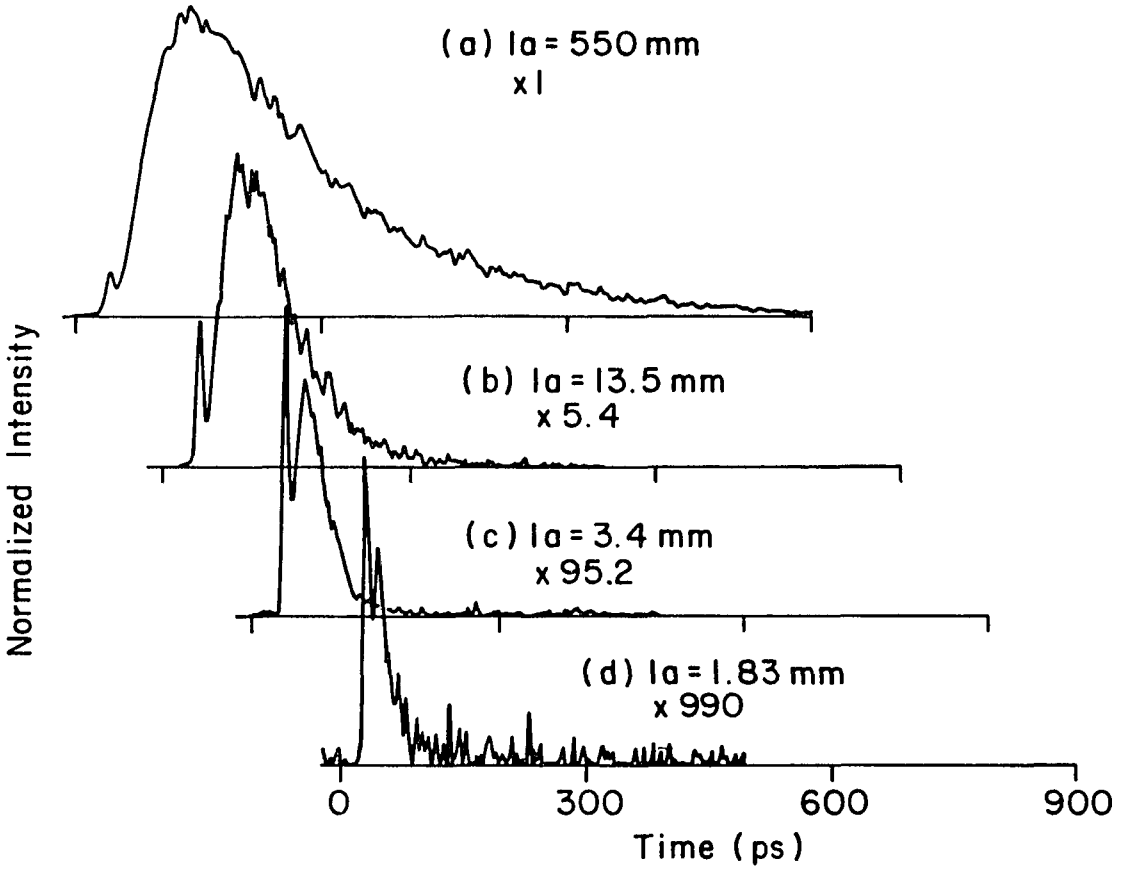

Fig.2.3 Transmitted pulse profiles through a slab of random medium of 10 mm thick with a 0.3 % concentration of latex beads of 0.296 μm diameter, at different amount of absorbing dye concentrations. The absorption lengths of these media are indicated on the curves.

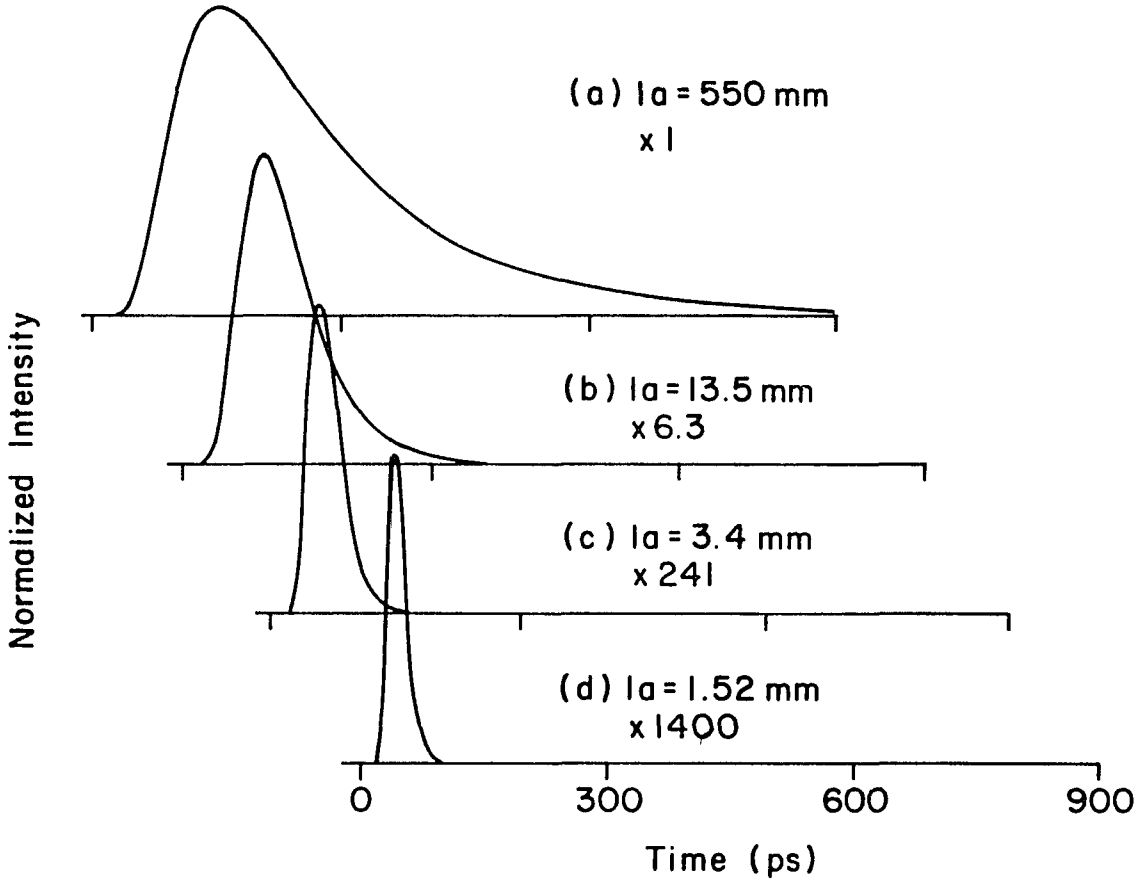

Fig.2.4 Theoretical plots of transmitted diffuse pulse profiles correspond to the case in Fig. 2.3. The transport mean free path l_t = 1.0 mm from the best fit is used in the computation.

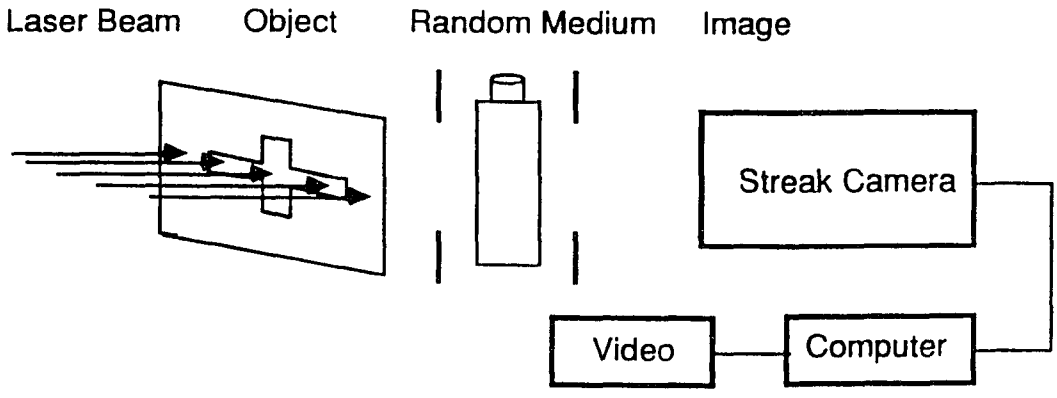

Inset : Imaging Setup

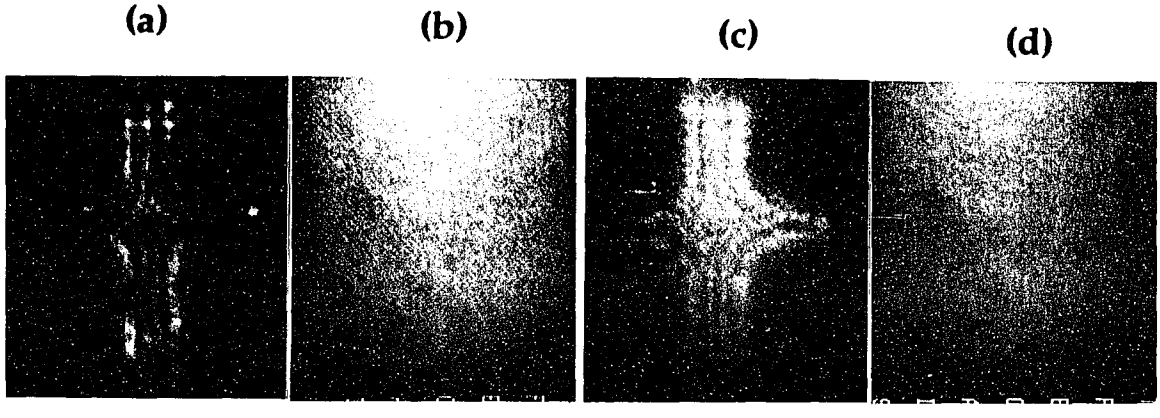

Images

Fig.2.5 Imaging setup (Inset) and photographic images of a CROSS: (a) No scatterer is in the cell; (b) scatterer in the cell, at $\lambda = 620\ nm$; (c) scatterer and malachite green in the cell, at $\lambda = 620nm$, $w/l_s = 25$, $l_a = 4.6\ mm$; (d) scatterer and malachite green in the cell, at $\lambda = 515\ nm$, $w/l_s = 25$, $l_a = 75\ mm$.

Chapter 3

The speed of the coherent component of femtosecond laser pulses propagating through discrete random scattering media

3.1 Introduction

Light propagating in a random scattering medium undergoes multiply scattering which splits a femtosecond light pulse into two components: a coherent (ballistic) and an incoherent (diffusive) component.[1,2] The incoherent component of the ultrafast laser pulse is temporally broadened and arrives much later than the coherent component because the scattered light undergoes a random walk with a large distribution of pathlengths.[2] Most recently, the average time of arrival and the temporal profile of the incoherent component of the transmitted pulse was measured and analyzed in various random media.[3-7] The coherent component arises from the coherent interference between the scattered waves and the primary wave. This interference keeps the coherent component propagating in the forward direction, increases the index of refraction, and reduces the speed of the light wave in the medium. In a homogeneous medium, the light waves are scattered by the individual atoms or molecules of the medium. Thus in a medium consisting of two kinds of substances mixed uniformly in atomic or molecular scale, the effective refractive index of the mixture is simply the volume fractional combination of the indices of the individual substances. This simple method to obtain refractive index may not be applied to the case of the mixed medium consisting of micro size scatterers, because the light scattering of micron size particle is different from the scattering of atom or molecule. Previous studies of the ballistic pulse using streak camera[2] did not have good enough time resolution

(time response of the streak camera is typically 10 ps) to accurately measure the pulse profile and the speed of the 100 fs ballistic pulse. As pointed out in Chapter 2, ballistic pulse carries the image information of hidden object inside or behind the scattering medium. Thus it is important to study the properties of the ballistic pulse. In this Chapter, the pulse profiles and the speed of the coherent component of 100 *fsec* laser pulse propagating through random scattering media were measured by femtosecond resolution cross-correlation method and the results were compared with theory.

3.2 Theory

A simple model which may account for the delay time (i.e. the reduction of the speed) caused by the scattering is that the increase in the group refractive index arises from the higher refractive index of the added scatterers. In this model, the effective refractive index of the medium is described by the volume fractional combination of the refractive indices of the water and latex beads. For a given volume fraction F of the latex beads, the effective group, phase index (n_g^e, n_p^e) of the scattering medium is simply given by:

$$n_{g,p}^{e} = n_{g,p}^{w}(1-F) + n_{g,p}^{l}F, \tag{3.1}$$

where $n_{g,p}^{w}$= 1.349, 1.332 and $n_{g,p}^{l}$= 1.638, 1.589 are the group and phase refractive indices of the water and latex bead at $\lambda = 625\ nm$, respectively. The group index is related to the phase index by $n_g = n_p - \lambda\frac{dn_p}{d\lambda}$, where λ is the wavelength in the vacuum.

The delay time Δt of the ultrafast laser pulse propagating through latex beads suspended in water medium of thickness L can be derived from eq. (3.1) and is given

by:

$$\Delta t = \frac{Ln_g^e}{c} - \frac{Ln_g^w}{c} = \frac{LF}{c}(n_g^l - n_g^w), \tag{3.2}$$

where c is the speed of light in the vacuum. $\Delta t = 0$ when laser pulses go through water.

A rigorous theoretical model which can be used to describe time delay of the coherent pulse is the coherent interference in the forward direction among the scattered light. This interference will reduce the traveling speed of the coherent pulse. M. Lax[1,9] has derived a rigorous theory for the refractive index of a scattering medium. The coherent pulse satisfies the wave equation:

$$[\nabla^2 + k^2 + 4\pi N r \vec{\varepsilon}_0 \cdot \vec{f}]\ \Psi_c(\vec{r}) = 0 \tag{3.3}$$

where k is the wave number in the medium without scatterers, N is the number density of the scatterer and can be computed from the volume fraction by $N = 3F/4\pi a^3$ (a is the radius of the spherical scatter), r is the ratio of the effective field acting on a scatterer to the average field in the medium, $\vec{\varepsilon}_0$ is the unit polarization vector of the wave, and $\vec{f}$ is the forward scattering amplitude of a single scatterer. For a plane wave, $\Psi_c = \exp(i\vec{r}\cdot\vec{k})$. Substituting this relation in eq. (3.3), the effective propagation constant k' for light wave is given by:

$$k'^2 = k^2 + 4\pi N r \vec{\varepsilon}_0 \cdot \vec{f}(\vec{k},\vec{k}), \tag{3.4}$$

where $\vec{f}(\vec{k},\vec{k})$ is the forward scattering amplitude by a single spherical scatterer computed with effective propagation constant and it can be computed from Mie scattering theory.[10]

Eq. (3.4) accounts the effect of the fields acting on one scatterer due to the presence of scattered field from other scatterers, i.e., multiple scattering. This situation is evident in the fact that ratio the r and the $\vec{f}$ on the right hand side of eq. (3.4) depends on k' instead of k. The forward scattering amplitude is complex, thus, k' is also complex. The real part of k' will give the effective phase index of refraction, while the imaginary part gives the attenuation coefficient of the intensity of coherent wave. For the electromagnetic wave, the ratio of the effective field acting on a small scatterer to the average field acting on the medium is given by[1,9] $r \approx ((n_p^e/n_p^w)^2 + 2)/3$. Since the attenuation per wavelength is small ($\mathrm{Im}k' \ll \mathrm{Re}k'$) and the change of index of refraction is also small, the ratio $r \approx 1$, and k is used instead of k' in computing the forward scattering amplitude in eq. (3.4). The effective propagation constant can be obtained as:

$$\mathrm{Re}k' = [k^2 + 4\pi N \mathrm{Re}(\vec{\varepsilon}_0 \cdot \vec{f}(\vec{k}, \vec{k}))]^{1/2}. \tag{3.5}$$

The imaginary part is given by:

$$\mathrm{Im}k' = [2\pi N \mathrm{Im}(\vec{\varepsilon}_0 \cdot \vec{f}(\vec{k}, \vec{k}))]/(Rek'). \tag{3.6}$$

Thus the intensity of the coherent wave through a slab of thickness L is attenuated by:

$$I = I_0 e^{-2\mathrm{Im}k'L} = I_0 e^{-N\sigma_t L}. \tag{3.7}$$

where σ_t is the total cross section and is related to the forward scattering amplitude via the cross section theorem : $\sigma_t = 4\pi/k \mathrm{Im}f(\vec{k},\vec{k})$. In our case, the medium can be considered non absorbing, so the total cross section is equal to the total scattering cross section (σ_s). The effective phase index n_p^e is given by:

$$n_p^e = \mathrm{Re}k'/k_0 = n_p^w + F\frac{3n_p^w}{2k^2a^3}\mathrm{Re}(\vec{\varepsilon}_0 \cdot \vec{f}(\vec{k},\vec{k})), \tag{3.8}$$

where F is the volume fraction of the scatterers and is related to the particle number density N by: $F = 4\pi a^3 N/3$.

In the small particle approximation which is the case in our experiment, the forward scattering amplitude is approximated by:[12]

$$\mathrm{Re}(\vec{\varepsilon}_0 \cdot \vec{f}(\vec{k},\vec{k})) = k^2 a^3 \frac{\varepsilon - 1}{\varepsilon + 2}, \tag{3.9}$$

where a is the radius of the small particle, k is the propagation constant in the background medium (water), and $\varepsilon = (n_p^l/n_p^w)^2$ is the relative dielectric constant of the scatterer (latex beads) to the background medium (water). The effective phase index is thus given by:

$$n_p^e = n_p^w(1 + 3/2F\frac{\varepsilon - 1}{\varepsilon + 2}). \tag{3.10}$$

The group index n_g^e is given by:

$$\begin{aligned} n_g^e &= n_p^e - \lambda\frac{dn_p^e}{d\lambda}, \\ &= n_p^w(1 + 3/2F\frac{\varepsilon - 1}{\varepsilon + 2}) - \lambda\frac{dn_p^w}{d\lambda}(1 + 3/2F\frac{\varepsilon - 1}{\varepsilon + 2}) \\ &\quad - n_p^w\lambda\frac{d}{d\lambda}3/2F\frac{\varepsilon - 1}{\varepsilon + 2} \\ &= n_g^w(1 + 3/2F\frac{\varepsilon - 1}{\varepsilon + 2}) - n_p^w 3/2\frac{F}{(\varepsilon + 2)^2}\lambda\frac{d}{d\lambda}(3\varepsilon). \end{aligned} \tag{3.11}$$

The last derivative term is given by:

$$\begin{aligned} \lambda\frac{d\varepsilon}{d\lambda} &= \lambda\frac{d(n_p^l/n_p^w)^2}{d\lambda} = \lambda(\frac{2\varepsilon}{n_p^l}\frac{dn_p^l}{d\lambda} - \frac{2\varepsilon}{n_p^w}\frac{dn_p^w}{d\lambda}) \\ &= \frac{2\varepsilon}{n_p^l}(n_p^l - n_g^l) - \frac{2\varepsilon}{n_p^w}(n_p^w - n_g^w) = -\frac{2\varepsilon}{n_p^l}n_g^l + \frac{2\varepsilon}{n_p^w}n_g^w. \end{aligned} \tag{3.12}$$

Substituting eq. (3.12) into eq. (3.11), we have:

$$n_g^e = n_g^w(1 + 3/2F\frac{\varepsilon - 1}{\varepsilon + 2}) - n_p^w \frac{3/2F}{(\varepsilon + 2)^2} 6(\frac{\varepsilon}{n_p^w} n_g^w. - \frac{\varepsilon}{n_p^l} n_g^l)$$

$$= n_g^w + 3/2F\left\{(\frac{\varepsilon - 1}{\varepsilon + 2})n_g^w + \frac{6}{(\varepsilon + 2)^2}(\sqrt{\varepsilon} n_g^l - \varepsilon n_g^w)\right\}. \qquad (3.13)$$

The delay time arises from the scattering can then be derived for the media of thickness L under the small particle approximation as :

$$\Delta t = \frac{Ln_g^e}{c} - \frac{Ln_g^w}{c} = \frac{L}{c}(n_g^e - n_g^w)$$

$$= \frac{3LF}{2c}[\, n_g^w \frac{\varepsilon - 1}{\varepsilon + 2} + \frac{6}{(\varepsilon+2)^2}(\sqrt{\varepsilon} n_g^l - \varepsilon n_g^w)]. \qquad (3.14)$$

Eqs. (3.2) and (3.14) are used to compared with the experimental results. Note that there were no fitting parameters in either models.

A more familiar technique[11,12] which directly computes the amplitude and the phase of the scattered field from all scatterers on a thin slab to a point far in front of the slab also yields the same result as eq. (3.8). This method could not account for the effect of the multiple light scattering in the medium. In fact, eq. (3.8) is the first order approximation of the scattering problem.

3.3 Experimental Method

The schematic of the second harmonic cross correlation experimental setup is shown in Fig. 3.1. Ultrafast laser pulses were generated from a colliding pulse mode-locked dye laser of 100 *fsec*, pulse repetition rate 82 *MHz*, wavelength λ= 625 *nm*, bandwidth $\Delta\lambda$= 10 *nm*, power 10 *mW*, and beam diameter 4 *mm*. The

laser beam was split into two beams. One beam was allowed to pass through random scattering media. The other beam was allowed to travel through an optical delay line which was controlled by a stepping motor of 1 μm accuracy (6.7 fs). The transmitted pulse and the reference pulse were focused by a lens onto a KDP(KH_2PO_4) crystal where the second harmonic wave (312.5 nm) was generated. The generated SHG light was detected by a photomultiplier tube (PMT) with a narrow band pass filter (310±10 *nm*) placed in front of the PMT. The signal was detected by a lock-in amplifier system. The temporal profile of the ballistic component of the scattered pulses were determined in terms of the cross-correlation function between the transmitted and the reference pulses. This cross-correlation technique is commonly used to measure the pulse duration of the ultrashort laser pulses.

Certain phase matching conditions[13] must be satisfied between the transmitted pulse and the reference pulse in order to generate the SHG cross correlation function signal. The phase matching conditions requires the polarization of the two laser beam be the same and the propagation directions of the two beams be parallel. Thus, the SHG cross-correlation method measure the transmitted light which has same polarization and propagation direction as the reference laser light. The eraly arriving ballistic light will be measured by the SHG method because they retain all the properties of the incident laser beam except that its intensity is attenuated by the scattering. The polarization of late arriving diffuse photons are randomized and the diffuse photons travel in all directions because they experience multiple scatterings inside the scattering medium. So SHG method can not measure the late arriving diffuse portion of the transmitted pulse. Some of the early arriving portion of the diffuse light which arrive at the same time or just after the ballistic pulse satisfy the phase matching condition because they experience only few scatterings and are not totally randomized. The

SHG method can also measure these early arriving diffuse photons if the early arriving portion of the transmitted pulse is not dominated by the ballistic photons. In the case of the scattering medium consisting discrete scatterers, the early arriving portion of the transmitted pulse is dominated by the ballistic pulse.

The measured temporal profile $I^{2\omega}(\Delta t)$ is the cross-correlation function of the transmitted pulse $I_s^{\omega}(t)$ and the reference incident laser pulse $I_0^{\omega}(t)$:

$$I^{2\omega}(\Delta t) \sim \int dt' \; I_0^{\omega}(\Delta t + t') \cdot I_s^{\omega}(t'), \tag{3.15}$$

where Δt is the optical time delay between these two pulses. The delay time Δt can be varied by the optical delay line. Thus the temporal profile of the cross-correlation function can be measured and the scattered pulse profile can be obtained by deconvolution. The zero time was taken at the peak of the cross-correlation curve when there was no scatterer in the water medium. The full-width at half maxima of the cross-correlation function of the laser pulse was measured to be 145 fs as shown in curve (a) of Fig. 3.2 which corresponded laser pulse duration of about 100 fs.

The random scattering medium was the latex beads of diameter $0.091 \mu m$ suspended in water. Different concentration random media were prepared by adding different amount of commercially available 10% concentration latex beads suspended in water into the water, where the characteristic "optical scattering parameter" $N\sigma_s L$ of the sample was varied up to 27, where N is the number density of the scatterer, σ_s is the total scattering cross section of a scatterer which was computed from Mie theory, and L is the thickness of the media.

3.4 Results and Discussions

The coherent component of the 100 fs ultrashort laser pulse propagating through a scattering medium did not appear to be broadened, but its speed and intensity were substantially reduced. Curve (a) (solid curve) of Fig. 3.2 illustrates the cross-correlation intensity profile of ultrafast pulses passing through a 1 cm thick of water medium, whereas curves (b), (c), and (d) (broken curves) of Fig. 3.2 show cross-correlation intensity profile of the coherent component of the ultrafast pulses passing through a scattering medium of latex beads (diameter 0.09 μm) suspended in water with same thickness but with different scatterer volume concentration of 1.03%, 2.15%, and 2.56%, respectively. The salient feature of the curves displayed in this figure is that the pulse profile remains essentially unchanged but its time of arrival is delayed. The delay time is increased as the scatterer concentration is increased. The intensity at the peak of curve (c) was $2.0 \cdot 10^{-6}$ times of the peak of curve (a). This intensity value was much larger than the expected value of $e^{-N\sigma_s L} = 3.7 \cdot 10^{-9}$. This higher intensity value could be a result of reduced scattering in the present case that there were more than one scatterer in a volume of one cubic wavelength[8].

Fig. 3.3 shows the experimental results for a scattering medium of 5 cm thick, where curve (a) is the result for laser pulse passing through water medium without scatterers, curve (b) and (c) are the measured SHG profiles for laser pulse passing through scattering medium of scatterer volume concentration of 0.21% and 0.37%, respectively. Again, the ballistic pulse profiles are essentially unchanged but its arrival time is increasingly delayed as the scatterer concentration is increased.

The delay times of arrival of the coherent pulse were measured for various medium thicknesses L (1, 2, 5, and 12.5 cm) at a series of volume concentrations of the scatterers F. The results versus parameter $L \cdot F$ is plotted in Fig. 3.4.

Squares, pluses, triangles and circles were experimental data measured from random media of different thicknesses. The delay time is found to be linearly proportional to the volume concentration of the latex beads and to the thickness of the media.

The delay time predicted from eq. (3.2) is plotted by the dash line in Fig. 3.4, which is in excellent agreement with the measured delay time. The most likely reason for this good agreement is that the size of the scatterer is smaller than the wavelength of light in the water, so that the light wave would see the scattering medium as a medium with an effective average index of the scatterer and water which is similar to mixing two kinds of liquids. It is important to note that the group index of refraction must be used in this model in order to fit the experimental data.

The delay time predicted by eq. (3.14) is plotted by the solid line in Fig. 3.4, which is a slightly smaller than the experimental data but within our experimental error.

In our case, ka is not much smaller than 1, so making correction to the small particle approximation taken in computing the forward scattering amplitude in eq. (3.8) would improve the agreement of Lax's theory with the experimental results because higher order terms give about 3.5% larger value of the forward scattering amplitude. A more detail calculation of the factor r would also improve the agreement of Lax's theory with the experimental results especially in the case of high concentration where the correlation between the scatterers are important.

3.5 Conclusion

The temporal profiles of the coherent component of 100 *fsec* laser pulses propagating through random scattering medium were found to be remained essentially unchanged while its speed was found to be substantially reduced. The time delay of arrival was found to be linearly proportional to the thickness of the media and the concentration of the scatterers in the scattering media over the range of "optical scattering parameter" $N\sigma_s L$ of less than 27. The delay time of arrival of the coherent component can be explained either by the simple theory in which the effective refractive index is the volume fraction combination of the refractive indices of the individual substances, or by the theory of the coherent interference of the scattered waves and the primary wave.

References

1 M. Lax, Rev. Mod. Phys. **23,** 287 (1951).

2 K. M. Yoo and R. R. Alfano, Opt. Lett. **15,** 320 (1990).

3 G. H. Watson, P. A. Fleury and S. L. McCall, Phys. Rev. Lett. **58,** 945(1987).

4 J. M. Drake and A. Z. Genack, Phys. Rev. Lett. **63,** 259(1989).

5 K. M. Yoo, Feng Liu and R. R. Alfano, Phys. Rev. Lett. **64,** 2647(1990).

6 A. Z. Genack and J. M. Drake, Europhys. Lett. **11,** 331(1990).

7 Ping Sheng ed., *Scattering and Localization of Classical Waves in Random Media,* (World Scientific, Singapore, 1990).

8 P. M. Saulnier, M. P. Zinkin, and G. H. Watson, Phys. Rev. **42,** 2621(1990).

9 M. Lax, Phys. Rev. **85**, 621 (1952).

10 M. Born and E. Wolf, *Principles of Optics,* 4th Edition, (Pergamon, New York, 1970), Pg. 633-664. See also the following two references.

11 H. C. van de Hulst, *Light Scattering by Small Particles*, (Dover, New York, 1981), Chap. 4, 6, and 10.

12 J. D. Jackson, *Classical Electrodynamics*, 2nd Edition, (Wiley, New York, 1975), Pg. 453-459.

13 A. Yariv, *Optical Electronics,* 3rd Edition, (Holt, New York, 1985), Pg. 236-246.

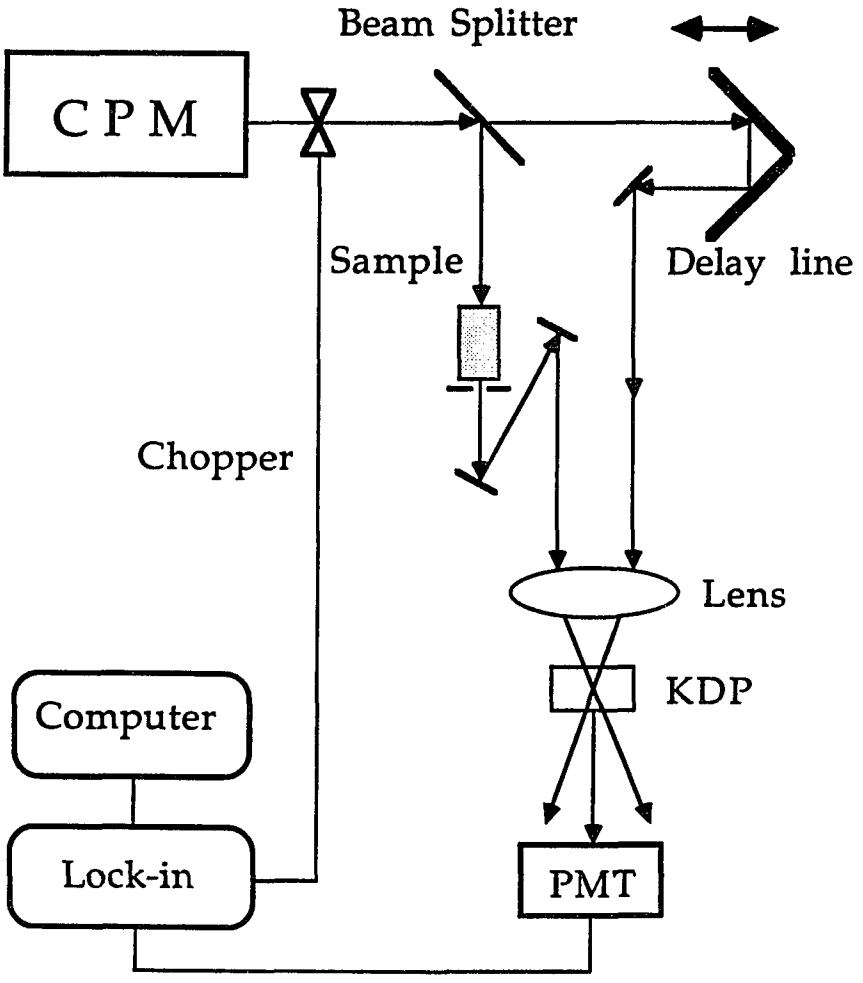

Fig.3.1 Schematic diagram of the experimental setup.

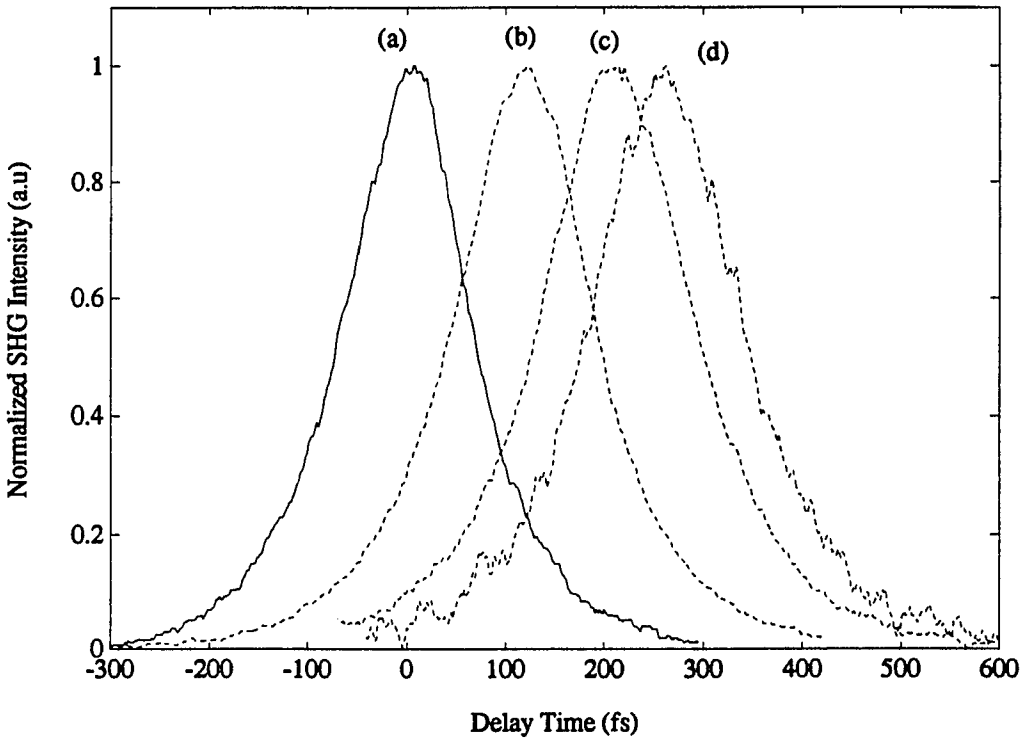

Fig.3.2 Normalized cross correlation intensity profile of the laser pulses when one beam passes through 1 cm thick medium of: (a) water; (b) 1.03% of; (c)2.15% of; and (d)2.56% of .091 μm diameter latex beads suspended in water. The arrival time of the laser pulse was taken at the peak of the curve.

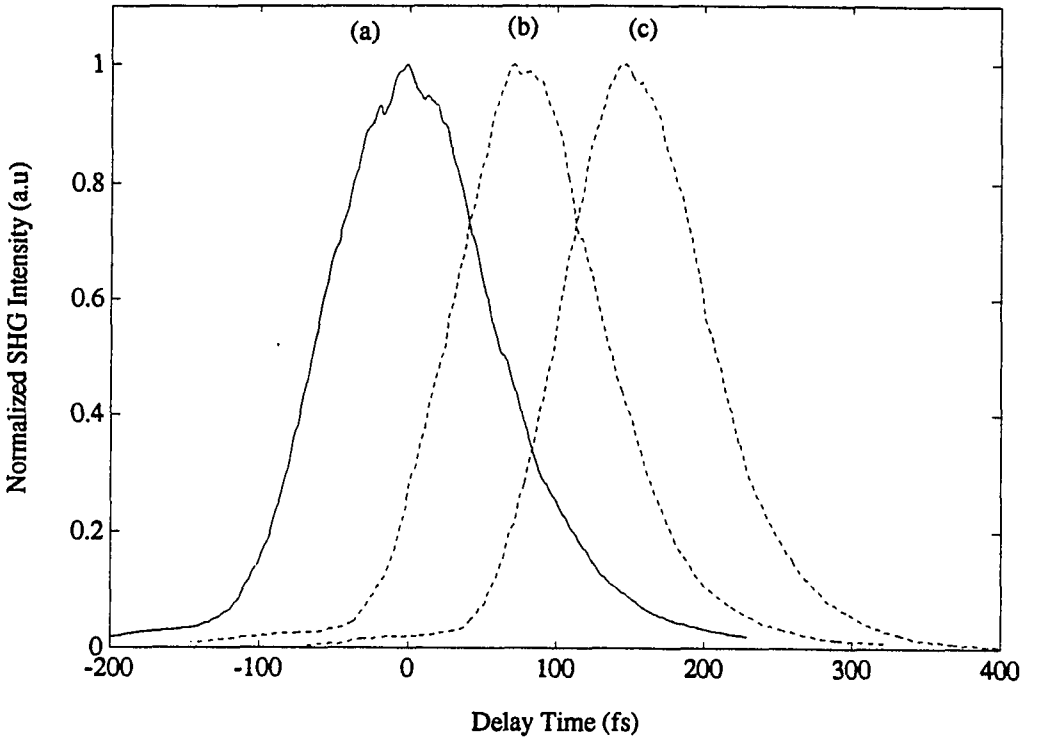

Fig.3.3 Normalized cross correlation intensity profile of the laser pulses when one beam passes through 5 cm thick medium of: (a) water; (b) 0.21% of; and (c) 0.37% of .091 μm diameter latex beads suspended in water. The arrival time of the laser pulse was taken at the peak of the curve.

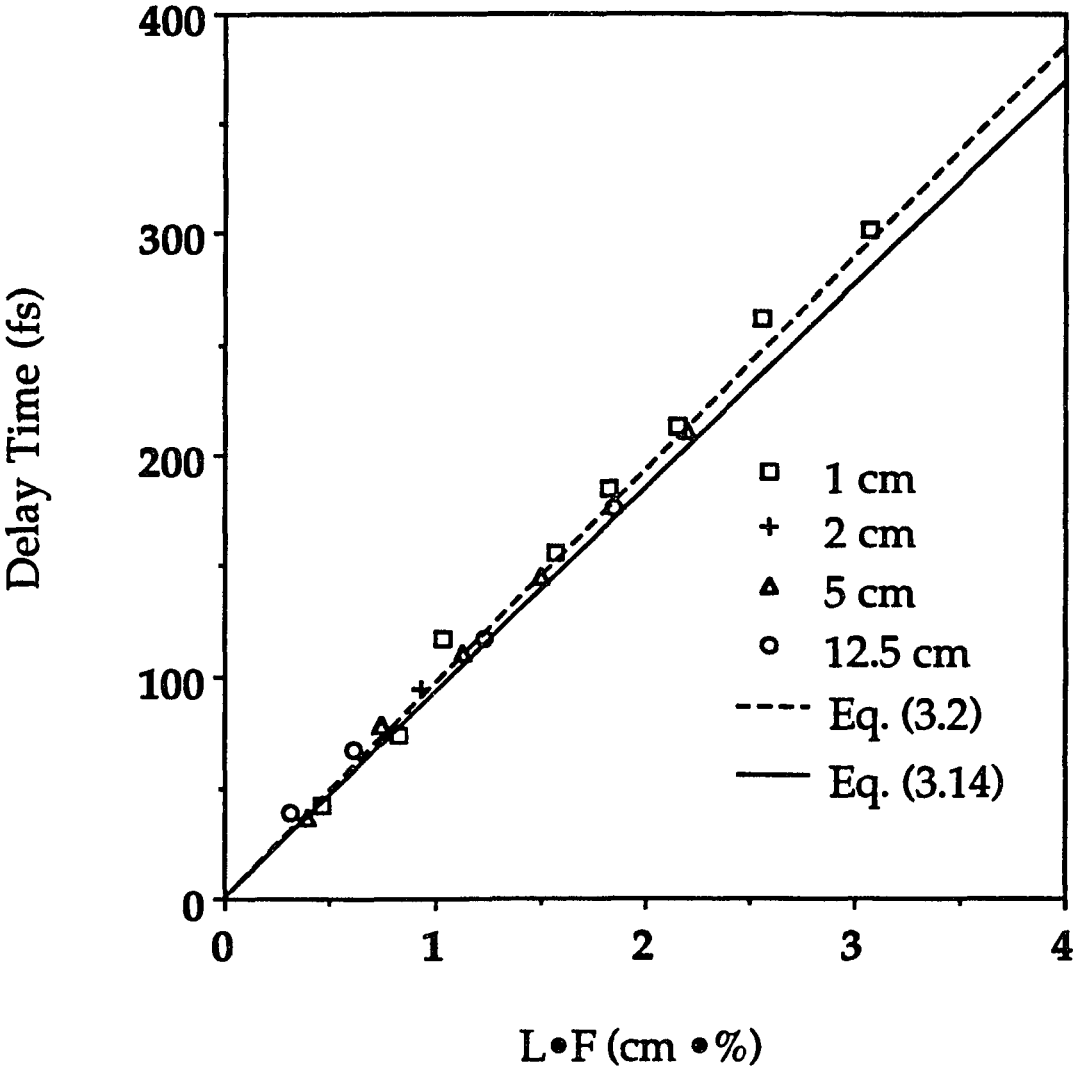

Fig.3.4 Plot of delay time of arrival of ultrafast laser pulse passing through random scattering medium versus $L \cdot F$, where L is the thickness of the sample, and F is the volume fraction of the latex beads in the sample.

Chapter 4

Pulse transmission and imaging through biological tissues

4.1 Introduction

Recently, there has been considerable interest to investigate ultrashort laser pulse propagation and light scattering in biological materials and discrete random media,[1-7] and to image hidden objects in random scattering media.[8-17] This effort has been motivated principally by the potential of developing light based diagnostic and imaging techniques for the medical community. The propagation of light in random scattering media is best studied using ultrashort laser pulses and ultrafast detection technology. Ultrashort laser pulses traversing through discrete scattering media have been shown to split into a **ballistic** (coherent) and a **diffuse** (incoherent) components.[4] The **ballistic** component arises from the coherent interference between the scattered waves and the primary wave. It propagates through the random medium undeviated in the forward direction with a pulse profile remaining essentially unchanged. The speed of the ballistic component of the 100 fs ultrashort laser pulses transmission through discrete scattering medium has been found to be reduced by scattering or the effective group index of the scattering medium.[18] The **diffuse** component undergoes multiple scattering and travels in all directions. The ballistic pulse forms the image (shadow) of an opaque object while the diffuse component contributes a bright background which will wash out the shadow if the random medium is sufficiently strong in scattering. The early portion of diffuse component consists of photons which have undergone a few scatterings in forward direction and traveled

through medium along some zig zag paths in the vicinity of the forward direction. These early arriving photons, hitherto referred to as **snake photons**, have been shown to retain some image information.[13, 17] The ballistic pulse is of particular interest because the spatial resolution of the image formed by it is of submillimeter scale and is limited by light diffraction. There have been several studies using ultrafast laser and time-resolved detection techniques to probe the optical properties of biomedical tissues.[6,7,19,20] However, previous transmission experiments through tissue were performed using thick tissues so that the ballistic component may be too weak to be observed, and the reflectance experiments were performed in a geometry that no ballistic component could be observed. Thus, the question whether a true distinct ballistic component exists for a light pulse transmitted through biomedical tissue remains an open issue.

In this Chapter, the temporal profile of 100 fs laser pulses transmitted through relatively thin biological tissues were measured using fs second harmonic cross-correlation (SHG) and ps synchroscan streak camera detection methods. No clear **distinct ballistic pulse** was observed upon passing through the tissues, unlike the case of a pulse transmitting through a random medium of discrete scatterers where the ballistic pulse was clearly observed.[4] The 100 fs pulse transmitted through biological tissues was found to be significantly broadened to 8 ps as the thickness of the tissue was increased to 7 mm. In a discrete random medium, the ballistic pulse remains undistorted-retaining its pulse profile. By detecting only the early portion of the transmitted pulse using SHG cross-correlation method, an opaque object hidden inside a thick tissue of 6.5 mm was imaged with submillimeter spatial resolution

4.2 Experimental Methods

The details of the experimental setups, SHG cross-correlation[11, 18] and synchroscan streak camera[21] detection techniques have been described previously in Chapter 3 and Chapter 2, respectively. Ultrafast laser pulses of 100 fs duration were generated from a colliding pulse mode-locked (CPM) dye laser system with a pulse repetition rate of 82 MHz, average power of 10 mW, and a wavelength centered at 625 nm. A part of the CPM beam were amplified by a copper-vapor laser (CVL) pumped amplifier system to 5 mW average power at a pulse repetition rate of 6.5 kHz. The amplified laser pulses were used in the SHG cross-correlation measurements and the laser pulses generated directly from the CPM laser were used in the streak camera measurements. In the SHG experiment, the laser beam was split into a signal beam and a reference beam. The signal beam was focused by a long focal lens (500 mm) to a narrow beam (diameter about 0.1 mm) incident on the tissue samples. The cross-correlation of the transmitted pulse and the reference pulse was obtained by focusing these two pulses into a KDP crystal where the second harmonic light generated was detected by a photomultiplier tube and a lock-in amplifier system. The reference pulse was scanned at various delay times with respect to the transmitted pulse in order to obtain the temporal profile of the transmitted pulse. The SHG cross-correlation technique can measure the early arriving photons of the transmitted pulse with time resolution on the fs time scale. In the streak camera measurement, CPM laser pulse was incident on a slab of tissue. The transmitted light through a small pinhole was collected by a lens and detected by a Hamamatsu synchroscan streak camera. The synchroscan streak camera measures the total temporal profile of the pulse transmitted through a random scattering medium which contains both the early arriving and later arriving photons with typical time resolution of 10 ps.

4.3 Results and Discussion

The SHG temporal profile of the transmitted pulse through slabs of chicken breast tissue of various thicknesses are shown in Figs. 4.1 and 4.2 on expanded and contracted time scales, respectively. Curve (a) in Fig. 4.1 shows the temporal profile of cross-correlation of the incident laser pulse. The FWHM of the cross-correlation function is found to be about 140 fs which corresponds to the incident laser pulse width of 100 fs. Curve (b) of Fig. 4.1 demonstrates the salient features of the transmitted pulse profile through the tissues of thickness 1.8 mm. Curves (a) and (b) of Fig. 4.2 show the curves of Fig. 4.1 on a contracted time scale. Curves (c) and (d) of Fig. 4.2 demonstrate the temporal profiles of the transmitted pulses through tissues of thickness 4.5 and 7.0 mm, respectively. The arrival time of the transmitted pulse is increasingly delayed as the tissue thickness is increased. The temporal profiles of the transmitted pulse through tissues are significantly broadened. The transmitted pulse becomes broader as the thickness of the tissue increases. For 7 mm thick tissue, the transmitted pulse is broadened to about 8 ps. The temporal profiles are not symmetrical, consisting of a fast rise and a slow decaying component. The profile of the transmitted pulse through tissues is much different from the one transmitted through discrete scattering medium (latex beads in water) where two distinct components of the transmitted pulse are observed: a ballistic and a diffuse component.[4] The principal reason for the absence of a clear distinct ballistic pulse may be due to the structure of biological tissues. The dielectric constant of tissue shows both discrete step and continuous random variation in space. Due to the continuous variation of the dielectric constant in biological tissue, the photons not only will be discretely scattered, but also will be bent continuously in a zig-zag pattern following the least optical path. Thus, the early arriving portion of the transmitted pulse

through tissue does not include a distinct ballistic pulse component which traveled through tissue undeviated, instead it consists of photons traveled through the tissue in various small zig zag paths. The continuous distribution of path lengths of the early arriving photon gives rise to a broadened early part of transmitted pulse. The early portion of the transmitted photons will be referred to as the snake photons since these photons traverse through the tissue along small zig zag paths in the vicinity of straight transmission.

As shown in Figs. 4.1 and 4.2, the arrival time of the transmitted pulse was delayed. The delay time increased as the thickness of the tissue increased. The delay time at the peak of the transmitted pulse measured using SHG cross-correlation method was plotted against the tissue thickness in Fig. 4.3. For thin tissues, the delay time depends linearly on the thickness of the tissue up to 6 mm. For thicker tissues, the delay time exceeds linear dependence due to the fact that photons undergo multiple scattering while traversing through the tissue. The linear dependence between the delay time Δt and the sample thickness L can described by an effective group index n_g of the tissue through relation $\Delta t = \frac{L}{c}(n_g - 1)$, where c is the velocity of light in the vacuum. The measured data was fitted by this relation using a standard least square fitting program we used in Chapter 2. An effective group index of 1.49 ± 0.02 for chicken breast tissue at 625 nm is obtained. The best fit is shown by the solid line in Fig. 4.3.

The transmitted pulse profiles through thick biological tissues have to be measured by synchroscan streak camera. The salient feature of the transmitted pulses through tissues of increasing thickness are shown in Fig. 4.4. The 100 fs incident laser pulse measured by the streak camera is presented by Curve (a) in Fig. 4.4. The

FWHM of the measured laser pulse is about 8 ps which is the time response of the streak camera system. Curves (b), (c), (d), and (e) of Fig. 4.4 show the temporal profiles of the transmitted pulse through samples of thickness 1.8, 7.0, 9.0, and 12.0 mm, respectively. The transmitted pulse becomes broader as the thickness of the tissue increases. Again, no distinct ballistic pulse component is observed. The early portion of the transmitted pulse contains the snake photons as depicted in Figs. 4.1 and 4.2. The long tail portion arrives much later in time corresponds to the diffuse component of the transmitted pulse in which the photons have undergone random walks in the tissue.

In Fig. 4.5(a), the measured transmitted pulse profiles by using the SHG and the streak camera methods are displayed on the same graph for a comparison as the solid and the broken curves, respectively. The arriving time of the SHG profile was shifted to match the peaks of the intensity of the measured profiles at the zero time. It is clearly that the pulse profile measured by the streak camera is quite different from the SHG profile. This difference is because the time response of the streak camera is 8 ps which broadened the measured pulse profile. The measured SHG profile was convoluted with a 8 ps Guassian response function and displayed in Fig. 4.5(b) along with the streak camera profile. The early arriving portion($\pm$10 ps) of those two temporal profiles are not very different indicating that SHG method measures the early arriving photons. The profiles deviate from each other at later times. The streak camera profile shows a long tail part, while the SHG profile has no signal beyond 25 ps from the peak. This may indicate that most of photons lost coherence after they migrated inside the tissue 25 ps longer than the early arriving photons. This phenomena needs to be further investigated.

These temporal profiles of the transmitted pulse through tissues measured either by SHG cross-correlation or by streak camera method can not be described well by the diffusion theory. The reason for the poor fitting is that in these experiments the thickness of the tissues are only about or smaller than 5 times the transport mean free path. The diffusion theory describes the transport of the photons in random scattering medium well when the thickness of the medium is about 10 or more times the transport mean free path.[21]

The transport mean free path and absorption length for chicken breast tissue were obtained to be 2.5 ± 0.5 mm and 60 ± 30 mm at 625 nm, respectively, by measuring the transmitted pulse profiles through thicker tissues and fitting the temporal profiles using diffusion theory.

These optical parameters are close to those given in Ref. 6. Assuming asymmetric scattering parameter g=0.9, the scattering length is computed to be 0.25 mm. Assuming the attenuation of the ballistic light follows Beer's exponential decay law, the intensity of ballistic light would be reduced by a factor of $7.5 \cdot 10^{-4}$ for the case of 1.8 mm thick tissue. The measured SHG peak intensity was found to be attenuated by a factor of $7.7 \cdot 10^{-6}$. The total integrated intensity of the transmitted pulse is reduced by a factor of $1.9 \cdot 10^{-5}$. Thus, the ballistic light would be observed, if presence, for the 1.8 mm thick tissue, because the expected ballistic intensity is 30 times larger than the actual measured transmitted pulse intensity. In discrete random medium with comparable optical parameters and larger thickness, a distinct ballistic component was clearly observed along with a diffuse component using streak camera detection method.[4,9]

Although no distinct ballistic pulse is present, we can still demonstrate that the early arriving snake photons can still be used to image an object hidden in a biological tissue. A bar code acting as an opaque object was sandwiched between two chicken breast tissues of total thickness of 6.5 mm (2.5 mm in front of and 4 mm in the back of the bar code). The bar code used consisted of two clear and one dark segment, the width of each is about 1.8 mm. The tissue sandwich was placed on a translational stage which was scanned perpendicularly to the laser beam. The profile of the transmitted pulse at early time is obtained by fs SHG cross-correlation technique. By fixing the delay time and scanning the object (no tissues) along a direction perpendicular to the laser beam, an one dimensional image of the object is obtained and is shown in Fig. 4.6(a). The plateaus and valleys in these intensity plots correspond to the clear and dark regions of the bar code, respectively. The intensity variation at the plateaus are caused by the fluctuation of laser pulses during the scan. Curve (b) of Fig. 4.6 shows the one dimensional image of the object hidden inside the tissues. The delay time was set at the rising peak (delay time 9.8 ps) of temporal profile of the snake component. Curve (c) of Fig. 4.6 shows the image at the delay time set at 14.5 ps about 4.7 ps later than the case of curve (b). The image resolution was on submillimeter scale. The image quality of curve (c) is worse than curve (b). This indicates that the earlier arriving photons are used for imaging the better the quality of image will be. The image quality for both curve (b) and (c) was not severely degraded. The other likely reasons for the distortion of the image was that the tissues were inhomogeneous and were not cut smooth enough. These results are consistent with recent work of Wang et. al[13] using a laser pulse of wider duration and a poorer time response detection system.

Biomedical imaging system requires snake photons to transmit through much thicker tissues in the order of 50 mm thick. This report shows the usefulness of the early arriving snake photons for imaging through tissues. There are many ways to increase the detectability of the early arriving photons such as: increasing laser power and pulse repetition rate, using better detectors (cooled CCD), using infrared lasers (fs Forsterite), and using other time gating methods (Kerr gate). It is still a great scientific and engineering challenge to develop a practical non-ionizing biomedical imaging system.

4.4 Conclusion

The temporal profile for 100 fs laser pulse transmitted through biological tissues was measured using both fs and ps time-resolved detection methods. No distinct ballistic component of the transmitted pulses with a profile of incident pulse through tissues was observed. The transmitted pulse was increasingly broadened as the thickness of the tissue was increased. The effective group refractive index can be determined from the delay time of arrival of the transmitted pulse through thin tissues of thickness less than 6 mm. The early arriving or snake photons was shown to carry enough information to image an opaque object embedded inside a tissue of 6.5 mm thick with spatial resolution on submillimeter scale.

References

1 M. Lax, V. Nayaramamurti, and R. C. Fulton, " Classical diffusive photon transport in a slab," in *Proceedings of the Symposium on Laser Optics of Condensed Matter, Leningrad, June 1987*, edited by J. L. Birman, H. Z. Cummins and A. A. Kaplyanskii (Plenum, New York, 1987), pp229-235.

2 G. H. Watson, Jr., P. A. Fleury, and S. L. McCall, Phys. Rev. Lett. **58**, 945-948(1987).

3 P. Sheng ed., *Scattering and Localization of Classical Waves in Random Medium*, (World Scientific, Singapore, 1990).

4 K. M. Yoo, and R. R. Alfano, Opt. Lett. **15**, 320-322(1990).

5 L. Goldman ed., *Laser Non-Surgical Medicine- New Challenges for An Old Application*, (Technomic, Lancaster, 1991)

6 W. F. Cheong, S. A. Prahl and A. J. Welsh, IEEE J. Quantum Elect. **26**, 2166-2185(1990).

7 B. C. Wilson and S. L. Jacques, IEEE J. Quantum Elect. **26**, 2186-2199(1990).

8 J. C. Dainty ed., *Laser Speckle and Related Phenomena*, (Springer-Verlag, Berlin, 1975), pp203-278.

9 K. M. Yoo, Feng Liu, and R. R. Alfano, Opt. Lett. **16**, 1068-1070(1991).

10 K. M. Yoo, Z. W. Zang, S. A. Ahmed, and R. R. Alfano, Opt. Lett. **16**, 1252-1254(1991).

11 K. M. Yoo, Qirong Xing, and R. R. Alfano, Opt. Lett. **16**, 1019-1021(1991).

12 P. P. Ho, P. Baldeck, K. S. Wong, K. M. Yoo, D. Lee, and R. R. Alfano, Appl. Opt. **28**, 2304-2310(1989).

13 L. M. Wang, P. P. Ho, C. Liu, G. Zhang, and R. R. Alfano, Science **253**, 769-771(1991).

14 S. Andersson-Engels, R. Berg, S. Svanberg, and O. Jarlman, Opt. Lett. **15**, 1179-1181(1990).

15 H. Chen, Y. Chen, D. Dilworth, E. Leith, J. Lopez, and J. Valdmanis, Opt. Lett. **16**, 487-489(1991).

16 J. C. Hebden, R. A. Kruger, and K. S. Wong, Appl. Opt. **30**, 788-794(1991).

17 K. M. Yoo, B. B. Das, and R. R. Alfano, Opt. Lett. **17**, 958-960(1992).

18 Feng Liu, K. M. Yoo, and R. R. Alfano, Opt. Lett. **16**, 351-353(1991).

19 M. S. Patterson, B. Chance, and B. C. Wilson, Appl. Opt. **28**, 2331-2336(1989).

20 D. T. Delpy, M. Cope, P. van der Zee, S. Arridge, Susan Wary, and J. Wyatt, Phys. Med. Biol. **33**, 1433-1442(1988).

21 K. M. Yoo, Feng Liu, and R. R. Alfano, Phys. Rev. Lett. **64**, 2647-2650(1990); errata, **65**, 2210-2211(1990).

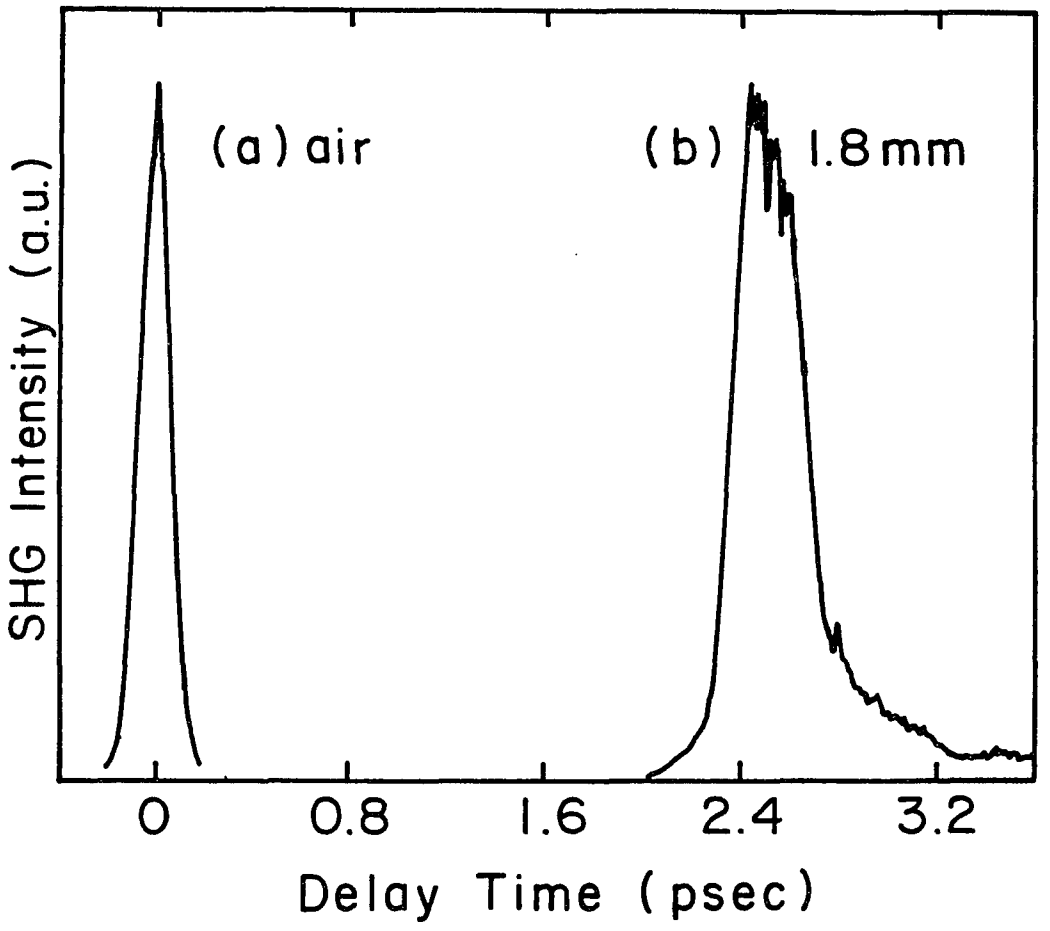

Fig.4.1 Normalized temporal profile measured by second harmonic cross-correlation of 100 fs ultrafast laser pulse transmitted through (a)air, and (b) 1.8 mm. The intensity at the peak of curve (b) is $7.7 \cdot 10^{-6}$ times of the peak intensity of curve (a). The zero time is set at the arrival time of the pulse transmitted through air.

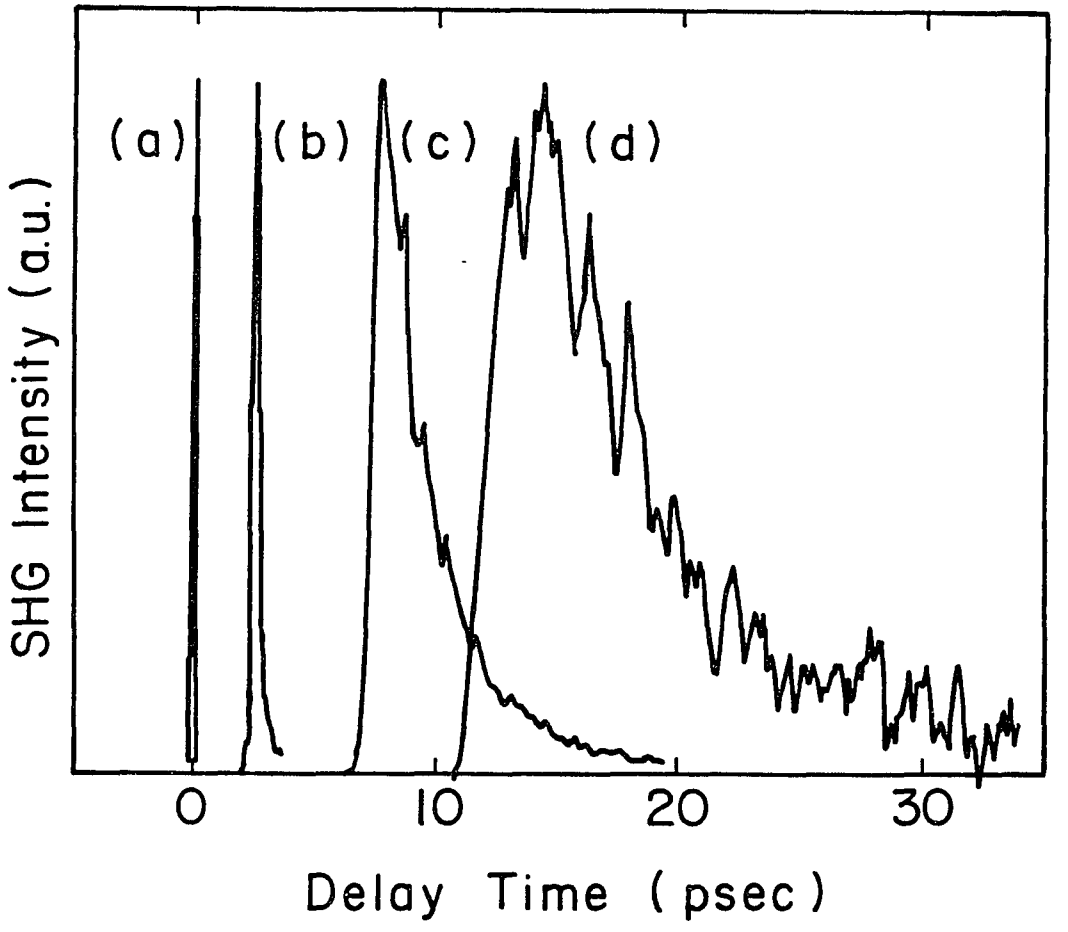

Fig.4.2 Normalized temporal profile plotted on a contracted time scale measured by second harmonic cross-correlation of 100 fs ultrafast laser pulse transmitted through (a)air, and (b) 1.8 mm, (c) 4.5 mm, and (d) 7.0 mm thick tissue. The peak intensity were of $7.7 \cdot 10^{-6}$, $1.2 \cdot 10^{-7}$, and $9.6 \cdot 10^{-9}$ times of the peak intensity of curve (a) for curve (b), (c), and (d), respectively.

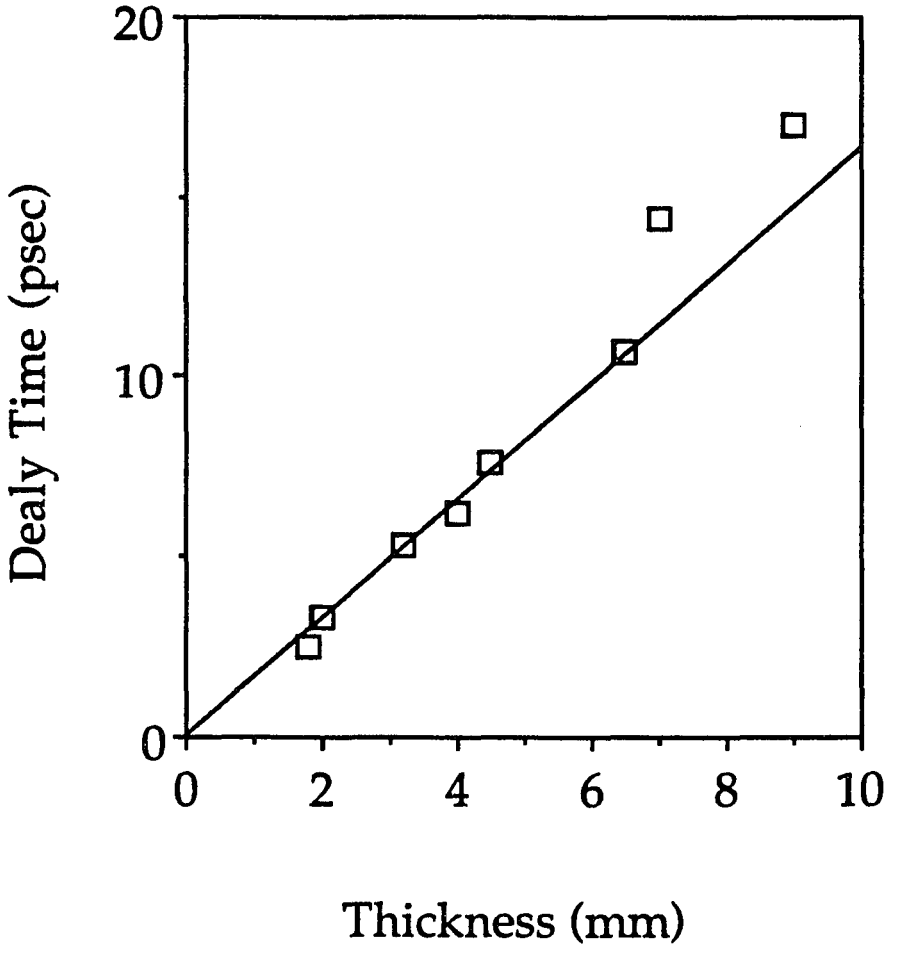

Fig.4.3 Plot of the delay time of arrival at the peak of a ultrafast laser pulse transmitted through tissues versus the thickness of the tissues. Experimental results are plotted by squares. The solid line is the best linear fit which the effective group index n_g = 1.49.

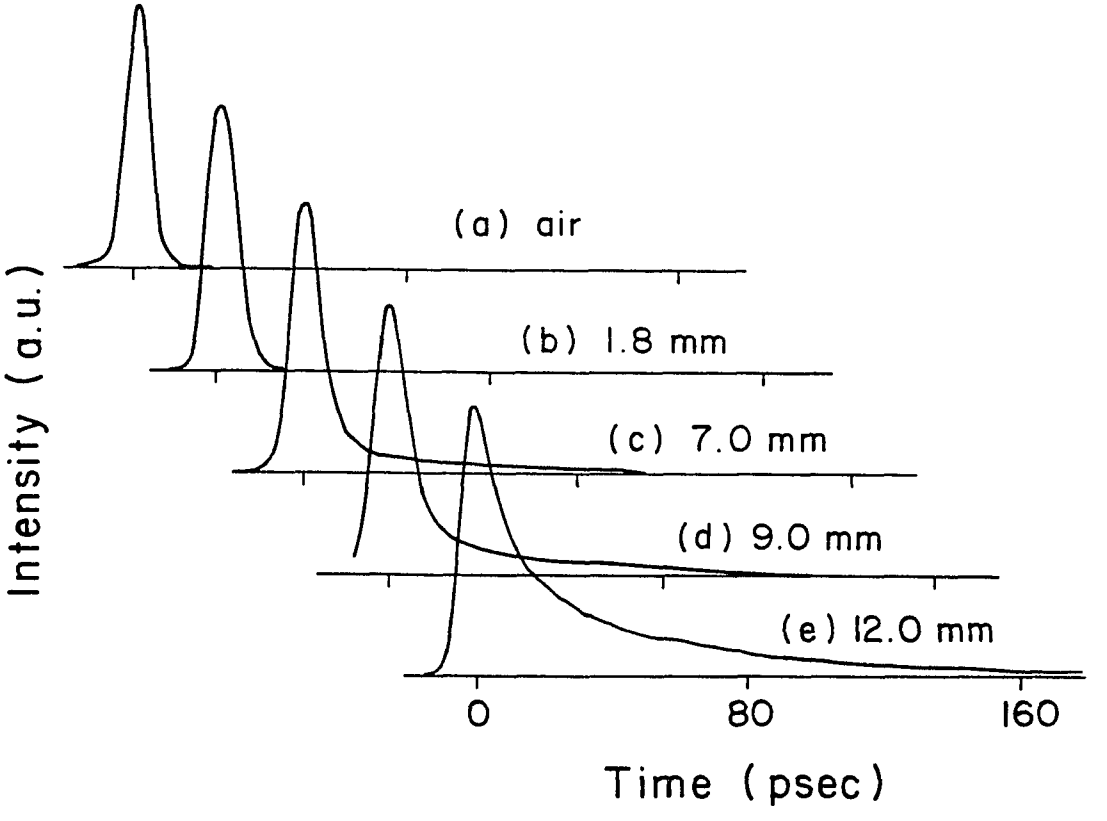

Fig.4.4 Normalized temporal profile measured by streak camera of 100 fs ultrafast laser pulse transmitted through (a) air, and (b) 1.8 mm, (c) 7.0 mm, (d)9.0 mm, and (e)12.0 mm thick tissues. The zero time was selected at the peak of the transmitted pulse.

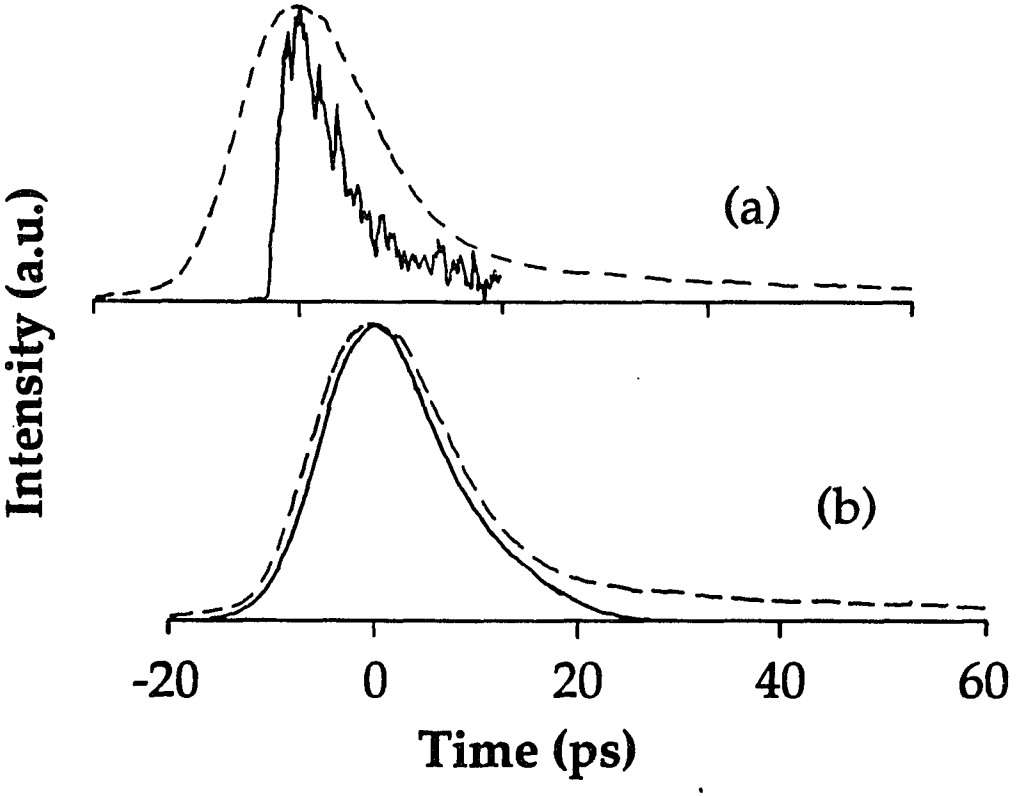

Fig.4.5 Normalized temporal profile of the transmitted pulse through 7 mm thick tissue measured by the SHG (solid curve) and the streak camera methods. (a)SHG profile unconvoluted, and (b)SHG profile convoluted with a 8 ps Gaussian response function.

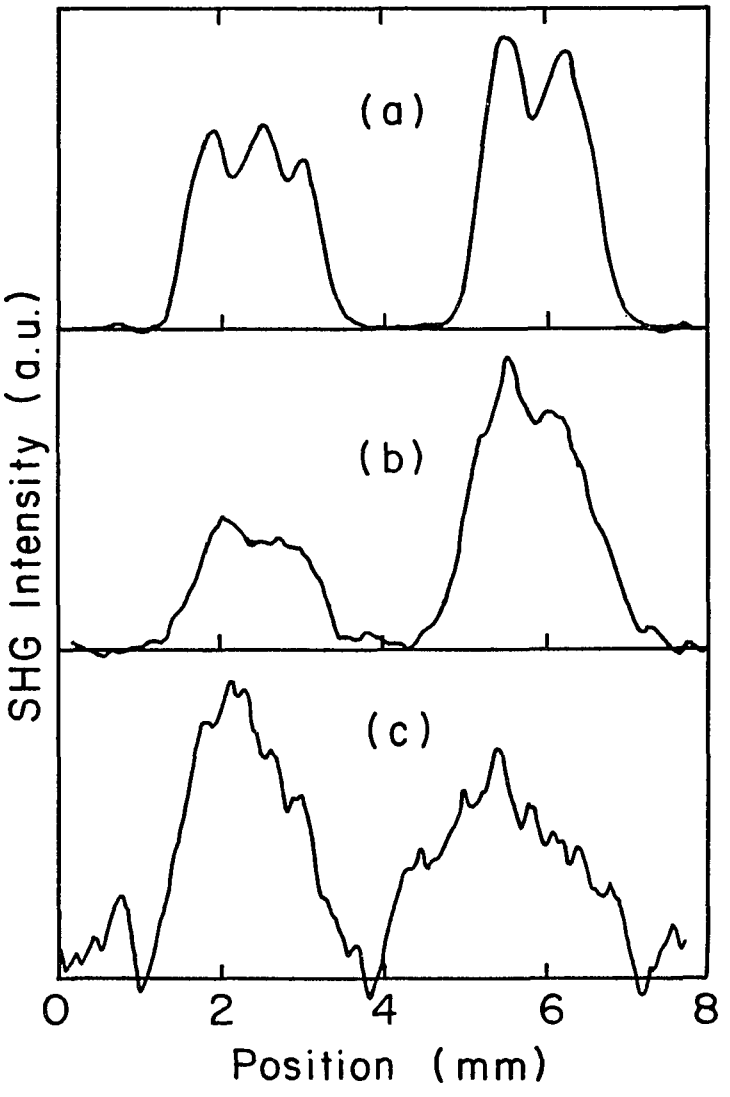

Fig.4.6 One dimensional images of a bar code measured by SHG cross-correlation technique at various time delays located (a) in air with zero time delay, (b) in 6.5 mm thick tissue with delay time set at 9.8 ps, (c) in 6.5 mm thick tissue with delay time set at 14.5 ps.

Chapter 5

Attenuation of transmitted photon intensity at various time intervals through uncompressed and compressed biological tissues

5.1 Introduction

Recently, various time-resolved methods have been introduced for imaging objects hidden in random media for potential prompt breast tumor detection.[1-7] The basis of time-resolved imaging techniques is that only the early arriving photons of the transmitted laser pulse is detected to view the image (shadow) of the object. While the later arriving photons which contribute noise are eliminated by time-resolved detection. The early arriving photons of ultrashort laser pulses transmission through an optically thin random medium of discrete scatterers is dominated by the ballistic component.[8] The propagation direction and the temporal profile of the ballistic photon remain unchanged while its intensity is reduced by a factor of e^{-w/l_s}, where w and l_s are the thickness and the scattering mean free path of the medium,[9] respectively. However, in a continuous random media such as a biological tissue, the ballistic component is absent and the early arriving portion of the transmitted pulse is dominated by snake photons. The snake photon is dominant in biological tissues because large scatterers present in tissues scatter the light mainly in the forward direction. These snake photons traverse through the medium along small zig zag paths slightly away from the straight line across the medium. Since snake photons traverse through the medium almost in a straight line, they carry the information of the scattering characteristics along this quasi-straight line path. The change in the

snake photon intensity can be used to detect the presence of a hidden object as shown in Chapter 4. The zig zag trajectories of the snake photons reduce the spatial resolution of the shadow of an object. The earlier arriving snake photons correspond to the smaller zig zag trajectories and are expected to give a better spatial resolution shadow. Unfortunately, the intensity of the earlier arriving photons is correspondingly lower.

In this Chapter, we present experimental studies on the intensity attenuation of the transmitted snake photons at various time intervals as the thickness of the biological tissue increases. Compression of tissues is shown to significantly make the photons to arrive earlier but the key optical properties of the tissue remain essentially unchanged.

5.2 Theory

A direct method to probe the transport of photons in a random scattering medium is to measure the distribution of photon arrival in the time domain; that is the temporal profile of the transmitted ultrafast laser pulse. When ultrafast laser pulse is incident normally at a point on a slab of random scattering medium with thickness w and transport mean free path l_t with $w/l_t \gg 1$, the temporal profile of transmitted photons at a circular pinhole of diameter a on the opposite side of the slab is predicted by the diffusion theory as[10]

$$I_z(t) = F\frac{D}{\pi w^2}[1 - \exp(-a^2/Dt)]$$

$$\cdot \sum_{m=1}^{\infty} m(\frac{\pi w}{d})^2 \sin\frac{m\pi w}{d}\cdot\exp(-Dt(m\frac{\pi}{d})^2)\cdot\exp(-\frac{vt}{l_a}), \qquad (5.1)$$

where $D = vl_t/3$ is the diffusion coefficient, $d = w + 2z_0$, $z_0 = 0.71l_t$ is the

extrapolation length, v is the speed of photons travel in the medium, l_a is the absorption length of the medium, and F is the collection factor which depends on the detection system. Eq. (5.1) is obtained by integrating eq. (2.6) over a small circular area of diameter a. The photon velocity, $v = \frac{c}{n_g}$, where n_g is the group index. We used the value $n_g = 1.49$ obtained in Chapter 4 in the computation. By fitting the experimental transmitted pulse profile with eq. (5.1) up to a collection normalization factor using the nonlinear least square numerical fitting program, two characteristic optical parameters, l_t and l_a, of biological tissues can be obtained.

As an illustration (the collection factor F is set to 1 in the following theoretical computations), the temporal profiles of the transmitted pulse are computed and displayed in a semilog plot Fig. 5.1 for $l_t = 2$ mm, $l_a = 100$ mm, diameter $a = 1$ mm, and different medium thickness $w = 5$, 10, 20, 40, 60, and 80 mm. The number of input photons is one. Thus, the intensity scale of the following theoretical plots is the attenuation factor of the intensity of the transmitted photons. The optical parameters l_t and l_a used in this case are close to that of tissues we used for the experiment in this study. As the thickness of the medium increases, the temporal profile of the transmitted pulse is broadened increasingly, its intensity decreases, and the arrival time of the peak intensity is delay more. Fig. 5.2 shows the transmitted pulse profiles for fixed medium thickness (60 mm) and different $l_t = 30$, 10, 6, 3, and 2 mm. Again as the l_t decreases, the transmitted pulse profile is broadened, its intensity decreases, and its peak intensity time is delayed. This indicates that as w/l_t increases, the transmitted pulse is broadened and its intensity is reduced significantly.

The temporal profiles for a fixed w/l_t value of 30 and different thickness and transport mean free path are shown in Fig. 5.3. The thickness and l_t are (a)15 and

0.5 mm, (b)30 and 1 mm, and (c)60 and 2 mm for curves (a), (b), and (c), respectively. The absorption length is 100 mm. This series of curves also show that as the medium thickness increases the transmitted pulse is delayed and broadened more. The intensity is decreased as the thickness increases. The peak intensity of curve (b) and (c) are enlarged by a factor of 17.2 and 515 as indicated in Fig. 5.3.

From these three illustrations, we see that as the medium thickness increases or the transport mean free path of the medium decreases, the transmitted pulse arrives later; the pulse profile is broadened more; and peak intensity decreases.

The integrated intensity $I(\Delta t)$ of the transmitted within a time interval of t_b to $t_b + \Delta t$ is obtained by integrating the transmitted pulse profile over the time interval:

$$I(\Delta t) = \int_{t_b}^{t_b+\Delta t} I_z(t)dt \ . \tag{5.2}$$

The time t_b is the ballistic time which is the least time photons take to traverse through the medium, $t_b = n_g w/c$. The solid curves of Fig. 5.4 show the integrated intensities of different Δt (10, 20, 50, 100, 200, 500, and 2000 ps from lowest curve up) against the thickness of the medium. In this case, l_t = 2 mm and l_a =100 mm. For thin medium, the integrated intensities do not depend on the time interval because the transmitted pulse is not broadened significantly. As the thickness of the medium increases, the transmitted pulse is broadened, the integrated intensity decays exponentially, the intensity within smaller time interval decays quicker with a larger exponent. The two broken curves in Fig. 5.4 are the expected ballistic intensity (computed using eq. (2.13)) for different mean cosine factor g = 0.9, and 0.6, which corresponds to the scattering mean path l_s of 0.2, and 0.8 mm, respectively. These two curves show that the expected ballistic intensity decay much faster than the

diffuse intensities.

Fig. 5.5 show the integrated intensities for fixed medium thickness (w=60 mm) and different l_t ranging from 60 to 2 mm plotted against parameter w/l_t. As w/l_t increases, the intensity of the transmitted photons within a time interval decreases exponentially. The smaller the time interval, the intensity decays quicker. The ballistic intensity for mean cosine factor g =0.9 and 0.6 are shown as the broken curves in Fig. 5.5, and decay much faster than the diffuse intensity for large w/l_t.

Fig. 5.6 shows the integrated intensities for fixed medium thickness w=50 mm, $l_t = 2$ mm, $l_a = 100$ mm, and different integration time Δt ranging from 10 ps to 8000 ps. This figure shows that the intergrated intensity changes nonlinearly with the increase of the integration time. At the small integration time, $\Delta t <$ 20 ps in this case, the integrated intensity increases linearly with the integration time. With increase of the integration time from 50 ps to 1500 ps, the integrated intensity increase quicker because most of the transmitted diffuse photons arrive in this time period. Further increase of the integration time does not increase the integrated intensity because not many photons arrive after 1500 ps.

Ultrashort laser pulses from the colliding pulse mode-locked dye laser system has a typical average output power of 10 mW and a wavelength centered in 625 nm. With 15 second instrument integration time, the number of incident photons is about $5x10^{17}$. Assuming the collection factor $F = 0.01$, there are about $2x10^3$ photons transmitted within the first 10 ps interval times in case of Fig. 5.6. This amount of photons are enough for detection using a streak camera. The number of the transmitted photons can be increaseed by increasing the incident laser power using solid state ultrafast laser system. From Fig. 5.5, the transmitted photon intensity can also be

increased by using a near IR ultrafast laser because tissues are less scattering in the near IR region (to be shown later), i.e. larger value of the transport mean free path l_t.

5.3 Experimental Method

The schematic of experimental arrangement is shown in Fig. 5.7 which closely follows the geometry governed by eq. (5.1). Ultrashort laser pulses of 100 fsec duration and wavelength centered at 625 nm were generated at a repetition rate of 82 MHz by a colliding pulse mode-locked (CPM) dye-laser system. The laser beam of diameter 4 mm was split into two beams: a reference beam to mark the zero time of the signal beam, and the signal beam is focused by a lens to a 100 μm spot on the biological sample. Biological tissues were placed between two glass slides. The tissues were compressed to various thicknesses by pushing the glass slides closer together. The transmitted pulse within a 1 mm diameter area centered along the optical axis of the incident beam was imaged 1:1 by a lens into the input slit of a Hamamatsu synchroscan streak camera. The temporal profiles of the transmitted photons were measured with a time resolution of about 8 ps. The width of the input slit of the streak camera was set to 80 μm. The average power of laser beam incident on the sample was about 8 mW.

Experiments were performed on chicken breast tissues of various thicknesses, and under different degrees of compression. The cross-section area of the tissue slab was at least 5x5 cm^2 in this experiment to insure that small amount of photons lost at the edge of the slab will not seriously affect the infinite slab assumption given in eq. (5.1). For thin sample with thickness less than 3 cm, a single slab of tissue was used. For thicker sample, a few, typically two, slabs of tissues were stacked together. The gain of the streak camera was fixed during the course of the

experiment so that the measured intensities of the transmitted photons from tissues of different thicknesses and compression condition can be compared with one another. Neutral density filters were used to reduce the incident beam intensity in order to avoid the saturation of the streak camera. The reference beam was used to mark the zero time and to monitor the intensity of the incident laser. The transmitted intensity is corrected by a factor of the neutral density filter and the intensity of the reference pulse. For each thickness and compression condition, several transmitted pulse profiles were recorded. For thicker tissues, the transmitted pulses were measured by two streak sweep speeds the slow streak sweep speed was used to measure the whole transmitted pulse profile, and the fast streak sweep speed was used to measure the early portion of the transmitted pulse profile with better time resolution.

5.4 Results and Discussion

Fig. 5.8 displays a series of transmitted pulse profiles through uncompressed tissues of increasing thicknesses. The time zero was set at the instant when the ultrafast laser pulse incident on the tissue. The solid lines are experimental results and the broken curves are the fitting by diffusion theory. The diffusion theory is expected to hold for thick tissues. By fitting eq. (5.1) to the transmitted pulse through the 5 cm thick tissue as shown in Fig. 5.8(d), the l_t and l_a are found to be 2.4 mm and 53 mm, respectively. These values were used to fit the measured transmitted pulse profiles for the thinner tissues with thicknesses 3.0, 2.2, and 1.25 cm as shown in curves (c), (b) and (a) of Fig. 5.8, respectively. The fitting is shown to be quite good for 3.0 cm thick tissue. The transmitted photons are found to increasingly arrive earlier than that predicted by the diffusion theory as the tissue becomes thinner than 2.2 cm (about 10 l_t). This result is consistent with our

previous studies on the transmitted pulse through discrete random medium.[11]

The effect of compressing a tissue on the temporal profiles of the transmitted pulse is shown in Fig. 5.9 for a 3.0 cm thick tissue. As the tissue is compressed to thinner thickness, the transmitted pulses arrived earlier with a narrower pulse profile. The best fit of eq. (5.1) to the uncompressed tissue transmitted pulse profile yields l_t and l_a equal to 2.6 and 60 mm, respectively. These values of l_t and l_a are used to compute the transmitted pulse profiles through the compressed tissue of different thickness. The fitting is rather good for thick compressed tissue shown by curve (c) of Fig. 5.9, indicating that l_t and l_a or optical properties of the tissue remain essentially unchanged under compression. Compressing it into a thinner tissue, shown by curve (b) of Fig. 5.9, the experimental result slightly deviates from the diffusion theory. Compressing it to a even thinner tissue (1.6 cm thick) as shown by curve (a) of Fig. 5.9, the diffusion theory is shown to fail to describe the photon transport in the thin compressed tissue.

Instead of using single set of l_t and l_a to fit all the experimental transmitted pulse profiles, one can use eq. (5.1) to best fit each experimental profile yielding some values of l_t and l_a. It is found that the optical parameters l_t ranges between 2.2 and 3.0 mm and l_a ranges between 40 and 90 mm for both uncompressed and compressed tissues. This gives characteristic optical parameters l_t and l_a for chicken breast tissue equal to 2.5±.5 and 60±30 mm at 625 nm, respectively.

The attenuation of snake photons intensity at different time intervals of arrival were measured on the chicken breast tissues of increasing thicknesses. The intensity of snake photon at time interval Δt was obtained by integrating photon intensity between t_b and $t_b + \Delta t$ of the transmitted pulse, where $t_b = 1.49\frac{z}{c}$ is the time taken

by photons transmitting straight across the tissue of thickness z. For each thickness, the integrated intensities over Δt were averaged over several measured transmitted profiles. The integrated intensities over Δt = 10 ps, 20 ps, 50 ps, 100 ps, 200 ps, and ∞ for the uncompressed tissues of different thicknesses are presented in Fig. 5.10. All these integrated intensities were computed with a normalization factor that the intensity of the laser pulse transmitted through air was 1. In our experiment, the arrival time of the transmitted photons was measured up to 2000 ps. The intensities of the photons decrease exponentially as the thickness of the tissue increases. For thin tissues with thickness less than 1 cm, the transmitted pulse is broadened by less than 10 ps. So the integrated intensities for different Δt of more than 10 ps are with same order of magnitude. For thicker tissues, the temporal profiles of the transmitted pulse become significantly broader than 10 ps as shown in Figs. 5.8 and 5.9. The integrated intensities $I(\Delta t)$ become highly dependent on the time interval Δt. For thick tissues, the semilog plot of $I(\Delta t)$ versus thickness shows a linear line with negative slope, indicating that $I(\Delta t)$ falls off exponentially. The larger negative slope for smaller time interval indicate that the intensity within smaller time intervals are reduced by larger exponential factors. The solid lines in Fig. 5.10 are the integrated intensities computed numerically from eq. (5.1) for different Δt, with an overall collection factor F = 0.016. The optical parameters l_t and l_a used in these computation were 2.4 mm and 53 mm, respectively. The collection factor F was set so that the total integrated intensity of the diffusion theory fit the experimental one for 5 cm thick tissue. The diffusion theory result agrees well with the experimental results for tissue thickness of 5 cm and $\Delta t \geq 50ps$. For thinner tissues, there are more photons detected experimentally than that predicted by the diffusion theory. The reason is that photons are scattered mostly in the forward direction because the size of the

scatterers in the tissue is large compare to the wavelength of the laser pulse. These forward scattered photons traverse through the tissues along quasi straight lines and thus arrive earlier.

The integrated intensities for tissues compressed to different thicknesses are shown in Fig. 5.11. The intensities of the early transmitted photons through compressed tissue increases by orders of magnitude as the tissue is compressed to a thinner one because the reduction in the thickness of the tissue. The magnitude of the integrated intensity of the transmitted photons of the squeezed tissue are of same order as the unsqueezed tissue of same thickness. This is another indication that the optical characteristics of tissues under different compression conditions do not change much. The solid lines in Fig. 5.11 are the diffusion theory results computed with overall collection factor $F = 0.05$ and same parameters l_t and l_a as the uncompressed tissue. The factor F was selected so that the experiment and theory agree with each other in the case of thick tissue (3.0 cm). The difference between experiment and theory is similar to the uncompressed tissue.

The contribution from noise on the integrated intensities arises mainly from the dark noise of the SIT detector. The error of the experimental data increases as the thickness of the sample increases and Δt decreases, where the intensity of the transmitted photons decreases. All experimental data for sample thickness less than 3.5 cm have errors less than 20%. For data for sample thickness 7 cm, the error is a few time the integrated intensities for $\Delta t \leq 200ps$. The magnitude of the dark noise is larger than the early arriving snake photon. So experimental data of 7 cm thick tissue for $\Delta t \leq 100ps$ are much larger than the diffusion theory as shown in Fig. 5.10. It is possible to get better signal to noise ratio by using a less noisy cooled CCD detector.

Using near IR laser sources can increase the signal to noise ratio because tissues are less scattering in the near IR region and deeper penetration is possible. Solid curve of Fig. 5.12 shows the measured transmitted pulse profile of near IR ultrasort laser pulse at a wavelength of 1060 nm through 5.7 cm thick chicken breast tissues. The ultrashort 1060 nm laser pulses are generated from a ND:YAG laser system. The pulse duration is about 5 ps, and the pulse repetition rate is 82 MHz. The average power used in the experiment was about 1 W and the integration time was 6 second. The experiment was performed in a geometry similar to the experiment performed in Chapter 2 as shown in Fig. 2.1. The beam diameter size of the incident laser beam was about 8 mm. The measured pulse profile was fitted using eq. (5.1) with diameter a=8 mm. The best fit, shown as the broken curve in Fig. 5.12, yields the optical parameter l_t = 5.1 mm and l_a = 71 mm. The transport mean free path for 1060 nm light is about twice of that for 625 nm light, and the absorption length does not change significantly. Experiments were repeated using tissue of different thickness and different incident spot on the tissue. The transport mean free path is 4.9±0.3 mm and the absorption length is 70±10 mm for the chicken breast tissue at 1060 nm. Thus, the chicken tissue is about twice less strong in scattering for the 1060 nm near IR light as compared to the 625 nm visible light. This shows that there are much more transmitted photons when near IR laser sources are used.

To detect small breast tumor early requires spatial resolution on the order of millimeter scale which implies that the gate time Δt to be about 10 ps. The optical parameters l_t and l_a for human breast tissues are similar to the values obtained here for the chicken breast tissues. From our data presented above, it is promising that early arriving transmitted light through human breast can be detected. However, living tissue may have different optical parameters. The optical parameters of living

tissues should be measured to compare with the results obtained here. To increase the transmitted signal, the power of the incident beam needs to be increased within the safety limit for human. The size of input slit of the streak camera could also be increased without compromising the time resolution of the detection system. By compressing the tissues, the intensity of the transmitted light through the tissues can be increased by several orders of magnitude.

5.5 Conclusion

Diffusion theory is shown to fail to describe the ultrafast laser pulse transmission through biological tissues of thickness thinner than $7l_t$. The attenuation of the snake photon intensity within different time interval were computed from the transmitted profiles and found to decrease exponentially on thickness of the tissue. There are significantly more photons arrived at early time than that predicted by the diffusion theory in thin tissues. The optical properties of biological tissue were found not change significantly under different compression conditions. The transport mean free path of the tissue in the near IR (1060 nm) is shown to be about two times of that in the visible spectral region (625 mm).

References

1 K. M. Yoo, Qirong Xing, and R. R. Alfano, Optics Letters **16**, 1021(1991).

2 P. P. Ho, P. Baldeck, K. S. Wong, K. M. Yoo, D. Lee, and R. R. Alfano, Appl. Opt. **28**, 2304(1989).

3 L. M. Wang, P. P. Ho, C. Liu, G. Zhang, and R. R. Alfano, Science **253**, 769-771(1991).

4 S. Andersson-Engels, R. Berg, S. Svanberg, and O. Jarlman, Optics Letters **15**, 1179(1991).

5 H. Chen, Y. Chen, D. Dilworth, E. Leith, J. Lopez, and J. Valdmains, Optics Letters **16**, 487(1991).

6 J. C. Hebden, R. A. Kruger, and K. S. Wong, Appl. Opt. **30**, 788(1991).

7 M. D. Duncan, R. Mahon, L. L. Tankersley, and J. Rentjes, Optics Letters **16**, 1868-1870(1991)

8 K. M. Yoo, and R. R. Alfano, Optics Letters **15**, 320(1990).

9 F. Liu, K. M. Yoo, and R. R. Alfano, Optics Letters **16**, 351(1991).

10 M. Lax, V. Nayaramamurti, and R. C. Fulton, in *Proceedings of the Symposium on Laser Optics of Condensed Matter, Leningrad, June 1987*, edited by J. L. Birman, H. Z. Cummins and A. A. Kaplyanskii (Plenum, New York, 1987), pp229-235.

11 K. M. Yoo, F. Liu, and R. R. Alfano, Phys. Rev. Lett. **64**, 2647(1990); errata, **65**, 2210(1990).

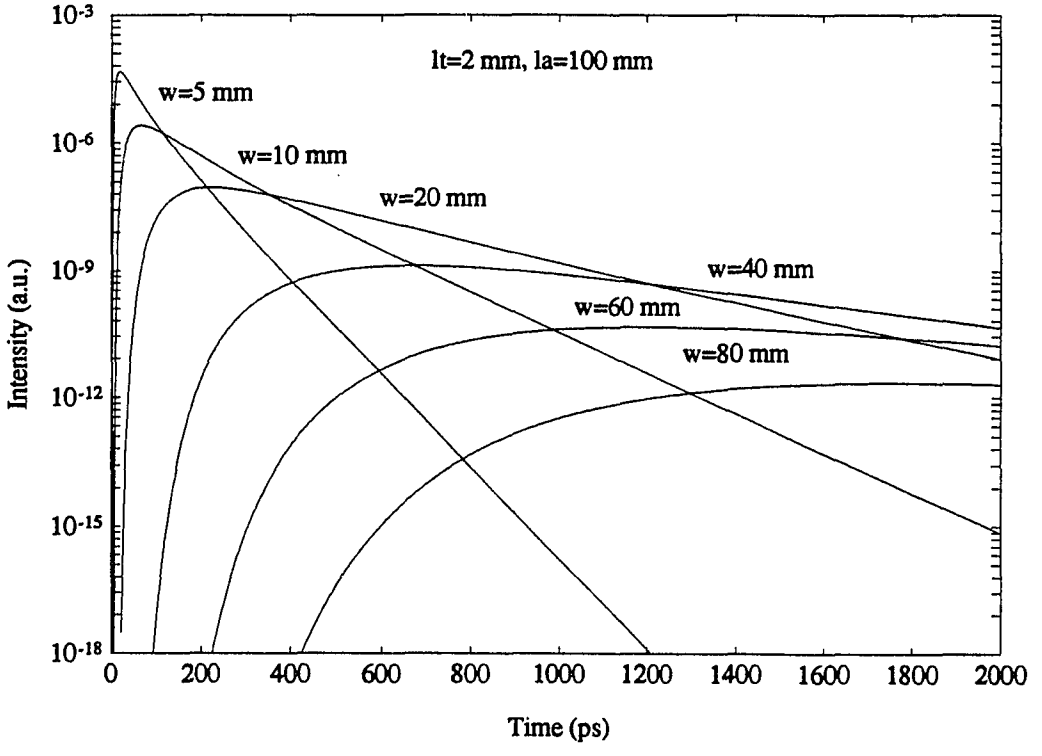

Fig.5.1 Semilog plot of the temporal profiles of the diffuse transmitted pulse computed using eq. (5.1) for different medium thicknesses. l_t , l_a, and pinhole diameter are 2, 100, and 1 mm, respectively.

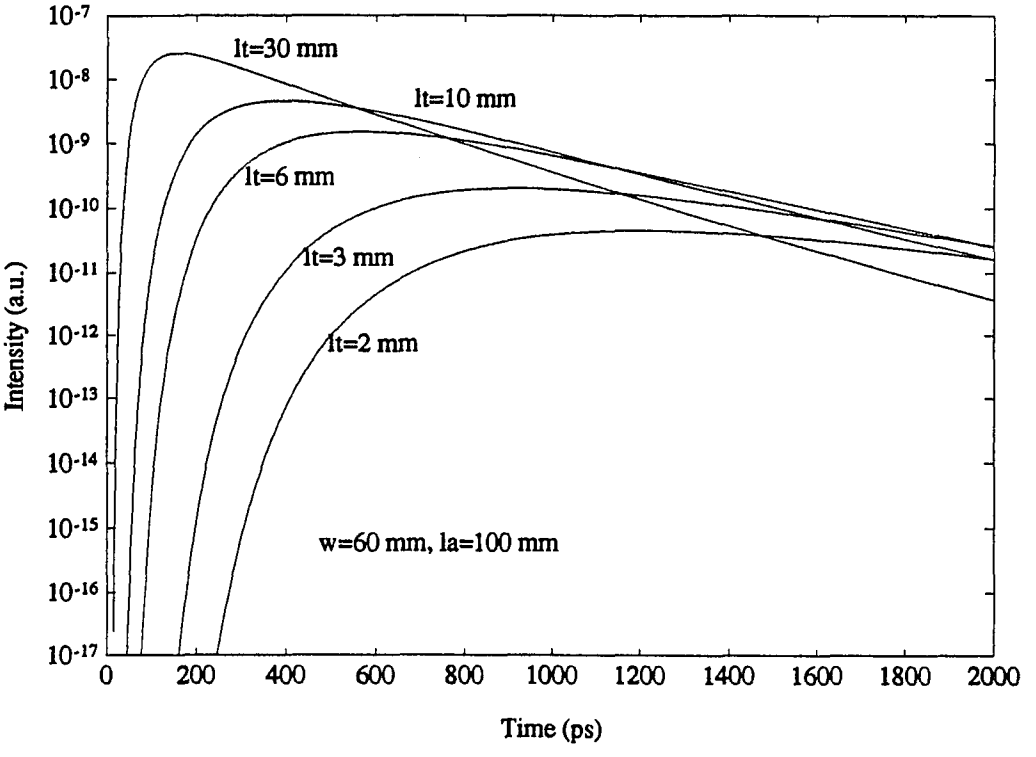

Fig.5.2 Semilog plot of the temporal profiles of the diffuse transmitted pulse computed using eq. (5.1) for different l_t. The medium thickness w , l_a, and pinhole diameter are 60, 100, and 1 mm, respectively.

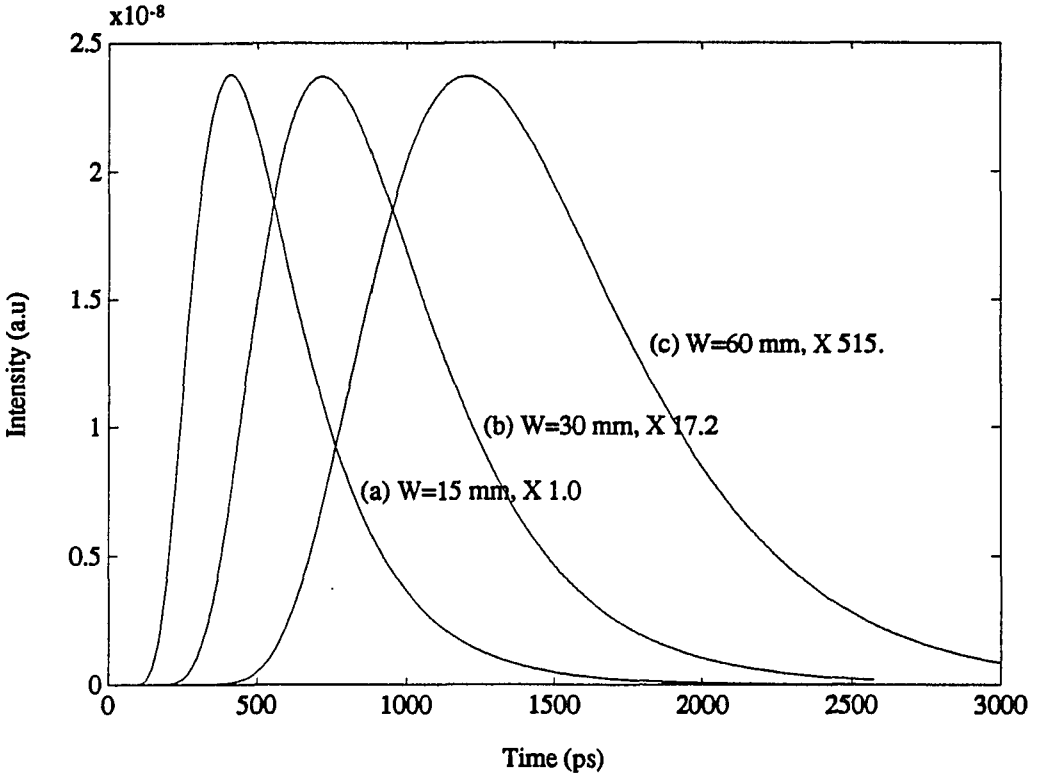

Fig.5.3 Plot of the temporal profiles of the transmitted pulse computed using eq. (5.1) for fixed $W/l_t = 30$. l_a, and pinhole diameter are 100, and 1 mm, respectively. The parameters W and l_t are (a)15 and 0.5 mm, (b) 30 and 1 mm, and (c) 60 and 2 mm for curves (a), (b), and (c), respectively.

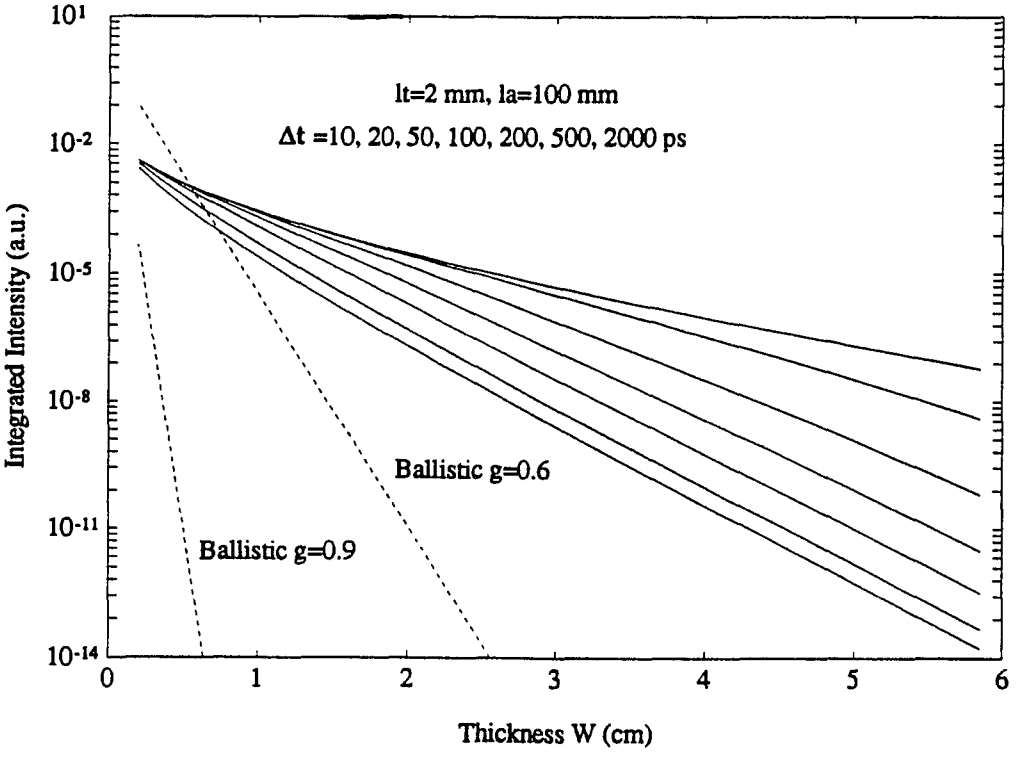

Fig.5.4 Semilog plot of the integrated intensities of the diffuse transmitted photons within different time intervals (solid curves) and the ballistic intensities of different mean cosine against the thickness of the medium. l_t, l_a, and pinhole diameter are 2, 100, and 1 mm, respectively. The integration time intervals (from lowest solid curve up) are 10, 20, 50, 100, 200, 500, and 2000 ps.

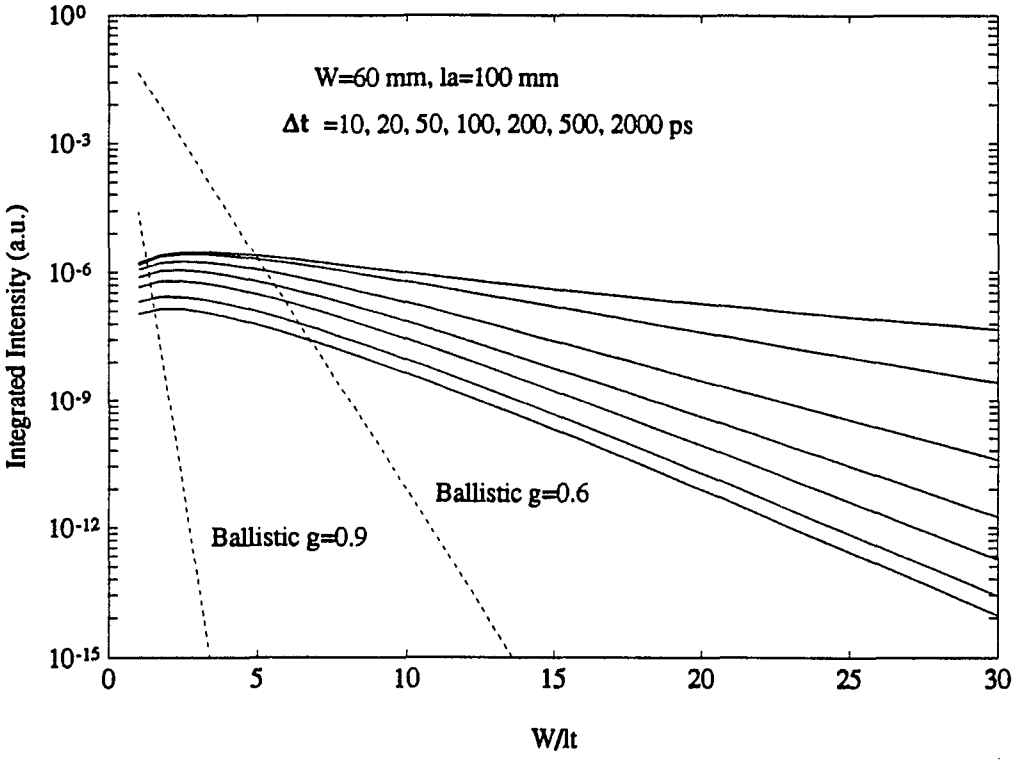

Fig.5.5 Semilog plot of the integrated intensities of the diffuse transmitted photons within different time intervals (solid curves) and the ballistic intensities of different mean cosine against parameter w/l_t. The medium thickness w , l_a, and pinhole diameter are 60, 100, and 1 mm, respectively. The transport mean free path l_t is changed from 60 to 2 mm. The integration time intervals (from lowest solid curve up) are 10, 20, 50, 100, 200, 500, and 2000 ps.

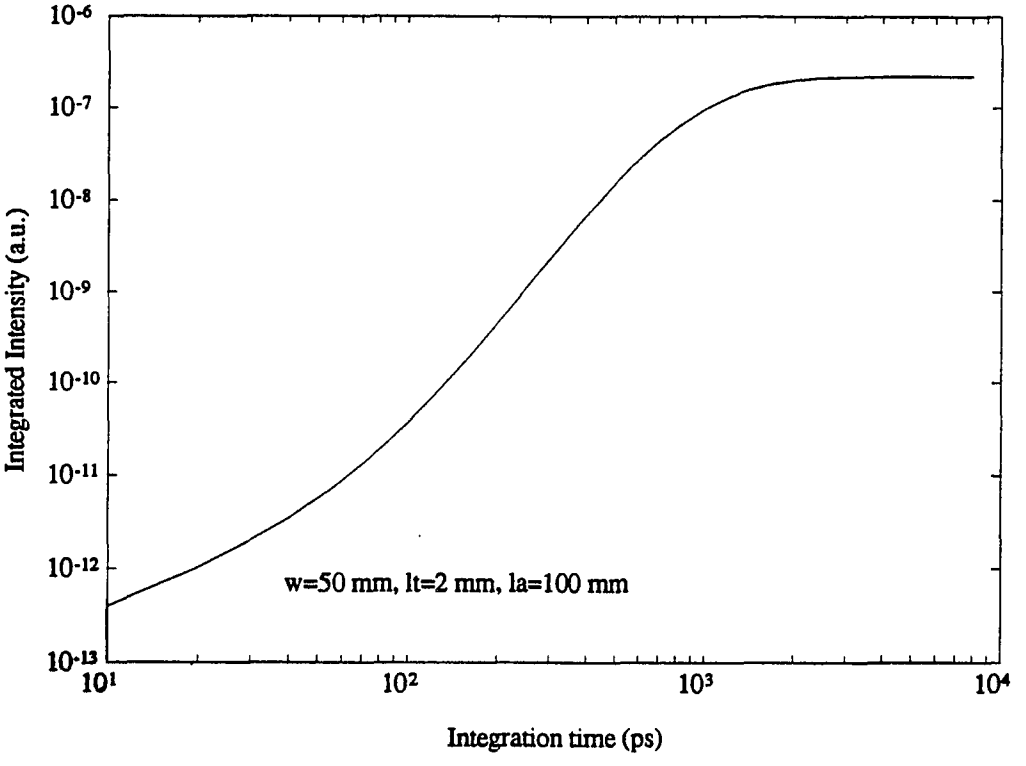

Fig.5.6 Loglog plot of the integrated intensities of the transmitted photons against the integration time Δt. w, l_t, and l_a are 50, 2, and 100 mm, respectively.

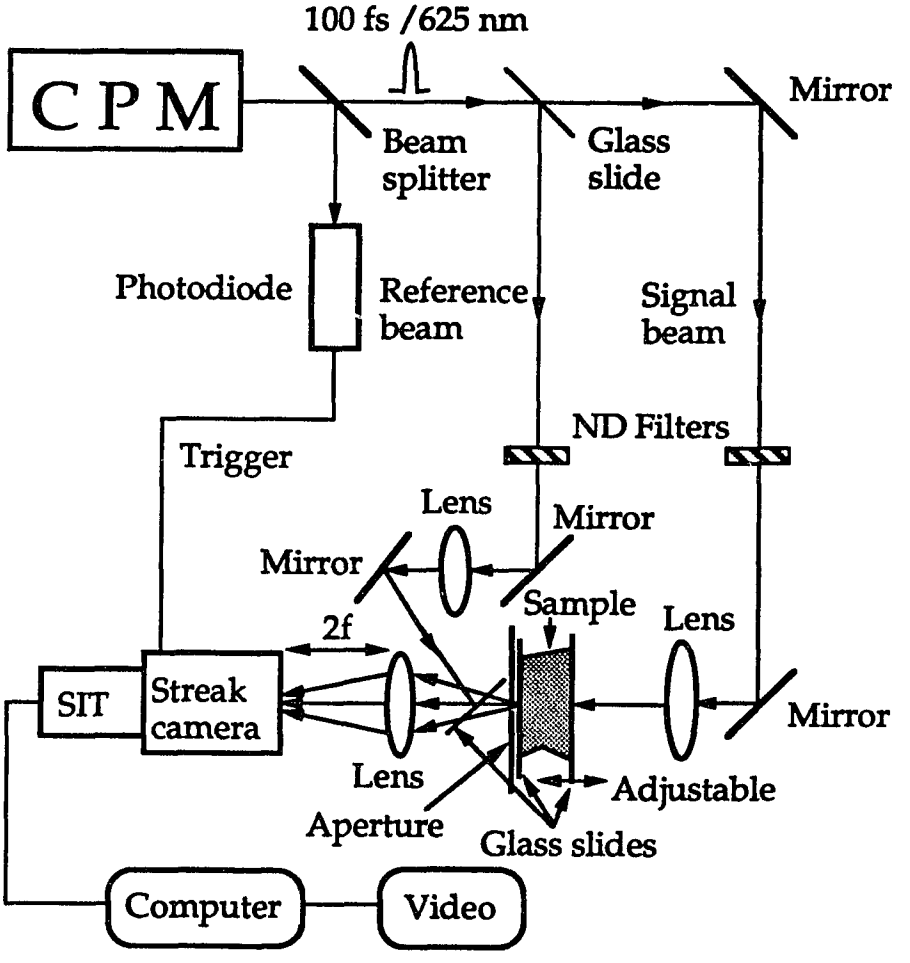

Fig.5.7 The schematic diagram of the experimental setup.

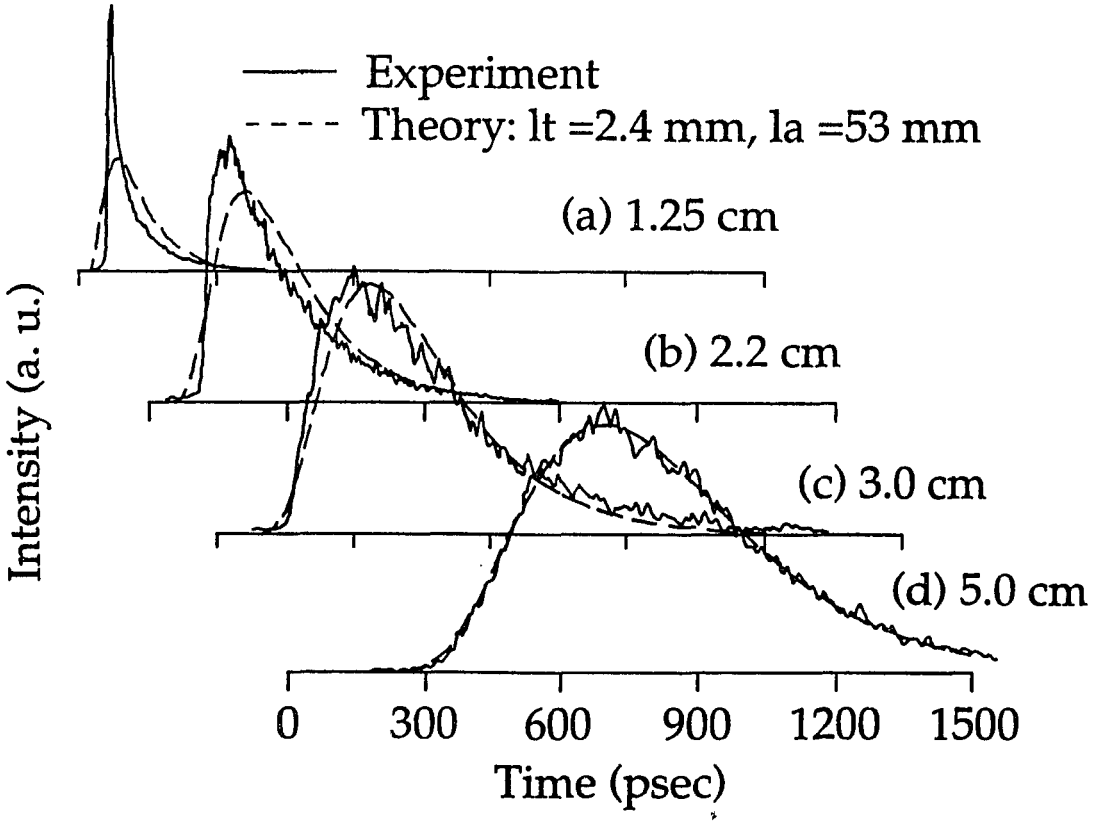

Fig.5.8 Normalized temporal profiles of 100 fs ultrafast laser pulses transmitting through uncompressed chicken breast tissue of thickness (a) 1.25, (b) 2.2, (c) 3.0, (d) 5.0 cm. The solid lines are the experimental results and the broken lines are the calculated fittings from diffusion theory. The corresponding fitting parameters for l_t and l_a are 2.4 and 53.2 mm, respectively.

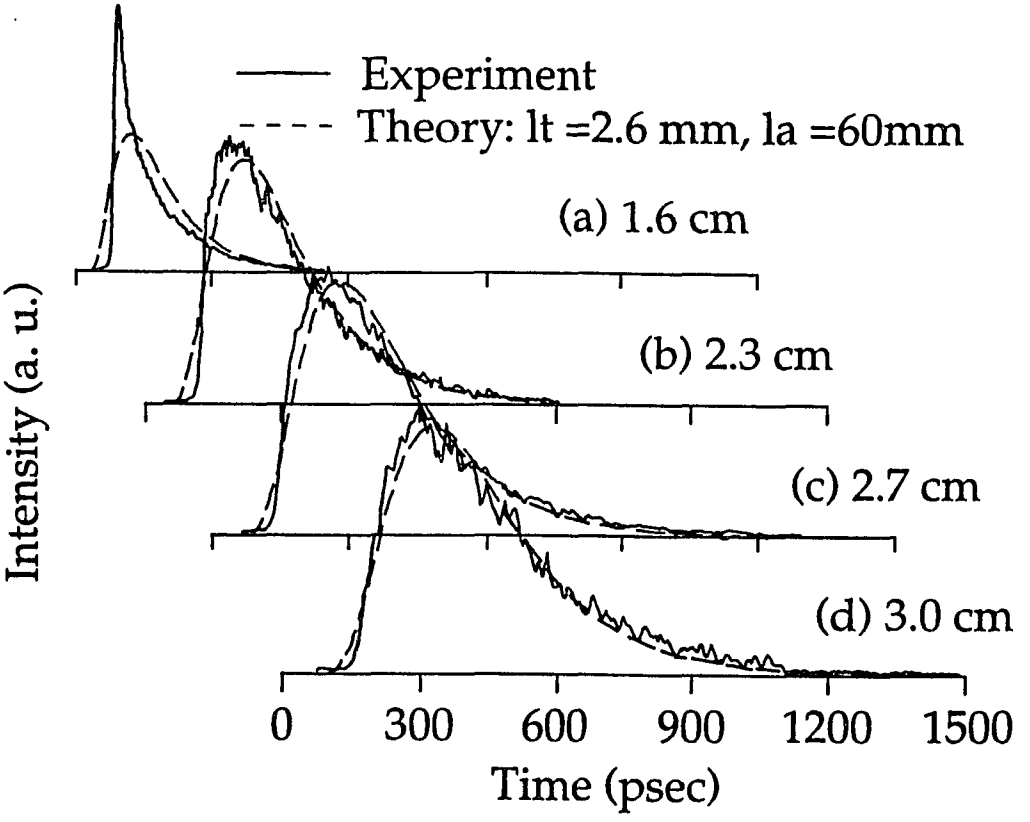

Fig.5.9 Normalized temporal profiles of 100fs ultrafast laser pulses transmitting through a 3.0 cm thick tissue compressed to different thicknesses of: (a) 1.6, (b) 2.3, (c) 2.7 cm, and (d) uncompressed. solid lines and broken lines are the experimental results and the diffusion theory fit, respectively. The fitting parameters l_t and l_a are 2.6 and 60 mm, respectively.

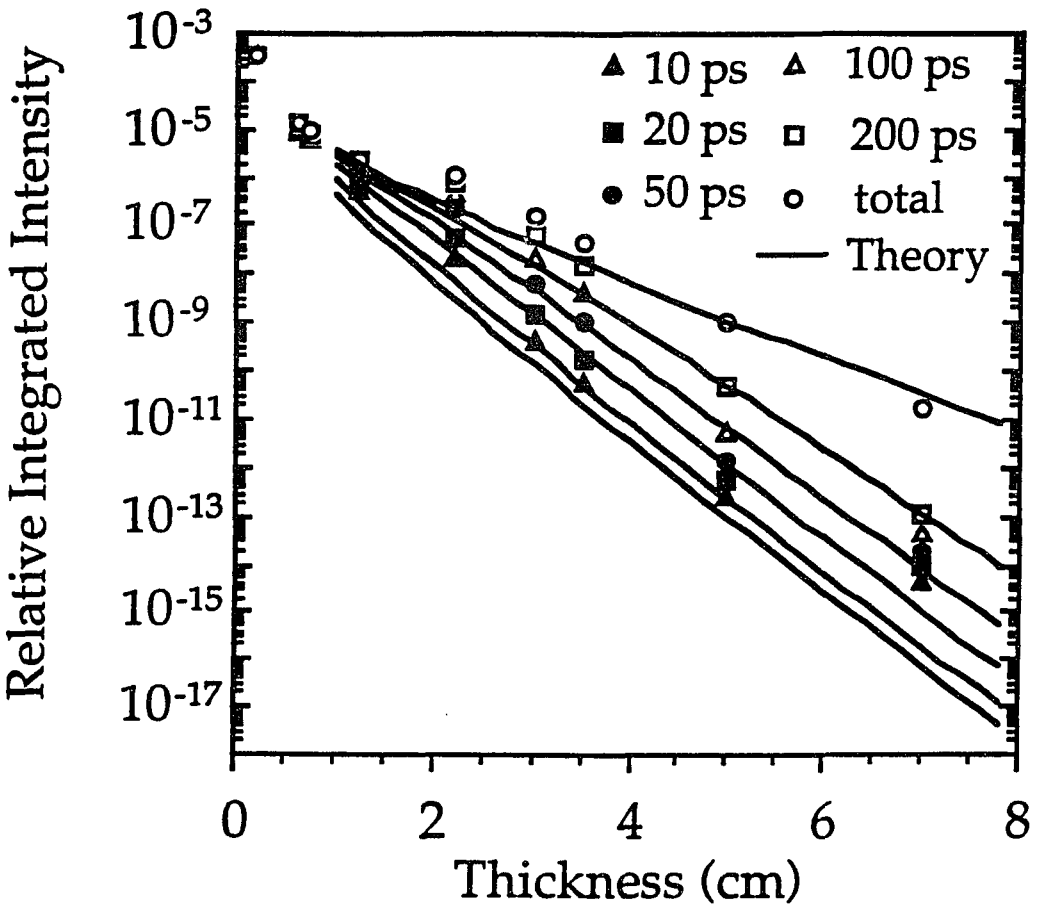

Fig.5.10 Integrated intensities of transmitted photons at various time intervals Δt through chicken breast tissues against tissue thicknesses. Integrated intensity of interval time Δt of 10, 20, 50, 100, 200 ps, and ∞ are plotted as darked triangle, darked square, darked circle, triangle, square, and circle, respectively. The solid lines are the integrated intensities computed from eq. (5.1) with collection factor of $F = 0.016$, and optical parameters $l_t = 2.4$ and $l_a = 53$ mm.

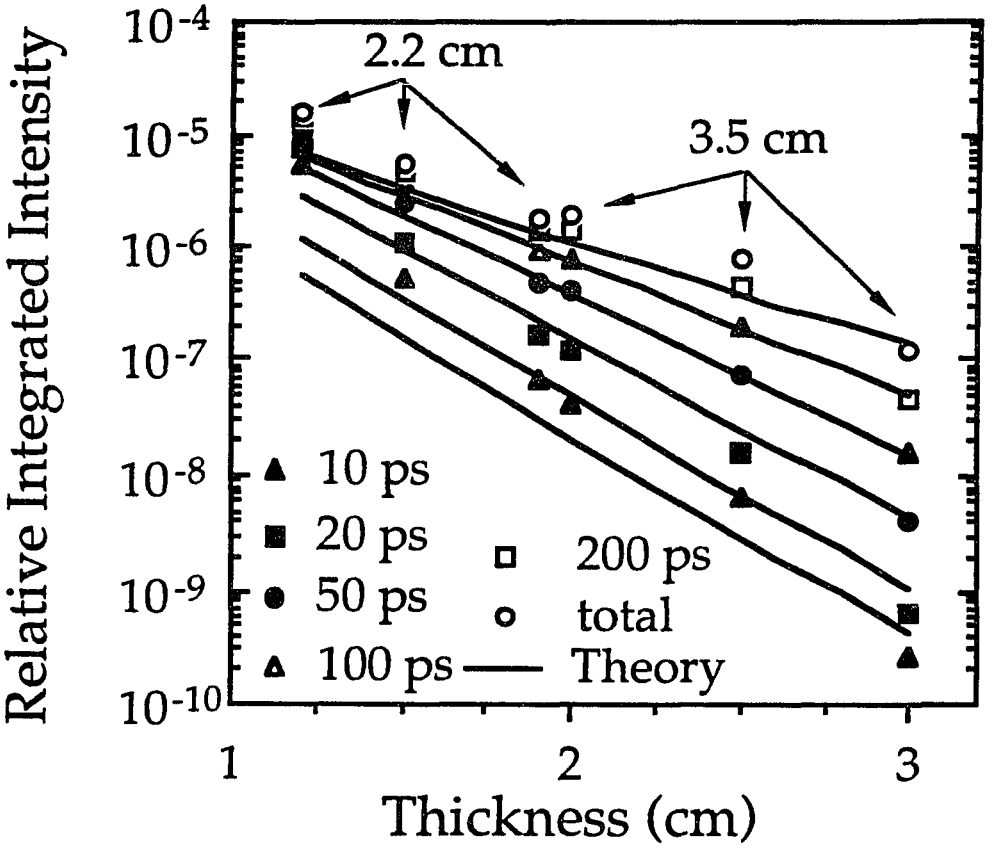

Fig.5.11 Integrated intensities of transmitted photon at various time intervals Δt through compressed tissues against tissue thickness. The marks indicate the thickness of the uncompressed tissue from which the tissue is compressed. Solid lines are the integrated intensities computed from eq. (5.1) with collection factor of $F = 0.05$, and $l_t = 2.4$ and $l_a = 53$ mm.

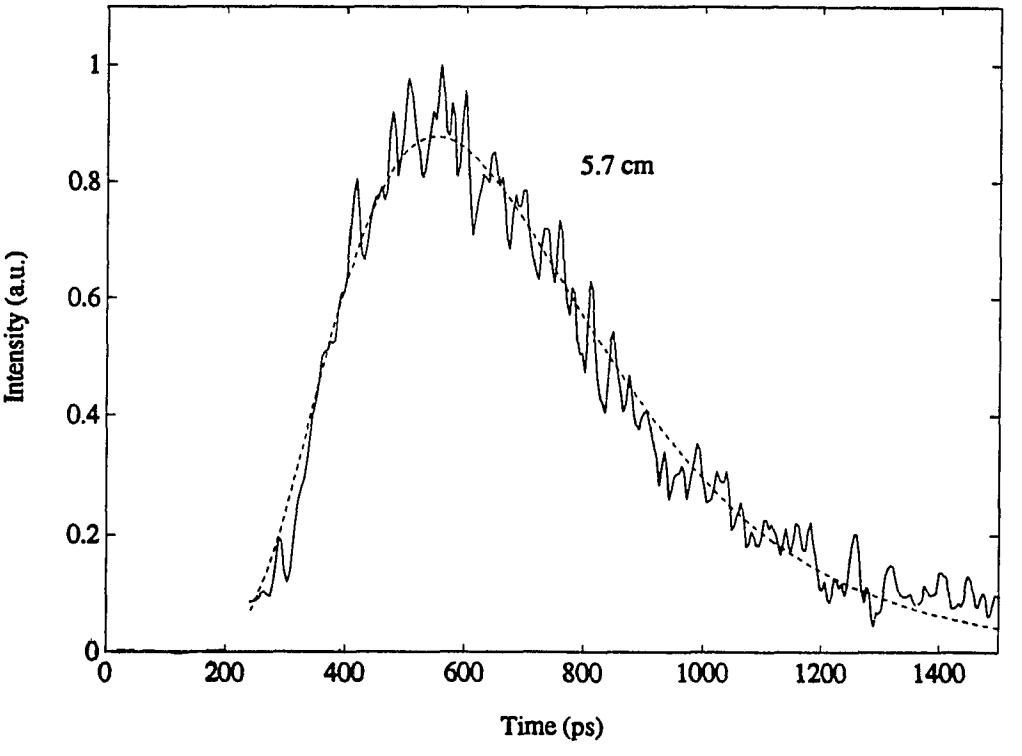

Fig.5.12 Normalized temporal profile of 5 ps 1060 nm near IR laser pulse transmitted through 5.7 cm thick chicken breast tissue. The solid and the broken curves are the experimental and the best fit by eq. (5.1) results, respectively. The fitting parameters l_t =5.1 mm, and l_a =70 mm.

Chapter 6

Should the photon flux or the photon density be used to describe the temporal profiles of scattered ultrashort laser pulses in random media?

6.1 Introduction

Diffusion theory has been widely used to describe the transport of photons in random media.[1-13] Analytical solutions of the diffusion equation for various boundary conditions are generally available. To probe photon transport, an ultrashort laser pulse which corresponds to an impulse of photons is incident on the scattering medium. The temporal profile of the scattered pulse at a given distance from the source, which corresponds to the distribution of photon migration path lengths, is measured and compared with theory. This time-resolved method has been widely used to study photon transport in random media.[7-12] The photon flux $j(\vec{r},t)$ has been commonly used to describe the temporal profile of the scattered pulse measured from the *surface* of random scattering medium.[7-13] However, in these cases, the calculated temporal profiles described by the photon flux and the photon density are essentially the same when the diffusion approximation is valid. Thus, whether the photon flux or the photon density should be used to describe the temporal profile of the scattered pulse has not been verified experimentally.

In this Chapter, we experimentally demonstrate that the photon density $n(\vec{r},t)$, instead of the photon flux $j(\vec{r},t)$, should be used to describe the temporal profile of the scattered pulse detected inside a random medium, while both the photon density and the photon flux can be used to describe the scattered pulse measured outside a

random medium. This study is important in the applications of ultrafast laser techniques to study light scattering phenomena and to obtain the optical properties of biomedical tissue for diagnostic and imaging purposes.

6.2 Theory

The temporal profile of a scattered ultrashort laser pulse in a random medium depends on the photon transport mean free path l_t and the absorption length l_a of the random medium, the distance between the source and detection sites, and the boundary conditions. Transport theory describes the light wave propagation and scattering in random media.[5] In transport theory, the propagation of the diffuse photon can be described by a quantity called diffuse intensity $I(\vec{r}, t, \hat{s})$, which is the number of photons traveling in the direction $\hat{s}$ at spatial position $\vec{r}$ in the medium per unit area per unit time. The diffuse intensity describes the experimentally measured scattered pulse profile in the time resolved experiment. The diffuse intensity satisfies the transport equation. However, transport equation is difficult to solve in most of cases.

The photon density $n(\vec{r}, t)$ is the total number of photon per unit volume at $\vec{r}$, and is related to the diffuse intensity by:

$$n(\vec{r}, t) = \frac{1}{v}\int I(\vec{r}, t, \hat{s})d\omega, \tag{6.1}$$

where the integration is performed over 4π solid angle of direction $\hat{s}$, and v is the velocity of the light in the medium. The net photon flux vector is the average of the propagating direction $\hat{s}$ and is given by:

$$\vec{j}(\vec{r}, t) = j(\vec{r}, t)\hat{s}_j = \int I(\vec{r}, t, \hat{s})\hat{s}d\omega, \tag{6.2}$$

where $\hat{s}_j$ is the unit direction vector of the net photon flux flow. The diffuse intensity

in the direction of the net flux $\hat{s}_j$. Define $\cos\theta = \hat{s}\cdot\hat{s}_j$. The diffuse intensity can be expand as around the mean flux flow direction $\hat{s}_j$:

$$I(\vec{r}, t, \hat{s}) = \sum_{l=0}^{\infty} I_l(\vec{r}, t) P_l(\cos\theta), \tag{6.3}$$

where $P_l(\cos\theta)$ is the Legendre polynominal of order l. This expansion is similar to the multipole expansion in electromagnetic theory. First term is the photon density (charge density), the second term is the net flux term (dipole). The higher order terms describe more details of the dependence of the diffuse intensity on the direction $\hat{s}$ (quadrupole, etc.). The first two terms I_0 and I_1 can be related to the photon density and the photon flux through eq. (6.1) and eq. (6.2), respectively.

By substituting eq. (6.3) into eq. (6.1), we have:

$$vn(\vec{r}, t) = \int \sum_{l=0}^{\infty} I_l(\vec{r}, t) P_l(\cos\theta) d\phi d\cos\theta = 4\pi I_0(\vec{r}, t). \tag{6.4}$$

From eq. (6.2), we have:

$$\vec{j(r}, t) = \int I(\vec{r}, t, \hat{s})\hat{s}\cdot\hat{s}_j d\omega$$

$$= \int \sum_{l=0}^{\infty} I_l(\vec{r}, t) P_l(\cos\theta)\, \cos\theta d\omega = 4\pi/3\, I_1(\vec{r}, t). \tag{6.5}$$

Inside a highly scattering medium, photons are scattered randomly many times so they travel almost uniformly in all directions. Therefore the higher order terms of eq. (6.3) can be neglected and this approximation is called diffusion approximation. In this diffusion approximation, the diffuse intensity can be approximated by:

$$I_d(\vec{r}, t, \hat{s}) \approx (vn(\vec{r}, t) + 3\vec{j}(\vec{r}, t)\cdot\hat{s})/4\pi. \tag{6.6}$$

The net photon flux $\vec{j}$ represent the diffusion propagation of the photon from the source and is not zero. The second term must be considerably smaller than the first

term, $vn \gg |\vec{j}|$, in order for this approximation to be valid. Inside a highly scattering medium, this condition holds. Thus the measured temporal profile can be approximately described by the photon density term, and can not be described by the photon flux term alone. On the medium boundary, the boundary condition, which is that no diffuse intensity flow inward to the medium, implies that this condition does not hold. Instead, the photon flux term is on the same order of the photon density in order to approximate the boundary condition. Therefore, on the medium boundary the photon density and the photon flux have same temporal profile. So both can be used to describe the scattered pulse profile measured from the surface of the medium.

Four experimental geometries shown in Fig. 6.1 were used to study whether the temporal profile of the scattered pulse should be described by $n(\vec{r},t)$ or by $j(\vec{r},t)$. These are: (i) a plane wave (large beam diameter) source and point detection through a slab of random medium, (ii) a point source and point detection inside an infinite random medium, (iii) a point source and point detection of the scattered pulse emitted from the surface of a semi-infinite medium, and (iv)a point source and point detection in a thick slab(semi-infinite) of medium with source inside and detection point changing from inside to the surface of the random medium.

In this diffusion approximation, the photon density can be shown from the transport equation to satisfy the diffusion equation and the photon flux is related to the photon density by: $j(\vec{r},t) = -D\hat{s}\cdot\vec{\nabla}n(\vec{r},t)$. The temporal profile of the photon density $n(\vec{r},t)$ at distance $\vec{r}$ from the source can be obtained from the solution of the diffusion equation as follows[12,13]

$$\frac{\partial n(\vec{r},t)}{\partial t} = D\nabla^2 n(\vec{r},t) - \frac{v}{l_a}\cdot n(\vec{r},t) + \delta(\vec{r})\delta(t), \tag{6.7}$$

where the δ- function term represents the impulsive photon source at time $t = 0$ and

position $\vec{r} = 0$, $D = \frac{1}{3} v l_t$ is the diffusion constant, and v is the speed of light in the scattering medium. The first term on the right hand side of eq. (6.7) is the diffusion term, and the second term is the absorption term.

In the experiment (i) where a plane wave is incident in a infinite slab, the photon density of the transmitted pulse at a point on the slab is given by: [12,13]

$$n_z(t) = \frac{1}{d} \sum_{m=1}^{\infty} (-1)^m (1 - \cos\frac{2\pi m z_0}{d}) \cdot \exp(-Dt(\frac{m\pi}{d})^2) \cdot \exp(-\frac{vt}{l_a}), \qquad (6.8)$$

and the photon flux is given by:

$$j_z(t) = \frac{D}{\pi w^2} \sum_{m=1}^{\infty} m(\frac{\pi w}{d})^2 \sin\frac{m\pi w}{d} \cdot \exp(-Dt(\frac{m\pi}{d})^2) \cdot \exp(-\frac{vt}{l_a}), \qquad (6.9)$$

where w is the thickness of the slab, $d = w + 2z_0$, and $z_0 = 0.71 l_t$ is the extrapolation length. Eq. (6.8) is obtained from integrating eq. (2.5) over the whole surface of the slab. Eq. (6.9) is same as eq. (2.7). Although eq. (6.8) and eq. (6.9) look differently, they give essentially the same temporal profile when diffusion theory is valid.

In an infinite medium geometry (ii), the temporal profile of the photon density at distance r from the source is given by:

$$n(\vec{r},t) = \frac{1}{(4\pi Dt)^{3/2}} \cdot \exp(-\frac{r^2}{4Dt} - \frac{vt}{l_a}), \qquad (6.10)$$

and the photon flux is given by:

$$j(\vec{r},t) = \frac{\hat{s} \cdot \vec{r}}{2t} n(\vec{r},t). \qquad (6.11)$$

Note, at large time t, n decays as $t^{-3/2}$ and j decays as $t^{-5/2}$. Therefore, the temporal profile of the photon density differs from that of the photon flux in an infinite medium. By comparing these computed profiles with the measured scattered pulse

profiles, one can determine whether the photon density or the photon flux gives a better description of the scattered pulse profile in an infinite medium geometry.

In a semi-infinite medium geometry (iii), with the boundary condition where the photon density vanishes on a plane at a distance z_0 from the medium surface, the temporal profile of the photon density at distance r from the source is given by:

$$n(\vec{r},t) = \frac{1}{(4\pi Dt)^{3/2}} \cdot \exp(-\frac{r^2}{4Dt} - \frac{vt}{l_a}) \cdot (1 - \exp(-\frac{z_0^2}{Dt})), \tag{6.12}$$

and the photon flux is given by:

$$j(\vec{r},t) = \frac{1}{(4\pi Dt)^{3/2}} \cdot \exp(-\frac{r^2}{4Dt} - \frac{vt}{l_a}) \cdot \exp(-\frac{z_0^2}{Dt}) \cdot \frac{z_0}{t}. \tag{6.12}$$

Note, at large time t, both n and j decay as $t^{-5/2}$. The temporal profiles of the photon density and the photon flux for this semi-infinite medium geometry are essentially the same at the source detection distance where the diffusion approximation holds (i.e. $r/l_t > 5$). Thus, for semi-infinite media one can not determine whether j or n should be used to describe the scattered pulse profile.

In the experiment geometry (iv), with the boundary condition where the photon density vanishes on a plane at a distance z_0 from the medium surface, the temporal profile of the photon density detected at distance d inside the medium with the source located at a further distance r inside the medium is given by:

$$n(\vec{r},t) = \frac{1}{(4\pi Dt)^{3/2}} \cdot \exp(-\frac{r^2}{4Dt} - \frac{vt}{l_a}) \left\{ 1 - \exp[-\frac{(z_0 + d)^2 + (z_0 + d)r}{Dt}] \right\}, \tag{6.14}$$

and the photon flux is given by:

$$j_z(\vec{r},t) = \frac{1}{(4\pi Dt)^{3/2} 2t} \exp(-\frac{r^2}{4Dt} - \frac{vt}{l_a})$$

$$\cdot\left\{r + (2d+2z_0+r)exp[-\frac{((z_0+d)^2 + (z_0+d)r)}{Dt}]\right\}. \qquad (6.15)$$

Note that when d=0, ie. detection at the surface of the medium, at large time t, both n and j decay as $t^{-5/2}$. The The temporal profiles of the photon density and the photon flux are essentially the same at the source detection distance where the diffusion approximation holds (i.e. r/l_t>5). The equations are similar to those of geometry (iii) case. As the detection point being moved into the medium (d increases), the temporal profiles of n and j begin to deviate from each other. Deep inside the medium (d/l_t large), ie. infinite medium case, the temporal profiles of n and j are very different. n decays as $t^{-3/2}$ which is slower than $t^{-5/2}$ j decays. The temporal profiles of the photon density and the photon flux are same as those in geometry (ii).

6.3 Experimental Method

The experiments were performed using streak camera and ultrashort laser pulses. Ultrafast laser pulses (100 fs/620 nm/82 MHz pulse repetition rate/10 mW) were generated from a colliding pulse mode locked (CPM) dye laser system. A part of the laser beam was split to trigger the synchroscan streak camera. The main part of the laser beam was further split by a glass slide for a reference pulse to mark the zero time of the main beam after it is scattered from random media. The experimental setup for experimental geometry (i) has been described in detail in Chapter 2. A schematics of the experimental setup for experiments (ii)-(iv) is shown in Fig. 6.2. To approximate the point source and point detection geometry, optical fibers (400 μm core diameter) were used to deliver the laser pulses into the scattering medium and to collect the scattered pulses. The scattered pulse profiles were measured by a Hamamatsu synchroscan streak camera. In experiments (ii) and (iii), a large random

scattering medium was used to ensure that it can be described by an infinite or a semi-infinite medium. A cylindrical tank of diameter 220 mm was used to contain the scattering medium. In an infinite medium represented by geometry (ii), the tips of the input and the collection fibers were placed at a height of 60 mm above the bottom of the tank, and the medium was 120 mm high. In geometry (iii), the medium was 60 mm high which was obtained by taking out half of the scattering sample from case (ii), and the tips of two optical fibers were just above the medium surface. The distance r were varied from 8 mm to 40 mm in both geometries. For experiment (iv), a cylindrical Pyrex glass cell of diameter 50 mm and height 100 mm was used. The tip of the input optical fiber was placed 25 mm above the bottom of cell, and the collecting fiber was mounted on a translation stage and inserted into the medium directly opposite to the input fiber as shown in Fig. 1(iv). The source detection distance r were set to 10 mm. The detection to medium surface distance d was varied from 0 to 25 mm by adding more scattering medium.

6.4 Results and Discussion

Transmitted pulse profiles of experiment (i) with slab thickness w = 10 mm are displayed in Fig. 6.3. Random medium used was latex beads of diameter 0.46 μm solution in water. Solid curve in Fig. 6.3(a) shows measured transmitted pulse profile with 0.84% of latex beads volume concentration. This transmitted pulse profile can be fitted well by both the photon flux (eq. (6.9), broken curves) and the photon density (eq. (6.8), dotted curves) using the same optical parameters: l_t = 0.25 mm and l_a = 330 mm. At lower latex beads concentration of 0.43% shown in Fig. 6.3(b), the transmitted pulse profile can also be fitted well by both n and j using l_t = 0.49 mm obtained from the scaling relation, and l_a = 330 mm. The fittings were

performed using a numerical standard least square fitting program. For this experimental geometry with $w/l_t > 10$, n and j have the same temporal profile and thus one could not tell which one will better describe the scattered pulse profile.

Intralipid (KabiVitrum Inc.) suspensions at various concentrations in water were used as random media in experiments (ii) and (iii). The scatterer is spherical with a mean diameter of 0.4 μm. The measured scattered pulse profiles $I(r, t)$ for geometry (ii) were fitted by eqs. (6.10) and (6.11), using a standard non-linear least square numerical fitting program, to determine whether n or j would give a better description of the scattered pulse profiles. The scattered pulse profiles from geometry (iii) were fitted by Eqs. (6.12) and (6.13). The fitting parameters l_t and l_a were obtained from the best fit of n or j for the case of large r and high scatterer concentration. In order to further determine whether n or j would give a better fit in geometry (ii), the parameters (l_t, l_a) obtained from the best fit for the case of large r were then used to fit the profiles in smaller r cases. The l_t used in fitting at different concentrations was extrapolated from the scaling relation: $l_t = l'_t \frac{F'}{F}$, where F is the volume fraction of the scatterers in the medium.

The temporal profiles of the scattered pulses for geometry (ii) are presented in Fig. 6.4. The solid curve of Fig. 6.4(a) shows the measured scattered pulse profile for an Intralipid suspension of volume concentration 0.48% and a source detection distance r=20 mm. The best fit of the photon density is shown by the dotted curve with l_t =1.3 mm and l_a=580 mm, while the best fit of the photon flux is shown by the broken curve with l_t=0.9 mm and l_a=$9 \cdot 10^4$ mm. The photon density fits the experimental curve better than the photon flux. Fig. 6.4(b) presents the experimental result at a shorter source detection distance (r=10 mm) where the photon density

shows a significantly better fit than the photon flux using the same l_t and l_a as used in Fig. 6.4(a). Fig. 6.4(c) shows the result for a lower Intralipid concentration and longer distance, 0.24% and r=30 mm, respectively. Both the photon density and the photon flux show rather good fits, although with different values of l_t, namely 2.6 mm for the photon density and 1.8 mm for the photon flux. The values of l_t and l_a obtained from the photon density fitting are the same as the values obtained from a pulse transmission experiment through a slab.[14] In addition, the absorption length obtained from the best fit by using the photon flux is clearly too long. This long absorption length is needed to compensate for the faster time decay of the photon flux ($t^{-5/2}$ instead of $t^{-3/2}$) in order to fit the later arriving portion of the scattered pulse. Overall, the temporal profile of the scattered pulse in an infinite medium is best described by the photon density.

The experimental results of geometry (iii) are shown in Fig. 6.5. A salient feature of the scattered pulse shows an early arriving component (the first narrow peak which is indicated by an arrow) in addition to the broad diffuse component. The solid curve in Fig. 6.5(a) displays the measured pulse profile for an Intralipid concentration of 0.48% and a distance r=30 mm. To minimize the effect of this early component on the fitting process, the numerical fittings were performed for the later arriving portion only. For instance, only the t >350 ps portion of the experimental profile was used in the fitting for Fig. 6.5(a). The early part of the theoretical curves were computed using the best fit parameters and plotted together with the later arriving part. The measured pulse profile is fitted by using eq. (6.13) (photon flux) and eq. (6.12) (photon density). Both fits yield l_t=1.6 mm and l_a=1200 mm, and their profile are same as represented by the broken curve. The measured temporal profile is fitted rather well by the diffusion theory for either n or j. By reducing the source

detection distance to r=20 mm, as shown in Fig. 6.5(b), both photon flux and photon density calculations also show a good fit to the measured pulse profile using the same optical parameters as for Fig. 6.5(a). These values of l_t and l_a are consistent with those obtained in experiment (ii) using the photon density fit. The slight difference in the fitting parameters between experiment (ii) and experiment (iii) can be attributed to the effect of the early arriving component observed in experiment (iii). This is shown in Fig. 6.5(c) where the experiment was done under the same condition as in Fig. 6.5(a) except a black plate (30 mm wide, 10 mm high, 1 mm thick) was inserted about 1 mm below the surface of the sample between the source and the detection fibers. This causes the early component to disappear. The fitting parameters l_t and l_a are 1.3 mm and 590 mm, respectively, which are the same as those obtained in experiment (ii) by the photon density fit. These results further show that the temporal profile of the scattered laser pulse in an infinite medium geometry should be described by the photon density.

The presence of a peak in the early arriving portion of the scattered pulse profiles shown in Figs. 6.5(a) and (b) is an interesting observation. The arriving time of the peak of this early component is about the time taken for light to travel from the source along the surface of the sample to the detection point using the refractive index of water (1.33). This observation indicates that light may be trapped and propagates ballistically along the surface of a random medium. This phenomena needs to be further investigated.

Experiment (iv) was performed using 0.296 μm diameter latex beads solution in the water. The measured temporal profiles for 0.25% scatterer volume concentration with d=0, 3.5, and 25 mm are shown as the solid curves in Fig. 6.6(a), (b), and (c), respectively. The broken, and dot lines are the best fittings by j (eq. (6.15)), and n

(eq. (6.14)), respectively.

The best fit by the photon density and the photon flux yields the same parameters for case (a), where the scattered pulse was measured from the medium surface d=0, l_t =0.9 mm and l_a =370 mm. The fitting curves in Fig. 6.6(a) show good agreement with the experiment and show again that in this case n and j have essentially the same temporal profiles. Fig. 6.6(b) show the scattered pulse profile detected just 3.5 mm below the medium surface with same scatterer concentration as Fig. 6.6(a). The best fits by n and j also show good agreement with the experiment result. However, best fit parameter l_t for j_z is 0.72 mm which is very much different from Fig. 6.6(a) fitting. While l_t is 1.06 mm for the photon density fit which is not very different from Fig. 6.6(a) fittings. Finally in Fig. 6.6(c), where the scattered pulse was detected deep inside the medium (d=25 mm), the best fit by j_z (l_t = 0.63 mm) is very different from the experiment curve. While the fitting by n show very good fit with almost same parameter l_t (1.11 mm). The transport mean free path can be obtained from Mie theory and is 1.05 mm which is very close to the value obtained from the n fittings. These results further show that the photon flux can only be used to describe the scattered pulse profile when it is measured from the surface of the medium. In general, the photon density can give a better description of the scattered pulse profile.

6.5 Conclusion

From these experimental results, we found that the measured scattered pulse profile can be consistently described by the diffuse intensity. In the diffusion approximation, the temporal profile of the scattered ultrashort laser pulse inside an infinite medium can be approximated by the photon density, while the temporal profile of the

backscattered pulse emitted from the surface of a semi-infinite medium can be described by either the photon density or the photon flux.

References

1 C. C. Johnson, IEEE Trans. Biomed. Eng. **17**, 129(1970).

2 R. J. Zdrojkowski, and N. R. Pisharoty, IEEE Trans. Biomed. Eng. **17**, 122(1970).

3 R. A. J. Groenhuis, H. A. Ferwerda, and J. J. Ten Bosch, Appl. Opt. **22**, 2456, and 2463(1983).

4 G. H. Weiss, R. Nossal, and R. F. Bonner, J. of Mod. Opt. **36**, 349(1989).

5 A. Ishimaru, *Wave Propagation and Scattering in Random Media*, Vol. 1, Chap. 9(Academic Press, New York, 1978).

6 P. Sheng ed., *Scattering and Localization of Classical Waves in Random Media*, (World Scientific, Singapore, 1990).

7 G. H. Watson, Jr., P. A. Fleury, and S. L. McCall, Phys. Rev. Lett. **58**, 945 (1987)

8 J. M. Drake, and A. Z. Genack, Phys. Rev. Lett. **63**, 259(1989).

9 M. S. Patterson, B. Chance, and B. C. Wilson, Appl. Opt. **28**, 2231(1989).

10 S. L. Jacques, IEEE Trans. Biomed. Eng. **36**, 1155(1989).

11 K. M. Yoo, Feng Liu, and R. R. Alfano, Phys. Rev. Lett. **64,** 2647 (1990); erratum Phys. Rev. Lett. **65,** 2210 (1990).

12 M. Lax, V. Nayaranamurti, and R. C. Fulton, in *Laser Optics of Condensed Matter*, J. L. Birman, H. Z. Cummins, and A. A. Kaplyanskii ed. 229-235(Plenum, New York, 1987).

13 G. H. Watson, S. L. McCall, P. A. Fleury, and K. B. Lyons, Phys. Rev. B **41**, 10947(1990).

14 Feng Liu, K. M. Yoo, and R. R. Alfano, (unpublished).

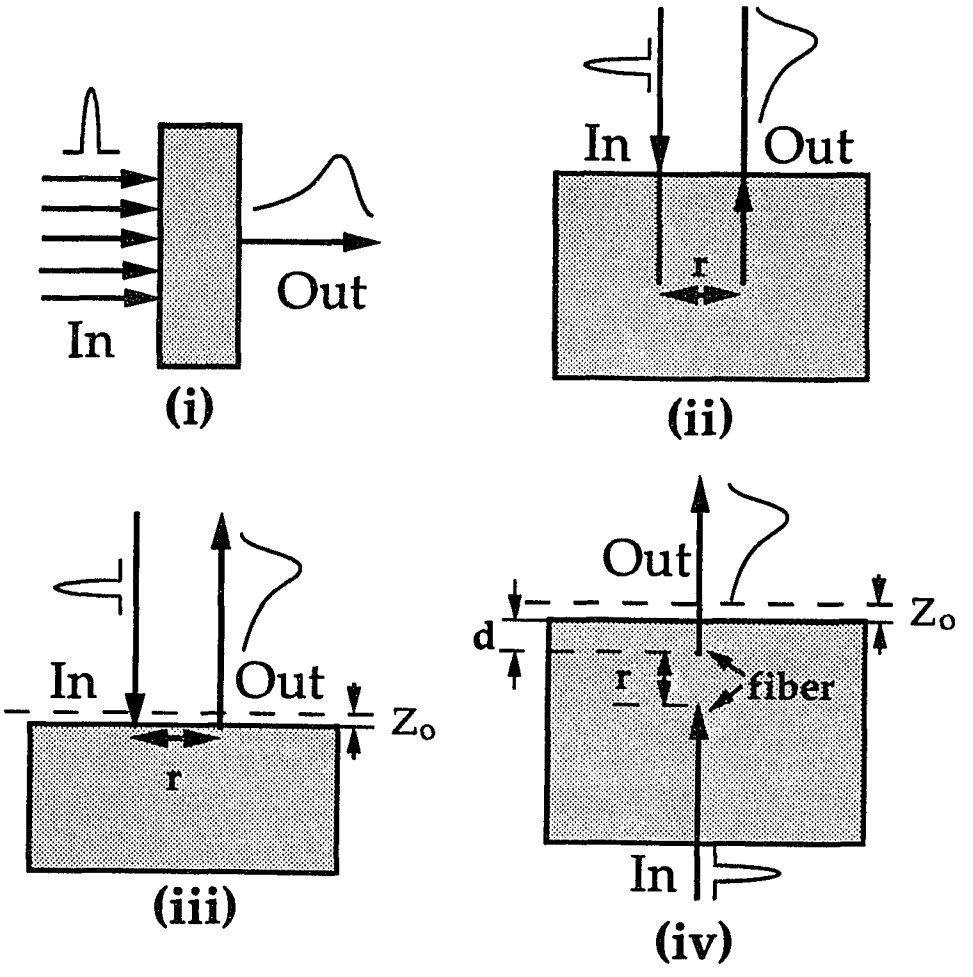

Fig.6.1 Schematic diagrams of different experimental geometry: (i) transmission through a slab medium; (ii) backscattering in an infinite medium; (iii) backscattering from the surface of a semi-infinite medium; and (iv) light scattering in a semi-infinite medium with source inside and detection point chaging from the surface to the inside of the medium.

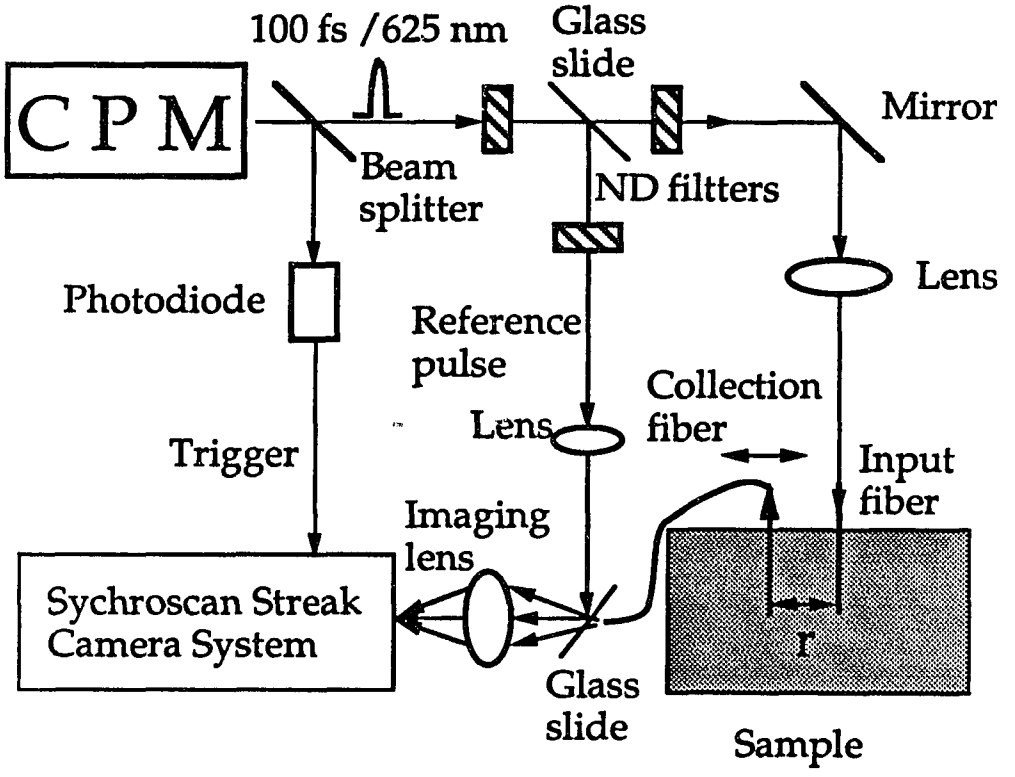

Fig.6.2 Schematic diagram of the experimental setup for experiments (ii)-(iv).

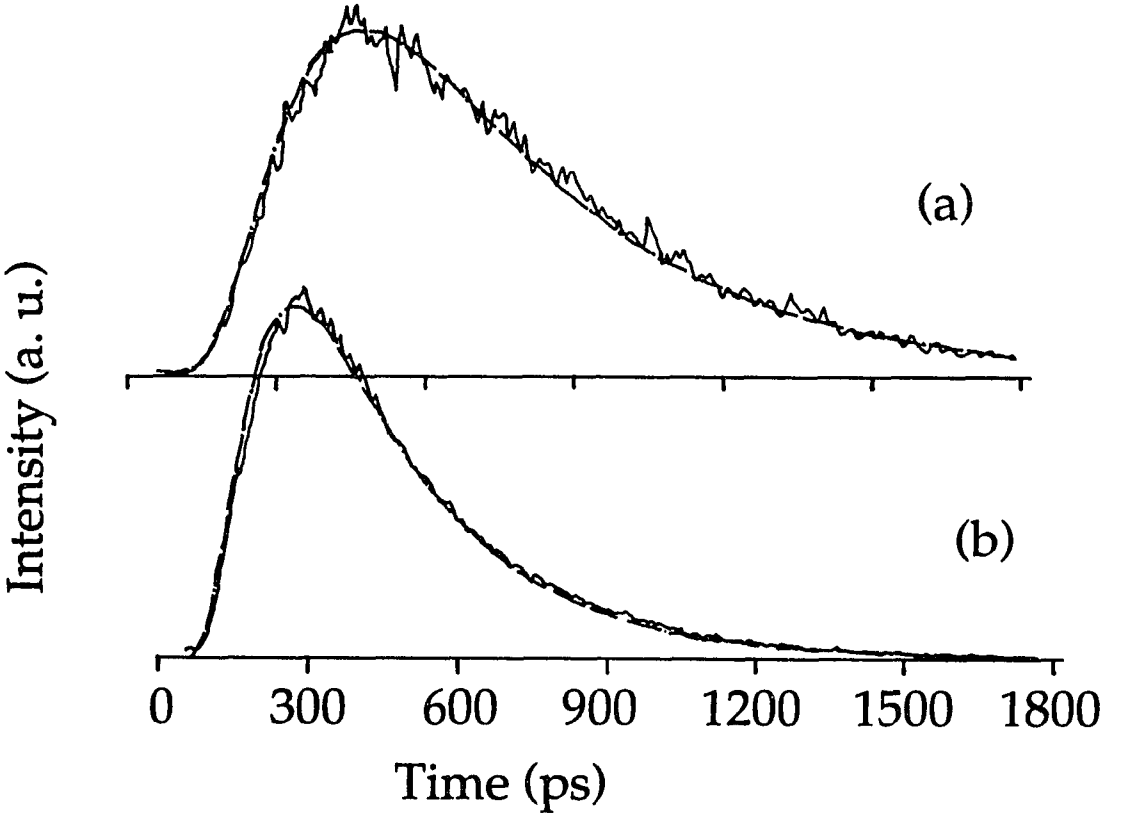

Fig.6.3 Normalized temporal profile of transmitted pulse through a slab of .46μm diameter latex beads solution of thickness z=10 mm. The solid, dot, and broken lines are the experimental, the fitting by eq. (6.8)(photon density), and the fitting by eq. (6.9)(photon flux), respectively. The volume concentration of the scatterer, and fitting parameter l_t (for both eq. (6.8) and eq. (6.9)), are: .84%, and .25 mm for Fig. 6.3(a); and .43%, and .49 mm Fig. 6.3(b). The absorption length l_a used in the fitting is 330 mm.

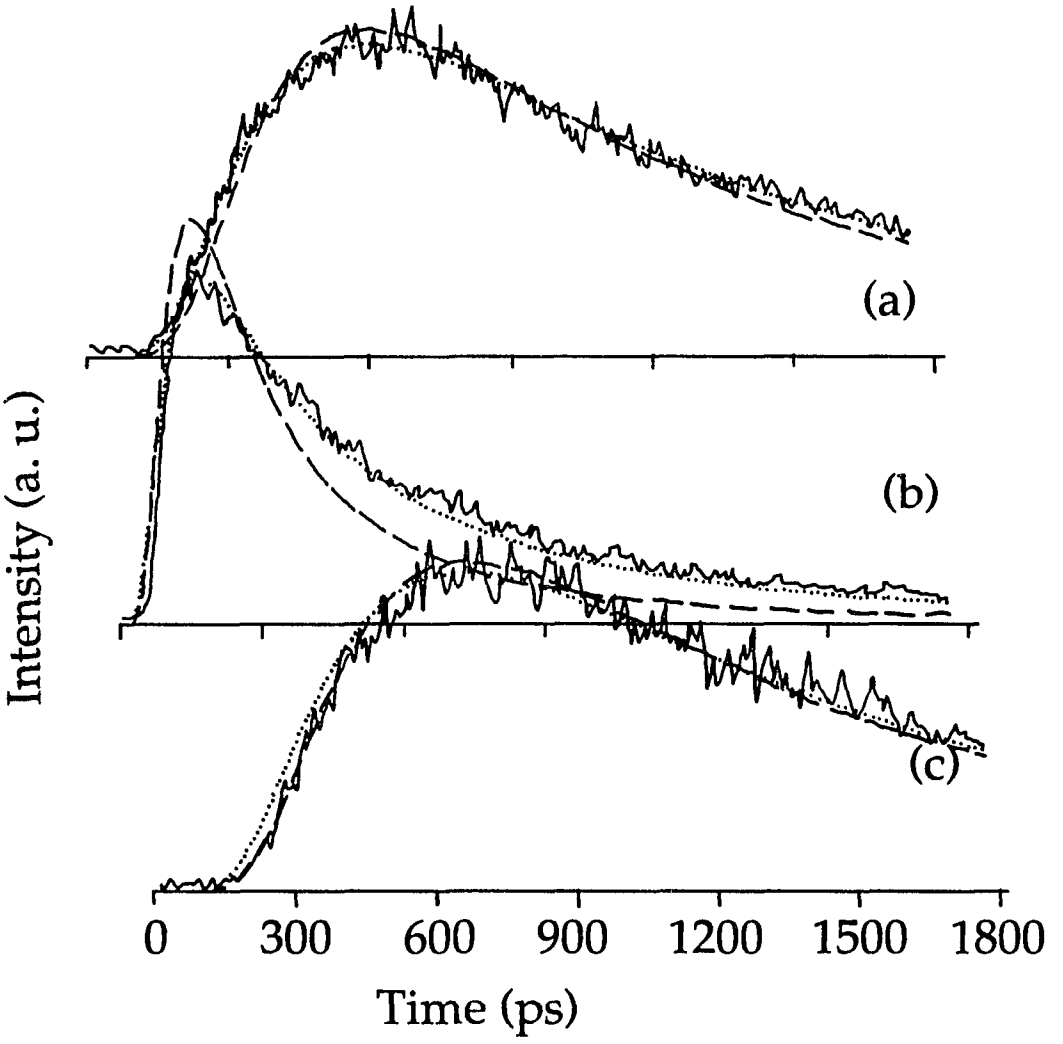

Fig.6.4 Normalized temporal profiles of a backscattered pulse in an infinite Intralipid solution for different r and scatterer concentrations: (a)20 mm and 0.48%; (b) 10 mm and 0.48%; and (c) 30 mm and 0.24%. The solid, dotted, and broken lines are the experimental results, the fitting by eq. (6.10), and the fitting by eq. (6.11), respectively.

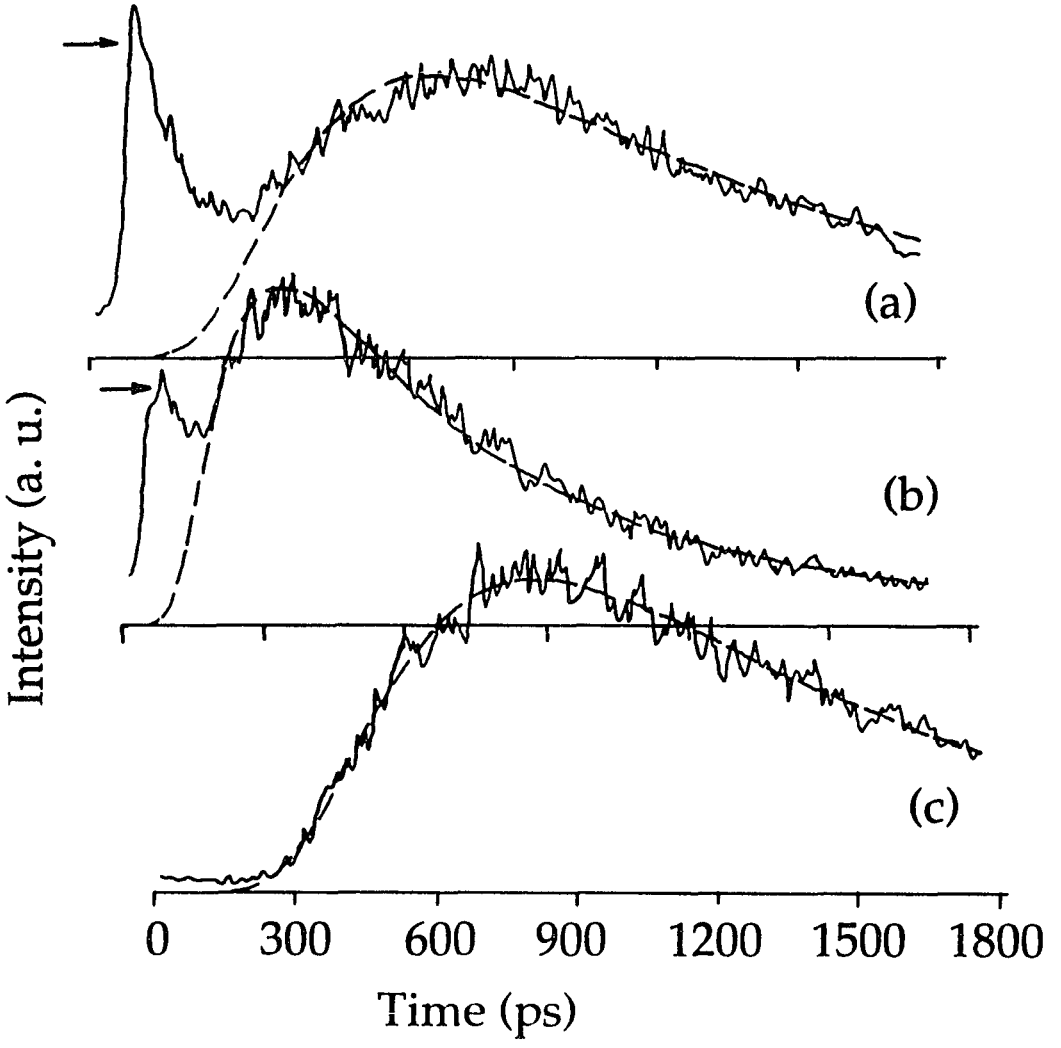

Fig.6.5 Normalized temporal profiles of a backscattered pulse from a semi-infinite Intralipid solution for different r and scatterer concentrations: (a)30 mm and 0.48%; (b) 20 mm and 0.48%; and (c)same as (a) but with a black plate inserted between the source and detection fibers. The solid and broken lines are the experimental results and the fitting by eqs. (6.12) and (6.13), respectively.

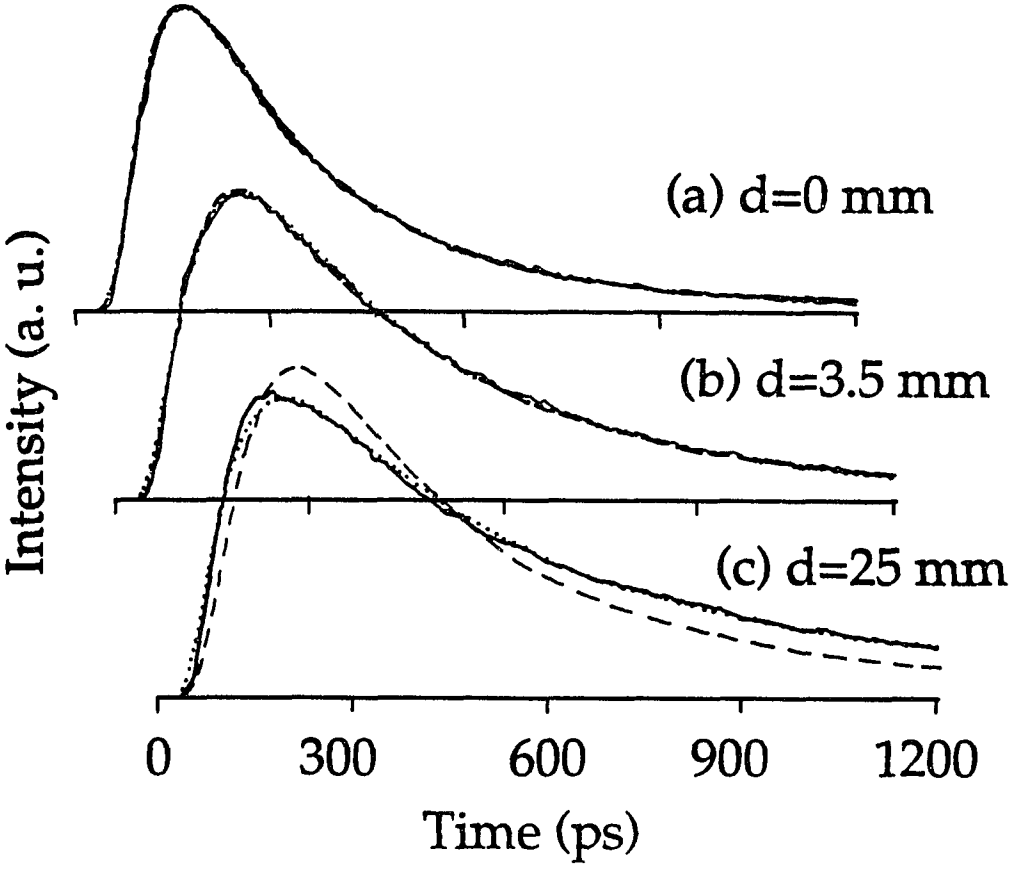

Fig.6.6 Normalized temporal profiles for different d. The solid, dot, and broken lines are the results of experimental, fitting by n (eq. (6.14)), and by j_z (eq. (6.15)), respectively. The source detection distance is 10 mm and d = 0, 3.5, and 25 mm for curves (a), (b), and (c), respectively. The best fitting parameters l_t and l_a for n and j_z fittings are: (a)0.88 and 370 mm, 0.87 and 350 mm; (b)1.06 and 890 mm, 0.72 and 760 mm; and (c)1.11 and 730 mm, 0.63 and 5000 mm, respectively.

Chapter 7

Summary

Ultrashort laser pulses and ultrafast time resolved detection techniques are used to study ultrashort laser pulse propagation in discrete random media and biological tissues. The speed of the ballistic component of the transmitted pulse through a slab of discrete scattering medium is found be reduced by the scattering. The reduction of the speed can be accounted by an effective medium description using an effective group index of refraction of the scattering medium. The effective group index can be obtained by the volume fraction combination of the refractive indexes of the scatterer and the background medium, or by the coherent interference between the scattered waves and the primary wave. The intensity of the diffuse component of the transmitted pulse is found to be preferentially attenuated with respect to the intensity of the ballistic pulse by the absorption. I demonstrated that an object hidden behind a highly scattering wall can be imaged by using the absorption effect.

Laser pulse transmission through a slab of biological tissues are studied. Unlike the case of pulse transmission through discrete medium, no clear distinct ballistic pulse is found. An experiment was performed to show that the early arriving component can be used for imaging through the tissue. The intensity of the transmitted photons through tissues arriving at various time intervals are measured and are found to decay exponentially with the thickness of the tissue. The earlier arriving photons decay quicker. Compression of the tissue is found not to change the key optical characteristics of the tissue. Diffusion theory is found to describe the transmitted pulse profile through thick tissues well, but it underestimates the intensity of the

early arriving photons.

The temporal profiles of the scattered ultrashort laser pulse with different experimental geometries are measured and analyzed by using the photon density and the photon flux given by the diffusion theory. It was found that the photon density instead of the photon flux should be used to describe the scattered pulse measured inside an infinite medium. Both the the photon flux and the photon density can be used to describe the scattered pulse profile measured at the boundary of the medium.

Chapter 8

Future research directions

In this thesis work, I have moved a small step closer to the understanding of the photon migration and light pulse propagation in random media. Much more theoretical and experimental studies are needed to better understand the basics of the light scattering in random media and to apply these understandings in material, biology, and health science. Some of the important future works are listed below.

1) Pulse propagation in tissues and the intensity of the early arriving transmitted light

The basics of the pulse propagation in biological tissues are necessary for biomedical diagnosis and imaging applications using laser technology. We have observed a broadened transmitted pulse through thin tissues which is fundamentally different from the pulse transmission through a single kind of discrete medium. One possible reason to explain this observation may be that tissues consist scatterers of a wide range of sizes. Theoretical work should be carried out to better understand this experimental observation. Pulse transmission through discrete scattering medium consisting different size scatterers should be experimentally investigated to see if a clear ballistic pulse exists.

We have shown that early arriving transmitted photons can be used to image object hidden inside random media. A better theoretical model than the diffusion theory is needed to correctly estimate the intensity of the early arriving transmitted photons and its dependence on the key optical parameters of the medium. This study will provide the feasibility of the time resolved transillumination imaging for human

breast cancer screening.

2) Imaging and microscopic characterization of random medium

The gross (macroscopic) properties of a random medium can be described by two key optical parameters, the transport mean free path and the absorption length, which can be obtained from the scattered pulse profile. The details of the fluctuation of the optical properties of the medium are unknown, such as the location of an inhomogeneity inside the medium. The possibility of determining the local optical properties inside the medium from the scattered pulse should be studied. This study can lead to a new technique for imaging a tumor inside human body.

3) Photon localization

Multiple scattered light in random medium interfere with each other. In a strong random scattering medium, it is predicted that the interference among the scattered lights will effectively reduce the rate of the photon migration in the medium to zero. This is so called photon localization phenomena. Ultrashort laser pulse and time resolved detection techniques are well suited to study the photon localization occurs as the functions of the properties of the medium, such as dielectric constant contrast of the scatterer to the surrounding medium, the size, shape of the scatterers.

The interference among the scattered light can be enhanced when the scattering medium is made ordered. This interference will make light scattered in certain directions, not randomly in all directions. The interference will also prohibit light wave propagation in certain wavelength band. The effect of the ordering of the medium on the pulse propagation should be studied.

Appendix

In this Appendix, we present some of the computer programs used in this thesis study. The programs are written in Rational Fortran (RATFOR).

A.1 Pulse profile eq. (2.7)

This is a RATFOR subroutine program used to compute the pulse profile given by eq. (2.7)

```
##################################################
##################################################
#       INPUT:
#       time (ps>)
#       lt (um)
#       la (um)
#       medium thickness (um)
#       index of the medium
#-----------------------------
#       OUTPUT:
#       intensity of the flux (per unit time)
##################################################
##################################################
#ifndef lint
#static char sccsid[] = "@(#)sublax.r 1.1 92/08/03";
#endif
#       program sublax.r: basic subroutine program to compute
#       temporal profile of point input transmitted through
#       whole surface on the oppsite side of slab. 4/9/92
#       ---------------------------------------
#       Modified 26/1/91 to include error standard.
#       Diffusion   5/1/90 modified to fix lt, change
#       length,   absorption considered.
#       from Lax Theory
#       --------------------------------
```

```
      subroutine gg(vv,xx1,xx2,wd,dex,uu)
      implicit double precision (a-h,o-z)
      common /fun1/pi,d,theta,theta1,dif,t
      if (vv <= 0.) { uu=0.
      }
      else {
# ------------------------------------
# paremeters
ero=1.e-8
z0=0.71*xx1  # for boundary condition
d=wd+2.*z0
pi=3.14159654
theta=wd*pi/d
theta1=2.*z0*pi/d
dif=.1*xx1/dex  # diffusion coefficient =vl/3 (um**2/fs)
ale=.3/xx2/dex     #absorption cofficent
# end parameters
# ------------------------------------
t=vv*1000.         #  t  time (fs)

call sum(ero,cjj,m)
uu=cjj*exp(-t*ale)*pi*dif/d**2
      }
      end

####
#     function subroutine, func(m)
subroutine func(m, funcm)
implicit double precision (a-h,o-z)
      common /fun1/pi,d,theta,theta1,dif,t
      fm=float(m)
      ff=(pi*2.*fm/d)**2*(dif*t)
ff1=(pi*(2.*fm-1)/d)**2*dif*t
      term2=-2.*fm*sin(2.*fm*theta1)*exp(-ff) #EVEN TERMS

term1=(2.*fm-1)*sin((2.*fm-1)*theta1)*exp(-ff1) #odd term
      funcm=term1+term2     #output
      end #end of function
####
####
#     subroutine to do infinet sum to certain accuracy,
#     SUM (from m=1 to m=inf) func(m)
#     func(m) is a subroutine.
subroutine sum(err,sumf,m)
```

```
implicit double precision (a-h,o-z)
tero=1.
m=1                  #initial condition
call func(m,sumf) #initial term
      while (tero .gt. err ) {
      nstart=m+1
      nfinish=2*m
      dsum=0.     # added part
      do i=nstart, nfinish {
      call func(i,funci)
      dsum=dsum+funci
      }
      sumf=sumf+dsum
      m=nfinish
      if (sumf .eq. 0.) {tero=1
      }
      else {
      tero=abs(dsum/sumf)
      }
      }
      end
####
```

A.2 Integrated intensity eq. (5.2)

Program to compute integrated intensities in Chapter 5. In this particular case, this program produce Fig. 5.6.

```
##########################################################
##########################################################
#       program called: qromb.f trapzd.f polint.f,
#       from "Numerical Receipes". These three programs
#       are available to public. They are integration
#       subroutine porgrams.
#--------------------------------
#       INPUT:
#       lt (um)
#       la (um)
#       medium thickness
#       pinhole diameter (um)
#       index
#--------------------------------
#       OUTPUT
#       integrated intensities vs. integration time from 10
#       ps to 8000 ps
##########################################################
##########################################################
#ifndef lint
#static char sccsid[] = "%Z%%M% %I% %E%";
#endif
#        program lpl4int1.r
#       compute integrated intensity density vs.
#       sample thickness for different time interval.
#       --------------------------------
#       point input , pin hole output
#       --------------------------------

      implicit double precision (a-h,o-z)
      real*8 tt(10)
      character*10 name3
##    COMMON BLOCKS
      common /fun1/pi,d,theta,theta1,dif,err,aale,ddia
      external func
      print*,"  transport mean free path tmfp (um) ? "
      read*, tmfp
```

```
      print*,"absorption lenth (um)"
      read*,ale
      #print*, " starting and ending thickness of slab (cm)"
      #read*, wstart,wend
      print*, " thickness of slab (um)"
      read*, wthic
      print*, " radius of pinhole (um)"
      read*, arad
      print*, "index of material"
      read*, dex
      print*, " output file name "
      read*,name3
      open(3,file=name3)
      print*, " read in terms to compute<5000"
      read*, ips
print*, "read in relative error for function"
read*, err
#-----------------unchanged paremeters
z0=0.71*tmfp  # for boundary condition
pi=3.141593
dif=.1*tmfp/dex  # diffusion coefficient =vl/3 (um**2 *fs)
aale=.3/ale/dex    #absorption cofficent
ddia=arad**2*.25/dif
d=wthic+2*z0 # (um)
theta=wthic*pi/d
theta1=2.*z0*pi/d
#-----------------end
#dw=(wend-wstart)/float(ips)  #step size of thickness
#      output file header
      write (3,*)"la=",tmfp, "la=",ale
      write(3,*)"index=",dex, "w=", wthic
      tint=0.
      ttspa=1.e+4
      ttout=0.
tball=wthic*10./3.*dex #(fs)
      tt(1)=tball
      tt(2)=tball
do i=1,ips {
if (ttout .gt. 1.e+7) { break}
tt(1)=tt(2)
tt(2)=tt(1)+ttspa
ttout=ttout+ttspa
if(ttout .gt. 1.e+5 ) {ttspa =2.e+4
}
```

```
 if (ttout .gt.2.e+5) {ttspa=5.e4
}
 if (ttout .gt. 8.e+5) { ttspa =1.e+5 }
call qromb(func,tt(1),tt(2),tint2)
tint=tint+tint2
ztt=ttout/1000. # change to ps
write(3,111)ttout, ztt, tint
111   format(1x, e12.6, 1x, e12.5,1x,e12.5)
}
      stop
      end
####----------------------------
#     function funcpl4(t)
#     common parameter provided through main program via
#     common block
      function func(t)
      implicit double precision (a-h, o-z)
      common /fun1/pi,d,theta,theta1,dif,err,aale,ddia
      common /fun2/twork
      twork=t
      if(t <= 0.) {
      func=0.
      }
      else {
      call sum(err,cjj,m)
      func=cjj*exp(-t*aale)*pi*dif/d**2*(1.-exp(-ddia/t))
      }
      return
      end
#-------------------------------
#     function subroutine, func(m)
subroutine funcpl4(m, funcm)
implicit double precision (a-h,o-z)
      common /fun1/pi,d,theta,theta1,dif,err,aale,ddia
      common /fun2/twork
      t=twork
      fm=float(m)
      ff=(pi*2.*fm/d)**2*(dif*t)
ff1=(pi*(2.*fm-1)/d)**2*dif*t
      term2=-2.*fm*sin(2.*fm*theta1)*exp(-ff) #EVEN TERMS

term1=(2.*fm-1)*sin((2.*fm-1)*theta1)*exp(-ff1) #odd term
      funcm=term1+term2     #output
      end                   #end of function
```

```
####----------------------------------------------
####
#       subroutine to do infinet sum to certain accuracy,
#       SUM (from m=1 to m=inf) func(m)
#       func(m) is a subroutine.
subroutine sum(err,sumf,m)
implicit double precision (a-h,o-z)
tero=1.
m=1                 #initial condition
call funcpl4(m,sumf)     #initial term
        while (tero .gt. err ) {
        nstart=m+1
        nfinish=2*m
        dsum=0.     # added part
        do i=nstart, nfinish {
        call funcpl4(i,funci)
        dsum=dsum+funci
        }
        sumf=sumf+dsum
        m=nfinish
        if (sumf .eq. 0.) {tero=1
        }
        else {
        tero=abs(dsum/sumf)
        }
        }
        end
```

A.3 Fitting program for Chapter 5

This is a standard least square fitting program used in the fitting computation in Chapter 5. The function subroutine can be easily changed to perform the fittings in Chapter 6.

```
#################################################
#################################################
#       program called: taurosv.f from "Numerical Receipes"
#       taurosv.f is a public domain
#       standard least fitting program.
#-----------------------------------------------
#       INPUT:
#       fitting parameter range for lt, la, and peak
#       normalization factor.
#       experiment pulse profile: time vs. intnesity.
#       index
#       pinhole diameter
#       medium thickness
#-----------------------------------------------
#       OUTPUT
#       best fit parameters: lt, la
#       theoretical pulse profile for best fit.
#################################################
#################################################
#ifndef lint
#static char sccsid[] = "@(#)fit2.r 1.3 92/11/26";
#endif
#       Program fit2.r
#       date 11-30-91,
#       for diffusion eq. fit
#       must be linked with taurosv.f
#
#       for infinite slab, point to point source
#       ----------------------------------------
#       must linked with function subroutine
#       sublaxpl4.r, and taurosv.f
#       ----------------------------------------
        subroutine fcn(npar, g,f,x,iflag)
        implicit double precision ( a-h, o-z)
        character * 12 anam, outfile
```

```
      character * 60 comfle,comfle1
      real*8  y(1024), z(1024), w(1024), x(6), c(1024)
      go to (10,60,60,60,120) iflag
 10   print *, "enter infile"
      read  *, anam
      open(1,file=anam)
      print *, "enter outfile"
      read *, outfile
      open(8,file=outfile)
      print *, "index, and pinhole diameter(um)"
      read*, dex,pdia
      print*, "thickness (um)"
      read*, wd
      ymax=0.
      yto=0.
      #read(1,*)comfle,comfle1
      print *, "yes"
      #read(1,*)ddjunk, ddjunk1
      do i=1,1024 {
      read (1,*,end=222)w(i), c(i)
      y(i) = c(i)
      if (y(i).gt.ymax) {ymax=y(i)
      }
#     #if (y(i).lt.0)y(i)=0.
      }
222   n=i-1
      nn=n-1
      do m=1,nn {
      yto=yto+(y(m)+y(m+1))*(w(m+1)-w(m))/2.
      }
#     write(6,*)"area=",yto
60    f=0.0
      zmax=0.
      zto=0.
      do i=1,n {
      call gg(w(i),x(1),x(2),wd,dex,pdia,z(i))
      if(z(i).gt.zmax) {zmax=z(i)
      }
      if(z(i).lt.0) z(i)=abs(z(i))
}
      do i=1,n {
      z(i)=z(i)/zmax*ymax*x(3)      #equal total intensity
      #f=f+(z(i)-y(i))*(z(i)-y(i))/sqrt(y(i)*y(i))
      f=f+(z(i)-y(i))*(z(i)-y(i))
```

```
}
      if (iflag.ne.3) return
120   print *,x(1),x(2),wd
      write(8,*)"%lt=",x(1)
      write(8,*)"%la=",x(2)
      write(8,*)"%thickness=",wd,"norm factor=",x(3)
      write(8,*)"%fcn=",f,"theory max=",zmax
      write(8,*)"%dia=",pdia,"index=",dex
      do m=1,nn {
      zto=zto+(z(m)+z(m+1))*(w(m+1)-w(m))/2.
      }
      rat=yto/zto
      write(8,*)"%total count exp.=",yto
      write(8,*)"%total count theo=", zto,"ratio=exp/theo",rat
      write(8,*)"fitda=["
      do i=1,n {
      com=(z(i)-y(i))/y(i)
      write(8,111)w(i), z(i)
#     write(18,*)w(i),com
}
111   format(1e10.5,1x,1e10.5)
      write(8,*)"];"
      close (8)
#     print *, "chi** =",xx
      end
####
#     FUNCTION SUBROUTINE
#     program sublaxpl4.r:    basic subroutine program to compute
#     temporal profile of point input transmitted through
#     a pin hole on the oppsite side of slab.      12/23/91
#     ---------------------------------------
#     Modified 26/1/91 to include error standard.
#     Diffusion   5/1/90 modified to fix lt, change
#     length,   absorption considered.
#     from Lax Theory
#     ----------------------------------
      subroutine gg(vv,xx1,xx2,wd,dex,pdia,uu)
      implicit double precision (a-h,o-z)
      common /fun1/pi,d,theta,theta1,dif,t
      if (vv <= 0.) { uu=0.
      }
      else {
# ------------------------------------
# paremeters
```

```
ero=1.e-6
z0=0.71*xx1  # for boundary condition
d=wd+2.*z0
pi=3.14159654
theta=wd*pi/d
theta1=2.*z0*pi/d
dif=.1*xx1/dex  # diffusion coefficient =vl/3 (um**2/fs)
ale=.3/xx2/dex     #absorption cofficent
ddia=pdia**2*.25/dif
# end parameters
# ------------------------------------
t=vv*1000.          #  t  time (fs)

call sum(ero,cjj,m)
uu=cjj*exp(-t*ale)*pi*dif/d**2*(1.-exp(-ddia/t))
       }
       end

####
#      function subroutine, func(m)
subroutine func(m, funcm)
implicit double precision (a-h,o-z)
       common /fun1/pi,d,theta,theta1,dif,t
       fm=float(m)
       ff=(pi*2.*fm/d)**2*(dif*t)
ff1=(pi*(2.*fm-1)/d)**2*dif*t
       term2=-2.*fm*sin(2.*fm*theta1)*exp(-ff) #EVEN TERMS

term1=(2.*fm-1)*sin((2.*fm-1)*theta1)*exp(-ff1) #odd term
       funcm=term1+term2     #output
       end #end of function
####
####
#      subroutine to do infinet sum to certain accuracy,
#      SUM (from m=1 to m=inf) func(m)
#      func(m) is a subroutine.
subroutine sum(err,sumf,m)
implicit double precision (a-h,o-z)
tero=1.
m=1                 #initial condition
call func(m,sumf) #initial term
       while (tero .gt. err ) {
       nstart=m+1
       nfinish=2*m
```

```
      dsum=0.     # added part
      do i=nstart, nfinish {
      call func(i,funci)
      dsum=dsum+funci
      }
      sumf=sumf+dsum
      m=nfinish
      if (sumf .eq. 0.) {tero=1
      }
      else {
      tero=abs(dsum/sumf)
      }
      }
      end
####
```

A.4 Scattering cross sections

This is a program computing the scattering cross section the momentum transfered cross section, and forward scattering amplitude for spherical particles. This program can also compute the scattering intensity vs. scattering angle. This program was written originally by Dr. P. Hu.

```
##############################################
##############################################
#       The input of this program can be easily changed to
#       compute cross sections vs. wavelength, particle
#       size. This version is corss sections vs. wavelength
#        for fixed size particle.
#============================================
#--------------------------------------------
#       INPUT
#       particle radius (um)
#       index contrast
#       index of the background medium
#       starting and finishing wavelength in vacuum
#--------------------------------------------
#       OUTPUT
#       wavelength vs. scattering cross section and
#       vs. momentum transfered cross section.
##############################################
##############################################
#ifndef lint
#static char sccsid[] = "%Z%%M% %I% %E%";
#endif
#       this program compute total Mie scattecross-section
#       and momentum-transfored cross-section.
#

complex*16 aa1,aa2,bb1,bb2,tt1,tt2,fors1,fors2,ex1
real*8aout,ra2,ra1,rfn1,rfn2,q1,q2,dex1,dex2,dex,s,s1,s2,pom,tw1,tw2,twav
#real*8ra,rfn1,q
integer ndim,ndim1,ii
print*,"ra=radius(mm),rfn1(>1),index in outside medium."
read*,ra2,rfn1,aout
print*,"starting and finishing wavelength in vacuum"
```

```
read*,tw1,tw2
#ra1=ra2/twav
tt2=(0,1)
write(22,*)"index=",rfn1
write(22,*)"outside index=",aout,"radius=",ra2
pom=0.
      do ii=1,51 {
twav=tw1+float(ii-1)*(tw2-tw1)/50.
ra1=ra2/twav*aout
ndim=int(ra1*2*3.14159+1.)
if (ndim.gt.5) {ndim=ndim+10
      }
      else {
      ndim=2*ndim
      }

call coout(ra1,rfn1,ndim,aa1,bb1,tt1,fors1,q1,ex1,s2)
dex1=dreal(tt1)*2./q1**2
s=real(ex1)*4./q1**2
s1=s2*2./q1**2
dex2=s/dex1 #     cos(theta) average
write(1,*)"momentum transfered=",s
#dex=dex1-s
#dex=(dex1-s)*3.141592654*ra2**2
#write(1,*)dex2
#write(2,*)q1,dex1,s,dex2,dex
write(3,111)q1,ndim,s,dex1,dex2
111   format(1f10.4,1x,1i5.2,1x,3e12.5)
#write(11,*)twav,dex1
dex=dex1*ra2**2*3.14159
#dex=1./dex1
#write(22,*)twav,dex    #lambda vs. Sigma(s)
#write(11,*)twav,dex    #.. .vs. 1/Qs

            }
      stop
      end
########################################
########################################

#     SUBROUTINE
#------------------------------
#calculates the scattering intensity at different angle
#(output: j ( angle between 1-179 degree )
```

```
#       int1(j) and int2(j)
#
#     ------------------------------------------
#     ------------------------------------------
#     changed to do total scattering and momentum
#     transfered cross-section
#     ------------------------------------------
#     output:       for ref. see van de Hulst. Page 127-128.

#     exsca:        the momentum transfered cross-section(complex);
#     extin: total scattering cross-section
#     tt:     forward scattering amplitude
#     ------------------------------------------
subroutine coout(ra,rfn1,ndim,aa,bb,tt,fors,q,exsca,extin)
complex*16 a(500),b(500),aa,bb,tt,cc,fors,exsca
real*8ra,rfn1,q,extin
integer ndim,j
#print*,"ra=radius/wavelength,rfn1,ndim"
#read*,ra,rfn1,ndim
q = 2*3.14159265358979*ra
call coef(a,b,ra,rfn1,ndim+1)
#call intensity(int1,int2,a,b,ndim)
cc=(0,1)
aa=(0.,0.)
bb=(0.,0.)
exsca=(0.,0.)
extin=0.
do j = 1,ndim {
fj=float(j)
aa=aa+a(j)*(2.*float(j)+1)
bb=bb+b(j)*(2.*float(j)+1)

#compute the total scattering cross-section
extin=extin+(xabs(a(j))+xabs(b(j)))*(2.*float(j)+1.)

#compute the momentum transfered cross-section
exsca=exsca+fj*(fj+2.)/(fj+1.)*(a(j)*dconjg(a(j+1))+b(j)*dconjg(b(j+1)))
exsca=exsca+(2.*fj+1.)/fj/(fj+1.)*a(j)*dconjg(b(j))
      write(8,*)j,a(j),b(j)
}
      tt=aa+bb
      write(1,*)"q=",q
#           write(1,*)"tt=",tt
#
```

```
#             write(1,*)"aa=",aa
#             write(1,*)"bb=",bb
#     ----------------------------
#     ----------------------------


#scattering amplitude
fors=tt/2./q
      write(1,*)"fors=",fors
return
end



subroutine intensity(int1,int2,a,b,ndim)
# This subroutine calculates the intensity of the
# scattered light for different polarization
# input :
#   ndim:  the dimension of the coefficients a and b
#    a  :  the coefficient of different partial waves
#          a(500)
#    b  :  the coefficient of different partial waves
#          b(500)
# return:
#  int1 :  the intensity scattered light with polarization 1,
#          int1(180) for different angle.
#  int2 :  the intensity scattered light with polarization 2
#          int2(180) for different angle.
real*8int1(180),int2(180),pix(500),taox(500),theta,dtheta,xtheta,c1,c2,cc,xabs
complex*16a(500),b(500),s1,s2
integer ndim,j,jj
theta = 0
dtheta = 3.14159265358979/180
do jj = 1,179 {
      theta = theta+dtheta
      xtheta = dcos(theta) #cos(theta)
      call pitao(pix,taox,xtheta,ndim) # calculates pi(x),tao(x),see
                                       # Kerker's book
      s1 = (0,0)
      s2 = (0,0)
      do j = 1,ndim {
            c1 = float(2*j+1)
            c2 = float(j*(j+1))
            cc = c1/c2
```

```
            s1 = cc*(a(j)*pix(j)+b(j)*taox(j))+s1
            s2 = cc*(a(j)*taox(j)+b(j)*pix(j))+s2
            }
      int1(jj) = xabs(s1)
      int2(jj) = xabs(s2)
      }
return
end



subroutine pitao(pix,taox,x,ndim)
# this subroutine calculates pi(x),tao(x) for diffrent partial
# wave index l upto ndim
#input:
#  x  : cos( theta ) , real
# ndim: integer
#return:
# pix  : real pix(500)
# taox  : real taox(500)
real*8pix(500),taox(500),plg(500),plgd(500),c,x
integer ndim,n
call plgf(plg,plgd,x,ndim)# calculates the Lergender polynomias
do n = 1,ndim {
      c = dsqrt(1.-x*x)
      pix(n) = plg(n)/c
      taox(n) = -plgd(n)/c
      }
return
end



subroutine plgf(plg,plgd,x,ndim)
#     this program calculate the p1(j) the associated legendre
#     function and its derivative
real*8plg(500),plgd(500),x
integer ndim,j
#     calculate first order associated legendre function
plg(1) = dsqrt(1.-x*x)
plg(2) = 3.*plg(1)*x
do j = 3,ndim+1
      plg(j) = (x*(2*j-1)*plg(j-1)-j*plg(j-2))/(j-1)
#     calculate derivative of ledendre function
```

```
#       plgd(j)=[plgd(j)]'*(sin(theta)**2)
do j = 1,ndim
       plgd(j) = -(j*plg(j+1)-(j+1)*plg(j)*x)
return
end



function xabs(x)
#this function calculates the sqare of the absolute value for
#a double precision complex value
real*8xabs
complex*16x
xabs = dreal(x)**2+dimag(x)**2
return
end



subroutine coef(a,b,ra,rf1,ndim)
#calculate the coefficients a and b for a shelled sphere scatterer
#input:
# ra  : inner radius / wave-length
# rf1 : refraction index in the core
# ndim: dimension of the coefficients of a and b
#return:
# a    : coefficients [see Kerker's book], a(500)
# b    : coefficients [see Kerker's book], b(500)
real*8psi1a(500),psi2a(500),psi1ad(500),psi2ad(500),kapa1a(500),kapa2a(
  500),kapa1ad(500),kapa2ad(500),topi,pi,qa,ra,zm1,rf1,
  z1a,ua1,ub1
complex*16xi1a(500),xi2a(500),xi1ad(500),xi2ad(500),a(500),b(500),da1,db1

integer ndim,n
pi = 3.14159265358979
topi = 2*pi
qa = topi*ra
zm1 = rf1
z1a = zm1*qa
call bessfunr(psi2a,kapa2a,xi2a,psi2ad,kapa2ad,xi2ad,z1a,ndim)
#functions at n*q
call bessfunr(psi1a,kapa1a,xi1a,psi1ad,kapa1ad,xi1ad,qa,ndim)
#functions at q
do n = 1,ndim {
```

```
#       calculate the coefficient a(n), kerker's book
#       formulas 5.1.29,5.1.31,5.1.33
#
        ua1 = zm1*psi2a(n)*psi1ad(n)-psi2ad(n)*psi1a(n)
        da1 = -psi2ad(n)*xi1a(n)+zm1*psi2a(n)*xi1ad(n)
        a(n)=ua1/da1
#        print*,'n,ua1,ua2,ua3,ua4,da1,da2,da3,da4'
#        print*,n,ua1,ua2,ua3,ua4,da1,da2,da3,da4,a(n)
#
#       calculate the coefficient b(n), kerker's book
#       formulas 5.1.30,5.1.32,5.1.34
#
        ub1 = -psi2a(n)*psi1ad(n)+zm1*psi2ad(n)*psi1a(n)
        db1 = zm1*psi2ad(n)*xi1a(n)-psi2a(n)*xi1ad(n)
        b(n)=ub1/db1
        }
return
end



subroutine bessfunr(psi,kapa,xi,psid,kapad,xid,x,ndim)
#input:
#   x : real
# ndim: integer
#return:
#psi   : real psi(500)
#psid  : real psid(500), derivative of psi
#kapa  : real kapa(500)
#kapad : real dapad(500), derivative of kapa
#xi    : complex xi (500)
#xid   : complex xid(500) , derivative of xi
#the difinations of the varables psi,kapa,xi can be found in
#                   Kerker's book.
complex*16xi(500),xid(500),ci
real*8psi(500),kapa(500),psid(500),kapad(500),bsj(0:500),bsy(0:500),x
integer l,ndim
call bessj(bsj,x,ndim+1)
call bessy(bsy,x,ndim+1)
ci = (0,1)
do l = 1,ndim {
        psi(l) = x*bsj(l)
        kapa(l) = -x*bsy(l)
        psid(l) = x/(2*l+1)*((l+1)*bsj(l-1)-l*bsj(l+1))
```

```
        kapad(l) = -(x/(2*l+1)*((l+1)*bsy(l-1)-l*bsy(l+1)))
        xi(l) = psi(l)+ci*kapa(l) #need to
        xid(l) = psid(l)+ci*kapad(l)    #check the sign,
                                  #     should be + ?
        }
return
end



subroutine bessj(bsj,x,ndim)
#    the subroutine bessj calculate the spherical
#         bessel function which is j[n](x) and has the relation to the
#         regular bessel function as
#        j[n](x) = sqrt(pi/(2x))j[n+1/2](x)
real*8bsj(0:500),sum,bjp,bj,bjm,bigno,bigni,bessjs,x,tox
integer iacc,n,ndim,m,i,j
parameter(iacc = 400,bigno = 1.e10,bigni = 1.e-10)
tox = 2./x
n = ndim+1
m = 2*((n+int(sqrt(float(iacc*n))))/2)
sum = 0.
bjp = 0.
bj = .0001
do j = m,1,-1 {
        bjm = (.5+j)*tox*bj-bjp
        bjp = bj
        bj = bjm
        if (j<=n)
              bsj(j) = bjp
        if (abs(bj)>bigno)
          {
           bj = bj*bigni
           bjp = bjp*bigni
           bessjs = bessjs*bigni
           sum = sum*bigni*bigni
           do i = 0,n
               bsj(i) = bsj(i)*bigni
           }
        sum = sum+(2*j-1)*bj*bj
        }
sum = dsqrt(sum)
do j = 0,n
        bsj(j) = bsj(j)/sum
```

```
bsj(0) = dsin(x)/x
return
end



subroutine bessy(bsy,x,ndim)
#     the bessy calculate the spherical
#          bessel function which is y[n](x) and has the relation to the
#          regular bessel function as
#         y[n](x) = sqrt(pi/(2x))y[n+1/2](x)
real*8bsy(0:500),x,tox
integer ndim,n,j
tox = 2./x
n = ndim+1
bsy(0) = -dcos(x)/x
bsy(1) = -dcos(x)/(x*x)-dsin(x)/x
do j = 2,n
       bsy(j) = (j-.5)*tox*bsy(j-1)-bsy(j-2)
return
end
```

Bibliography

Agranovich, Z. S., and V. A. Marchenko, *The Inverse Problem of Scattering Theory*, (Gorden and Breach, New York, 1963).

Andersson-Engels, S., R. Berg, S. Svanberg, and O. Jarlman, Opt. Lett. **15**, 1179-1181(1990).

Baltes, H. P. ed., *Inverse Source Problems in Optics*, (Springer-Verlag, Berlin, 1978).

Born, M., and E. Wolf, *Principles of Optics*, 4th Edition, (Pergamon, New York, 1970), Pg. 633-664.

Chen, H., Y. Chen, D. Dilworth, E. Leith, J. Lopez, and J. Valdmains, Opt. Lett. **16**, 487(1991).

Cheong, W. F., S. A. Prahl and A. J. Welsh, IEEE J. Quantum Elect. **26**, 2166-2185(1990).

Dainty, J. C. ed., *Laser Speckle and Related Phenomena*, (Springer-Verlag, Berlin, 1975), pp203-278.

Debye, P., Ann. Physik. **30**, 59(1909).

Delpy, D. T., M. Cope, P. van der Zee, S. Arridge, Susan Wary, and J. Wyatt, Phys. Med. Biol. **33**, 1433-1442(1988).

Dorsinville, H. R., R. R. Alfano, and N. H. Schiller, "Calibrating a picosecond streak camera", *The photonics design and applications handbook*, H23-25(1986).

Drake, J. M., and A. Z. Genack, Phys. Rev. Lett. **63**, 259(1989).

Duncan, M. D., R. Mahon, L. L. Tankersley, and J. Rentjes, Optics Letters **16**, 1868-1870(1991).

Feng, S., C. Kane, P. A. Lee, and A. D. Stone, Phys. Rev. Lett. **61**, 834 (1988)

Fork, R. L., B. J. Greene, and C. V. Shank, Appl. Phys. Lett. **38**, 671(1981).

Freund, I., M. Rosenbluh, and S. Feng, Phys. Rev. Lett. **61**, 2328(1988)

Fujimoto, J. G., S. De Silversti, E. P. Ippen, R. Margolis, and A. Oseroff, Opt. Lett. **11**, 150 (1986)

Genack, A. Z., and J. M. Drake, Europhys. Lett. **11**, 331(1990).

Goldman, L. ed., *Laser Non-Surgical Medicine- New Challenges for An Old Application*, (Technomic, Lancaster, 1991).

Groenhuis, R. A. J., H. A. Ferwerda, and J. J. Ten Bosch, Appl. Opt. **22**, 2456, and 2463(1983).

Hebden, J. C., R. A. Kruger, and K. S. Wong, Appl. Opt. **30**, 788-794(1991).

Ho, P. P., P. Baldeck, K. S. Wong, K. M. Yoo, D. Lee, and R. R. Alfano, Appl. Opt. **28**, 2304-2310(1989).

van de Hulst, H. C., *Light Scattering by Small Particles*, (Dover, New York, 1981), Chap. 4, 6, and 10.

Ishimaru, A., *Wave propagation and scattering in random media*, Vol. **1 & 2**,(Academic Press, New York, 1978).

Jackson, J. D., *Classical Electrodynamics*, 2nd Edition, (Wiley, New York, 1975).

Jacques, S. L., IEEE Trans. Biomed. Eng. **36**, 1155(1989).

Johnson, C. C., IEEE Trans. Biomed. Eng. **17**, 129(1970).

Lax, M., Rev. Mod. Phys. **23**, 287(1951).

Lax, M., Phys. Rev. **85**, 621(1952).

Lax, M., *Symmetry principles in solid state and molecular physics*, (Wiley, New York, 1974), pp 198.

Lax, M., V. Nayaramamurti, and R. C. Fulton, " Classical diffusive photon transport in a slab," in *Proceedings of the Symposium on Laser Optics of Condensed Matter, Leningrad, June 1987*, edited by J. L. Birman, H. Z. Cummins and A. A. Kaplyanskii (Plenum, New York, 1987), pp229-235.

Liu, F., K. M. Yoo, and R. R. Alfano, Opt. Lett. **16**, 351-353(1991).

Liu, F., K. M. Yoo, and R. R. Alfano, (unpublished).

Mie, G., Ann. Physik. **25**, 377(1908).

Patterson, M. S., B. Chance, and B. C. Wilson, Appl. Opt. **28**, 2331-2336(1989).

Press, W. H., B. P. Flannery, S. A. Teukolsky, and W. T. Vetterling, *Numerical Recipes*, (Cambridge, New York, 1986).

Reynolds, G. T., Microsc. Acta 83, 55 (1980)

Saulnier, P. M., M. P. Zinkin, and G. H. Watson, Phys. Rev. **42**, 2621(1990).

Shapiro, S. L., ed. *Ultrafast Laser Pulses*, (Springer-Verlag, Berlin, 1984).

Sheng, P., ed. *Scattering and Localization of Classical Waves in Random Medium*, (World Scientific, Singapore, 1990).

Stephen, M. J., and G. Cwilich, Phys. Rev. B **34**, 7564(1986).

Ultrafast Phenomena, Vol. I-VII(Springe-Verlag, Berlin).

Wang, L. M., P. P. Ho, C. Liu, G. Zhang, and R. R. Alfano, Science **253**, 769-771(1991).

Watson, G. H., P. A. Fleury, and S. L. McCall, Phys. Rev. Lett. **58**, 945-948(1987).

Watson, G. H., S. L. McCall, P. A. Fleury, and K. B. Lyons, Phys. Rev. B **41**, 10947(1990).

Weiss, G. H., R. Nossal, and R. F. Bonner, J. of Mod. Opt. **36**, 349(1989).

White, B., P. Sheng, M. Postel, and G. Papanicolou, Phys. Rev. Lett. **63**, 2228 (1989)

Wilson, B. C., and S. L. Jacques, IEEE J. Quantum Elect. **26**, 2186-2199(1990).

Yariv, A. *Optical Electronics,* 3rd Edition, (Holt, New York, 1985), Pg. 236-246.

Yariv, A. and P. Yeh, *Optical Waves in Crystal: Propagation and Control of Laser Radiation*, (Wiley, New York, 1984), Pg. 549

Yoo, K. M., and R. R. Alfano, Opt. Lett. **15**, 320-322(1990).

Yoo, K. M., Feng Liu, and R. R. Alfano, Phys. Rev. Lett. **64**, 2647-2650(1990); errata, **65**, 2210-2211(1990).

Yoo, K. M., Feng Liu, and R. R. Alfano, Opt. Lett. **16**, 1068-1070(1991).

Yoo, K. M., Z. W. Zang, S. A. Ahmed, and R. R. Alfano, Opt. Lett. **16**, 1252-1254(1991).

Yoo, K. M., Qirong Xing, and R. R. Alfano, Opt. Lett. **16**, 1019-1021(1991).

Yoo, K. M., B. B. Das, and R. R. Alfano, Opt. Lett. **17**, 958-960(1992).

Zdrojkowski, R. J., and N. R. Pisharoty, IEEE Trans. Biomed. Eng. **17**, 122(1970).